TAMPEREEN TEKNILLINEN YLIOPISTO
TAMPERE UNIVERSITY OF TECHNOLOGY

Sarita Hernesniemi

Wetting and Reactivity between Nitride Ceramics and Molten Copper and Silver Alloys

Julkaisu 1040 • Publication 1040

Tampere 2012

Tampereen teknillinen yliopisto. Julkaisu 1040
Tampere University of Technology. Publication 1040

Sarita Hernesniemi

Wetting and Reactivity between Nitride Ceramics and Molten Copper and Silver Alloys

Thesis for the degree of Doctor of Science in Technology to be presented with due permission for public examination and criticism in Konetalo Building, Auditorium K1702, at Tampere University of Technology, on the 25th of May 2012 at 12 noon.

Tampereen teknillinen yliopisto - Tampere University of Technology
Tampere 2012

ISBN 978-952-15-2813-2 (printed)
ISBN 978-952-15-2836-1 (PDF)
ISSN 1459-2045

ABSTRACT

Wetting and reactivity were studied for molten Cu-Cr, Cu-Zr and Ag-Zr alloys on two nitride ceramics AlN and Si_3N_4. The aim of the study was to understand the interfacial behaviour of these metal alloys in molten state on each ceramic. The potential for the successful application of these material combinations can be evaluated by measuring the contact angle formed in the wetting test. Wetting test is also a suitable method for producing interfacial reactions and analysing them after the experiment. If good bonding is the most important requirement, the wetting should be as good as possible and the reactivity should not produce cracking in the materials. On the other hand, if a high temperature material is needed for metal alloy handling applications, the wetting should not be too good and the reactivity should be limited to avoid the cracking of the materials.

High vacuum sessile drop experiments were carried out with polished substrate samples by *in-situ* alloy manufacturing. During the experiment the development of contact angles and other dimensions were determined as a function of time and the spreading rate was used to evaluate the kinetics of the reactive wetting. After the experiment the adhesion of the drop to the surface was evaluated through possible crack formation and chemical analyses for the interfaces were carried out with SEM and EDS. Thermodynamic calculations for predicted reactions were carried out to determine the driving forces for these reactions. The results were used to identify the phases revealed at the interface after the wetting experiments.

Among the studied Cu- and Ag- base metals with Cr- and Zr-additions only the Ag-Zr alloy on Si_3N_4 showed perfect wetting. Same alloy on AlN produced the contact angle of 15°±2°. The best wetting with copper alloys was obtained with the CuCr1,5 alloy on Si_3N_4 showing the contact angle of 75°±2°. Other studied combinations did not produce wetting. Interfacial reactivity was revealed with all Zr-and Cr-additions. The formation of ZrN and Cr_2N was confirmed by SEM analyses. Significant amounts of oxygen were also found in most cases and it was concluded that oxygen interfered wetting, even if no separate oxygen-containing phases were found in interfacial layers. The AlN substrate cracked after wetting experiments due to the strong bonding of

interfacial layers. The Si_3N_4 substrate did not crack, even if the observed reaction layers were several micrometers thick. Since oxygen was found in the interfacial layers even in these high vacuum experiments it will probably have a strong influence on the behaviour in real applications. It may even prevent some of the observed interactions by interrupting the process of wetting.

PREFACE

This research work was carried out in Tampere University of Technology, in Outokumpu Copper R&D unit in Pori and in Institut National Polytechnique de Grenoble (INPG) with funding of Outokumpu Oyj Foundation during 1999-2005.

I want to express my gratitude to my supervisor professor Tuomo Tiainen from Tampere University of Technology for his support and advice.

I want to express my gratitude also to Dr Nicholas Eustathopoulos from Institut National Polytechnique de Grenoble for enabling this research work and his indispensable advice during my stay in his research group in years 2000-2001. I also want to direct my sincere thanks for Dr Pavel Protsenko and Mr Michel Jeymond in the team for all the possible help in carrying out this work. All the three furnaces used in this study are located in the INPG.

I am also very grateful for Dr Elina Huttunen-Saarivirta from Tampere University of Technology for all her help as well as I am grateful for all the help from the personnel of Outokumpu Copper R&D during this research work.

Finally I want to express thanks to all my family and friends during the many years of completing this work.

LIST OF SYMBOLS

a_i =	thermodynamic activity of component i
$a_{(i)j}$ =	thermodynamic activity of component j in solution of i
C_0 =	instantaneous concentration
C_e =	concentration in equilibrium
D =	diffusion coefficient
e =	thickness of interfacial layer
f_α =	surface fraction of phase α
f_d =	driving force
F_s =	surface free energy
$F(\tau)$ =	time dependent constant in equation 13
$\Delta G^0_{f(i)}$ =	standard Gibbs free energy of formation of the compound i
ΔG_M =	Gibbs energy for reaction
h=	height
$\Delta \bar{H}^\infty_{i(j)}$ =	partial enthalpy of mixing at infinite dilution of a solute in a solvent j
k=	Wenzel coefficient in equation 5
K =	material constant in equation 11
m =	mass
m=	coefficient in equation 10
M=	molar mass
n =	numerical constant in equation 14
n_v =	number of moles of component v
P_i =	partial pressure of species i
$P^{d(MO)}_{O2}$=	partial pressure of the decomposition of oxide MO
$P^{ox(M)}_{O2}$=	oxygen partial pressure of the oxidation of metal M
P^{l}_{O2}=	equivalent partial pressure at a solid/liquid interface
R,r=	radius
R_a =	average height of asperities on a measured surface
R_{ms} =	mean squared roughness data point for the measured surface
R_t =	range of collected roughness data points for the measured surface
t =	time
T =	temperature
T_M =	melting temperature
V=	velocity
V=	volume
W_a =	work of adhesion
W_c =	work of cohesion
x_i =	molar fraction of component i
x_i^{eq}=	molar fraction of component i for a reaction at equilibrium
y =	deviation from stoichiometry in non-stoichiometric compound
Γ_i^j=	relative adsorption of species i with respect to species j
$\gamma^\infty_{O(A)}$=	activity coefficient of species I at infinite dilution in a solvent
δ^{max} =	local maximum inclination of the real surface
ε^B_O=	Wagner interaction parameter between oxygen and solute 1
θ=	contact angle
θ_a=	advancing contact angle

θ_{app}= apparent contact angle
θ_{Cassie} = Cassie contact angle on chemically heterogeneous surface
θ_D = dead or in-effective contact angle in reactive wetting
θ_f= final contact angle
θ_m= measured contact angle
θ_r = receding contact angle
θ_W= Wenzel contact angle on a rough surface
θ_Y= Young contact angle
θ_α = contact angle of phase α
θ_β = contact angle of phase β
η = dynamic viscosity
ρ = density
σ_{LV}= liquid/vapour surface energy
σ_{SV}= solid/vapour surface energy
σ_{SL} = solid/liquid interfacial energy
Φ_L = triple line angle between liquid-solid in Smiths relation in equation 12
Φ_V = triple line angle between vapour-solid in Smiths relation in equation 12
Φ_S = wetting ridge angle in Smiths relation in equation 12
Φ_1 = Smith's equilibrium contact angle
Ω= Volume

Chapter 1. Introduction

Nitride ceramics are of great interest in applications where good thermal shock resistance is required. The specific properties of different nitrides have made them appealing in several applications. Aluminium nitride (AlN) has a combination of good thermal conductivity and high electrical resistivity, which makes it a good substrate material for electronics industry. Silicon nitride has excellent strength also at high temperatures. This makes it a good material for example for gas turbines. Nitrides have also a good chemical resistance at high temperatures and in aggressive environments, such as molten metals.

Growing demands on materials performance have necessitated the joining of dissimilar materials. In many cases it is the only way to fulfil the new requirements, such as a combination of low weight and high strength. To enhance the adhesion and wetting between two non-reactive materials some reactive element is often added to the brazing alloy to provoke the adhesion between the materials. In the metallurgical industry a need exists on materials for molten metal handling. Wetting and reactivity are here either desired or undesired properties, depending on application. Anyway they will play significant role when selecting a material for a definite application. Nitride ceramics are generally poorly wetted by most molten metals; only some nitride forming metals make an exception.

In this study the interest is in clarifying the interfacial phenomena between molten copper-zirconium, copper-chromium and silver-zirconium alloys and AlN and Si_3N_4 ceramics. The studied parameters are wetting and reactivity. The shape of a liquid droplet characterizes the wetting on a solid surface at the studied temperature and in a specific atmosphere. The wetting is studied by the sessile drop method which allows the continuous observation of the shape of the liquid droplet during the experiment. Zirconium and chromium are both reactive alloying elements which thermodynamically are expected to react in the experiment with all the studied ceramic substrates. Wetting will also be influenced by this reaction. The spreading of the liquid droplet on the substrate surface and the final contact angle which describes the wettability will be altered by this reaction. In this work the kinetics of this reactive wetting will

be studied and some hypotheses concerning the mechanisms which control the reaction and the spreading of the liquid will be presented.

The factors which influence the wetting will be also studied and discussed. The most important of these are the cleanliness of the substrate surface, its roughness and the influence of oxygen on the wetting. Oxygen is dissolved to a great extent in Cu and Zr. These effects should be considered already in sample preparation. This is important for the comparison with other studies, since the final contact angle depends on numerous things and in order to reproduce experiments a lot of details should be known about the materials, test conditions and measurements.

Finally the reactivity is studied using the solidified sessile drop samples. Adhesion can only be evaluated qualitatively, since no data for liquid CuZr alloy was found for calculating the exact work of adhesion. The reaction products are identified from the cross-section of sample. The results for wetting and reactivity are then compared with the thermodynamic data and the previous studies carried out on these materials.

Chapter 2. Theoretical background of wetting and reactivity

The basic equations on wetting and adhesion apply for ideal solid surfaces. Some additional factors must be taken into account when discussing real surfaces. Such factors are, for example, surface roughness and chemical discontinuity points.

2.1. Ideal surface

Wetting is characterised by wetting angle, which is the contact angle at the triple line in system that contains the solid surface S, liquid drop L on solid surface and vapour phase V. The triple line means the line common for solid, liquid and vapour phases. Such system is shown in figure 2.1. The liquid phase is considered to be perfectly wetting if the contact angle is 0°, and partially wetting if the angle is between 0° and 180°. The latter case is further divided into two subcases: if the contact angle is smaller than 90° the system is called as wetting. If the contact angle is larger than 90°, the system is characterised as non-wetting. These three cases are described in figures 2.1.a) - c).

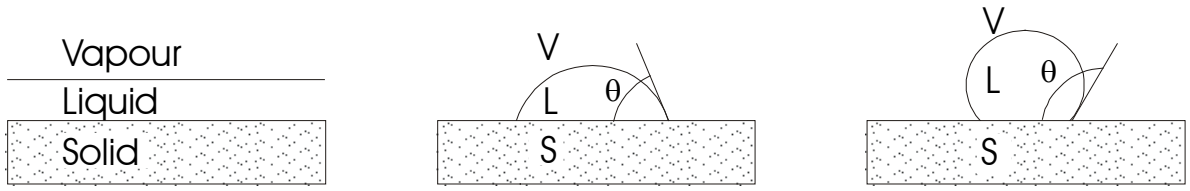

a) b) c)

Figure 2.1. Three different basic cases in wetting: a) perfect wetting, b) wetting system ($\theta < 90°$), c) non-wetting system ($\theta > 90°$) /1/.

Let us consider a system consisting of a horizontal, undeformable, perfectly smooth and chemically homogeneous solid surface, vapour atmosphere and a non-reactive liquid. In thermodynamic equilibrium the relation between contact angle θ_Y and sur-

face energies σ_{SV}(solid – vapour), σ_{SL}(solid – liquid) and σ_{LV}(liquid – vapour), can be described by the Young's equation /1/:

$$\cos\theta_Y = \frac{\sigma_{SV} - \sigma_{SL}}{\sigma_{LV}} \qquad (1)$$

At the solid – liquid interface the adhesion depends on the interactions between the atoms of solid and liquid phases. The strength of bonding at that interface is characterized with the work of adhesion W_a. This work can be thought as the energy per unit surface that is required to separate the liquid and solid phase under isothermal conditions. This work of adhesion is described by Dupré equation /2/:

$$W_a = \sigma_{SV} - \sigma_{SL} + \sigma_{LV} \qquad (2)$$

Combining these two equations we get the Young-Dupré equation /2/:

$$\cos\theta_Y = \frac{W_a}{\sigma_{LV}} - 1 \qquad (3)$$

This equation combines the opposite forces which are present at the solid – liquid interface. One of the forces is derived from the interaction between solid and liquid phases (W_a) which promotes the liquid spreading and the other originates from the cohesive forces inside the liquid (σ_{LV}) at solid substrate. The work of cohesion can be thought to form analogously with the work of adhesion, describing the energy needed to separate a liquid volume into two pieces for creating two new liquid surfaces. The equation to describe the work of cohesion is written as:

$$W_c = 2\,\sigma_{LV} \qquad (4)$$

Both the work of adhesion and the work of cohesion are illustrated in figure 2.2.

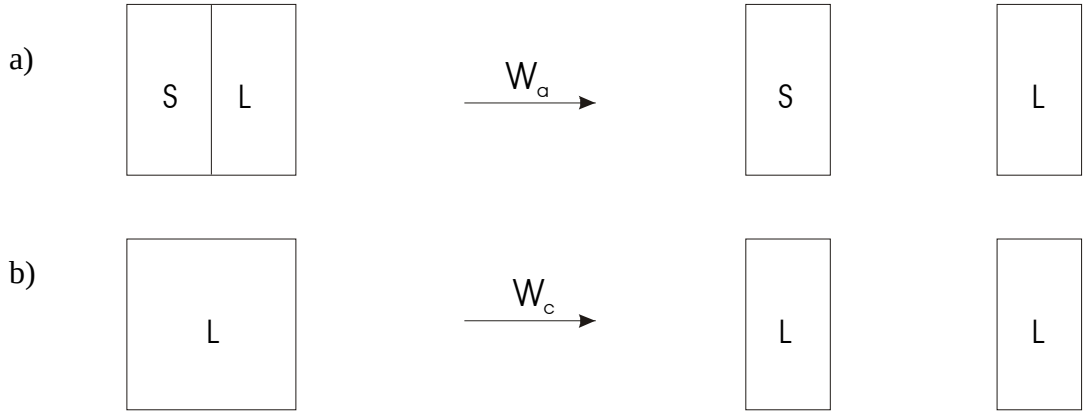

Figure 2.2. Schematic presentation of the reversible separation of interfaces, and the consequent work of adhesion W_a (fig 2.2a) and work of cohesion W_c (fig 2.2b) /2/.

2.2. Real surface

At real surfaces the measured real contact angle value varies around the ideal contact angle θ_Y, changing between advancing and receding contact angle values. The advancing contact angle θ_a is the angle observed immediately after spreading and the receding contact angle θ_r is the angle observed after the recoiling of liquid front. The measured angle θ_m is somewhere between these values $\theta_r < \theta_m < \theta_a$.

Deviation from Young's contact angle values comes from obstacles at the spreading or the receding liquid front. Such blockage of the triple line can be due to two types of surface defects:

1. Topological irregularities such as surface roughness can cause physical blocking and so the transition of the triple line to incorrect location.

2. Chemical heterogeneity which originates from impurities at the surface or from the different chemical composition at different places of the surface. Both these change the value of surface energy σ_{SV} and therefore also the value of interfacial energy σ_{SL}.

2.2.1. Influence of surface roughness on contact angle

First studies on the influence of surface roughness on contact angle values were carried out by Wenzel /3/. He added to the analysis the influence of actual surface area, which is larger than the geometrical surface area due to surface roughness. He described the effect with the Wenzel coefficient k. This coefficient is the ratio between actual and ideal planar area (k > 1). Now the contact angle can be written as:

$$\cos\theta_W = k \cos\theta_Y \qquad (5)$$

where θ_W is the contact angle on rough surface. This model supposes that the only influence of roughness comes from the increased surface area. According to equation (5) the contact angle increases in non-wetting systems ($\theta_Y > 90°$) and decreases in wetting systems ($\theta_Y < 90°$) due to the surface roughness.

Shuttleworth and Bailey /4/ took into account the local geometry of the surface defects and they made a hypothesis on the hysteresis in contact angle. They predicted that the surface asperities could lock the triple line into positions described in figure 2.3, for two-dimensional case. According to this assumption the triple line is stopped to a position where the local contact angle is equal to Young's contact angle. If that is the case the measured contact angle could be larger or smaller than on ideal surface. These two angles, advancing and receding contact angles are described with following equations:

$$\theta_a = \theta_Y + \delta^{max} \qquad (6)$$

$$\theta_r = \theta_Y - \delta^{max}, \qquad (7)$$

where δ^{max} is the local maximal inclination of the real surface.

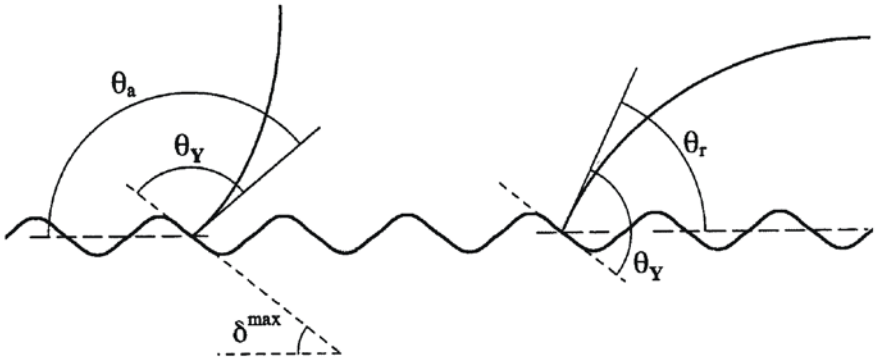

a) b)

Figure 2.3. Illustration of the contact angle on rough surface (roughness described by maximal inclination δ^{max}), which can vary between the maximum (advancing a)) and the minimum (receding b)) contact angles /4/.

Other studies, like Dettree /5/ and Eick /6/ have shown that in practice the contact angle can assume any value between θ_a and θ_r. The variation comes from the vibrational energy which is induced by the used equipment. This additional vibrational energy is always present to some degree, and it partially explains the variations in measured contact angle values for different installations and in different experimental conditions.

2.2.2. Influence of chemical inhomogeneity

The effects originating from the presence of two chemically different phases resemble the effects of surface roughness. Assume that the two different phases α and β are in the form of strips which are perpendicular to the triple line. Equation to describe this situation was first presented by Cassie /7/:

$$\cos\theta_{Cassie} = f_\alpha \cos\theta_\alpha + (1 - f_\alpha)\cos\theta_\beta \quad (8)$$

where f_α is the surface fraction of phase α, and θ_α and θ_β are the equilibrium contact angles on phase α and β, respectively. The phase α is supposed to be wetting ($\theta_\alpha < 90°$) and phase β is supposed to be non-wetting ($\theta_\beta > 90°$).

If the different phases are parallel to the triple line the obtained contact angle will be the minimum receding angle for the better wetting phase β, and the maximum advancing angle for phase α. Definitions for the advancing and receding contact angles were given in the previous chapter.

2.3. Dynamics of wetting

In the previous section the static equilibrium contact angles in the beginning of contact and after achieving equilibrium were studied. Now the intermediate situation will be studied. This dynamic stage is generally called spreading and it includes all the phenomena occurring between the initial and the final contact stages. The treatment is carried out separately for non-reactive and reactive cases.

2.3.1. Non-reactive wetting

The driving force f_d which promotes the isothermal spreading of liquid and therefore wetting of solid substrate can be described with the following equation 9 /9/, which gives the change in the surface and interfacial energy F_s for a differential movement dx of the triple line along the substrate surface:

$$f_d = -\frac{dF_s}{dx} = \sigma_{SV} - \sigma_{SL} - \sigma_{LV}\cos\theta = \sigma_{LV}\left[\cos\theta_f - \cos\theta\right] \quad (9)$$

In the equation the angles θ_f and θ are the final equilibrium contact angle and the instantaneous contact angle in the system, respectively.

The spreading of a liquid can be either inertial or viscous depending on the properties of the liquid. In the case of low viscosity the spreading has been presented to follow the spreading law presented by de Gennes /9/:

$$R^{3m+1} = V^* t \Omega^m, \tag{10}$$

where m is an experimental coefficient evaluated in /9/, V^* is γ/η (surface energy / fluid viscosity), t is time and Ω is the drop volume. In the case of a viscous liquid viscous dissipation of energy in the drop limits spreading. The dependence of the spreading on viscosity η, described as the differential growth of drop radius dR over time dt (dR/dt), was shown by Tanner /8/ and de Gennes /9/ to follow the equation:

$$\frac{dR}{dt} = \frac{\sigma_{LV}}{3\eta \mathrm{K}} \tan\theta\left(\cos\theta_f - \cos\theta\right) \tag{11}$$

Here K is a numerical constant with the value close to 10. This equation holds for viscous materials such as glass which has a total spreading time of 10^2 s. The viscosity of liquid metals is small and therefore their spreading times are in general as small as 10^{-1}–10^{-2} s and the equation 10 must be used. The non-reactive spreading of metals on different substrates has been studied by several authors as presented, e.g., in the articles /10, 11, 12/.

Another effect occurring during the spreading is presented in figure 2.4. Here the substrate is deformed in front of the triple line. In fact the situation in figure 2.1. is the vector projection of the situation in figure 2.4. According to Smith /13/ this deformation of the surface corresponds to the final equilibrium state at triple line. This equilibrium is formulated in Smiths relation:

$$\frac{\sigma_{SV}}{\sin\Phi_L} = \frac{\sigma_{SL}}{\sin\Phi_V} = \frac{\sigma_{LV}}{\sin\Phi_S} \qquad (12)$$

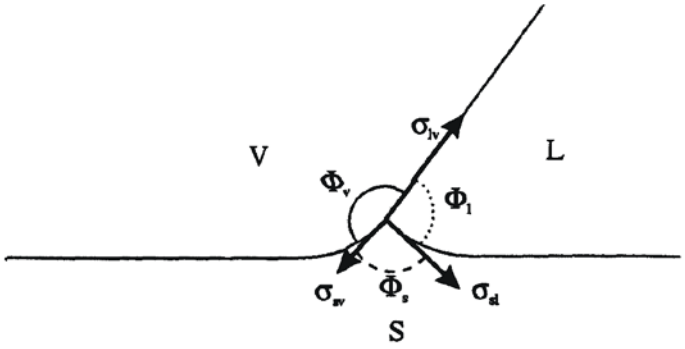

Figure 2.4. Smith's relation for equilibrium state at the triple line in the case of deformable substrate surface /13/.

With viscoelastic substrates this deformation can be measured locally and according to Carre and Shanahan /14/ the movement of this "wetting ridge" could control the overall wetting. For example studies carried out by Saiz et al /15/ suggest that the formation of the triple line ridge controls also the spreading in reactive wetting. Eustathopoulos in /16/ concludes that on ceramic surfaces the growth rate of ridges is not high enough to control the spreading. Next subchapter presents the background and current understanding of reactive wetting.

2.3.2. Reactive wetting

Two possible types of chemical reactions occurring at the liquid – solid interface exist: dissolution of the substrate by liquid or the formation of a new phase at the interface. It is also possible that reaction layer forms after sufficient amount of initial dissolution, thus combining the two types.

Dissolutive wetting

There are two different wetting cases with dissolution. Dissolution can occur without any significant changes in the surface and interfacial energy values σ_{LV} and σ_{SL}. An example of dissolutive wetting without any new compound formation is the wetting of HfB_2 by molten Ni /17/. This kind of reactive wetting was studied by Warren et al /18/. They modeled the liquid B on substrate A as described in figure 2.5. Here A and B do not form any compounds at the ambient temperature and there is no remarkable solubility of B to A, but there is a solubility of A to B.

When the drop B, which is pure from A, is placed on the substrate A the equilibrium is attained via three kinetically different stages. In the first stage the liquid spreads non-reactively to the substrate and stops at the Young's equilibrium contact angle. This spreading takes place in approximately 10^{-2} s and there is only negligible amount of dissolution. Same kind of spreading would occur if the drop B was saturated by A, and no further stages two or three i.e. dissolution would occur.

The second stage of reactivity is the dissolution of the substrate at the interface and the change in the geometry of the cross section of the system, as shown in figure 2.5.c). Now the contact angle is neither the Young's angle nor the Smith's equilibrium contact angle. The contact angle can be considered as the Smith's angle Φ_1 only microscopically, as in figure 2.5c) (magnified part), assuming that the triple line stays in the same plane with the original substrate. Time for this dissolution (t_2 in the figure) is of the order of 10^2 s. After much longer time, perhaps even years, the total equilibrium shape is formed in the third state, as shown in part d) of figure 2.5.

The second case in dissolutive wetting includes the presence of tension-active species in the system where also new compounds may be formed either to the interface or on the drop surface. Tensio-active species has a tendency of adsorbing to the surface and there it can decrease significantly the surface energy values σ_{LV} and/or σ_{SL}. An example of this kind of system is the Fe/Al_2O_3 system /19/, where additions of elements S, Se and Te increase the contact angle by adsorbing to the Fe/Al_2O_3 interface. The re-

duction of σ_{SL} is much lower than the reduction of σ_{LV} by these elements. In this case large contact angles, such as 160° were observed.

More recent examples of studies on dissolutive wetting where new compounds are formed to the system are Ni-Ti alloys on HfB_2 /16/ and Au-Ni alloys on ZrB_2 /20/. Other studies which have been carried out to understand this kind of wetting and also the transitions between non-reactive and dissolutive wetting have been conducted during last years. Examples of these are e.g. Ag-Cu alloys on Cu /12/, Si on Cu /10/, Sn on Au /21,22/. Not clear understanding exists on the mechanisms which control the spreading in these systems. The basic difference as compared to other types of theories on the spreading of the drop triple line is the strong convective movement which has been found in these systems and its influence on the final contact angle is under discussion.

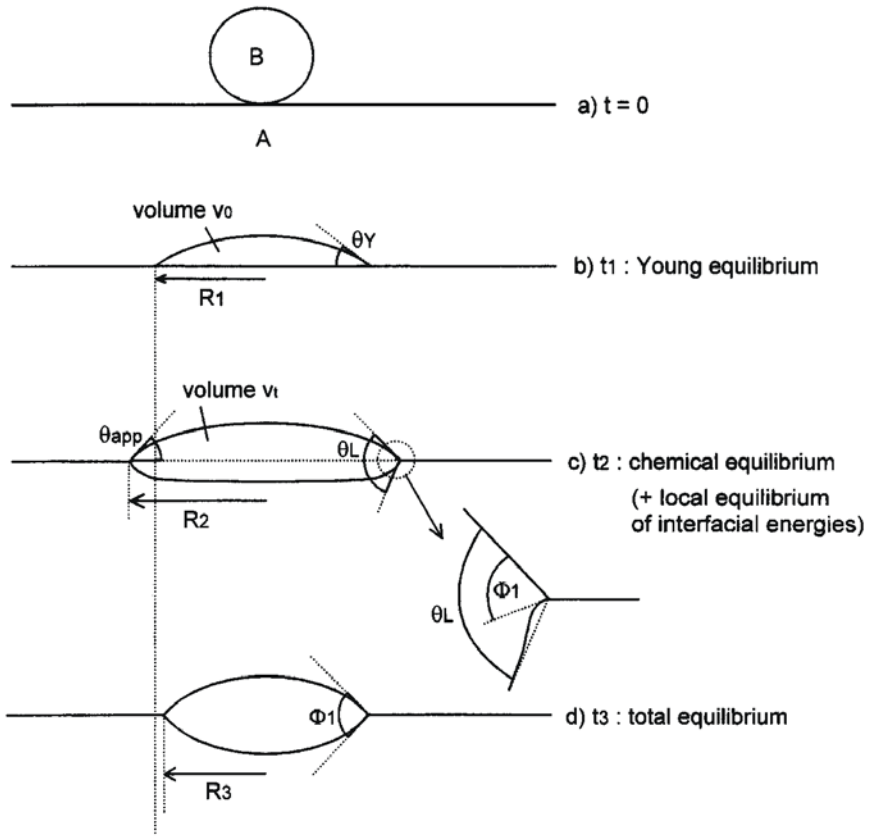

Figure 2.5. Dissolutive wetting according to the model of Warren et al in /18/.

In ref. /23/ Bougiouri et al found an example of a system (NiSi alloys on C) which transfers from dissolutive wetting to a formation of new interfacial layer after a sufficient amount of Si is dissolved and a SiC layer can form to the interface.

Formation of 3-dimensional compounds

When the thermodynamic and kinetic conditions are favourable, a continuous, dense 3-dimensional layer can form in the solid - liquid interface. The final wetting behaviour depends on the final chemical composition of the interface, not on the intensity of reactions. If the final interfacial product is the same for different substrates, the wetting will also be the same. This result has been verified by authors Espié et al /24/, Kritsalis et al /25/ and Landry et al /26/.

The first fundamental study of reactive spreading was carried out by Landry and Eustathopoulos with pure liquid aluminium on vitreous carbon substrate. In this study the growth of the reaction product (Al_4C_3) was observed during the sessile drop experiment. The results are presented in figure 2.6. The reaction product is wetted better than the original substrate /27/. In the spreading curve measured in this experiment three different stages can be observed. Stage A-B presents the deoxidation of liquid aluminium surface. After that there is the nonlinear stage B-C, where the wetting starts. During this phase the reaction occurs at the interface until at point C the interface has completely reacted. After this point there is a linear region C-D in the curve. Now the spreading rate is equivalent with the reaction rate and it stays constant with time (Landry /26/ and Dezellus /28/). The spreading stops at the equilibrium contact angle of Al on Al_4C_3 at point D.

Deviations from this kind of spreading can occur when the reaction is controlled by the diffusion of the active element from the liquid to the triple line where the reaction takes place. This phenomenon was studied by Mortensen et al /29/. In this case the spreading rate decreases continuously due to the reduction of the diffusion field as described in figure 2.7. The diffusion field is considered to be proportional to the volume of the drop liquid where the diffusion can take place near the triple line.

According to Mortensen et al. the rate of diffusion controlled spreading can be estimated with the following equation:

$$\frac{dR}{dt} = \frac{2DF(\tau)}{en_v}(C_0 - C_e)\theta \qquad (13)$$

where D is the diffusion coefficient of the reacting element in the liquid phase and F(τ) is a constant depending on time (typically in a sessile drop experiment lasting some tens of minutes this constant is close to 0,04). C_o and C_e are the instantaneous concentrations of the reactive solute at the triple line and in the equilibrium with the reaction product, respectively. The quantity e is the thickness of reaction product at the triple line, n_v is the number of moles of reactive species per unit volume of drop and θ is the instantaneous contact angle.

Hodaj et al /30/ have added to this equation the influence of interfacial reaction layer growing behind the triple line. If the diffusion through the formed interfacial the layer is significant, some of the active element will be consumed in the thickening of layer behind the triple line. This is introduced in the equation with angle θ_D which is the dead or in-effective angle proportional to the decrease in the flux of active element to the triple line. In equation (13) θ is thus replaced by $(\theta-\theta_D)$.

As an example of a case where the reactions near the triple line and not the diffusion phenomena control the wetting, silicon alloys wetting on carbon substrate have been studied. The reactive spreading was shown to occur in three different stages in the reactive wetting study by Dezellus et al. /31/ After fast start of spreading immediately at the contact, the second phase of spreading seen in the contact angle – time curve is taking place with decreasing rate as the new reaction layer is formed. The authors describe this quasi-linear spreading in comparison to the final strictly linear constant rate spreading until the final contact angle θ_f is reached. In this stage the kinetics of the substrate dissolution process controls the reaction layer formation.

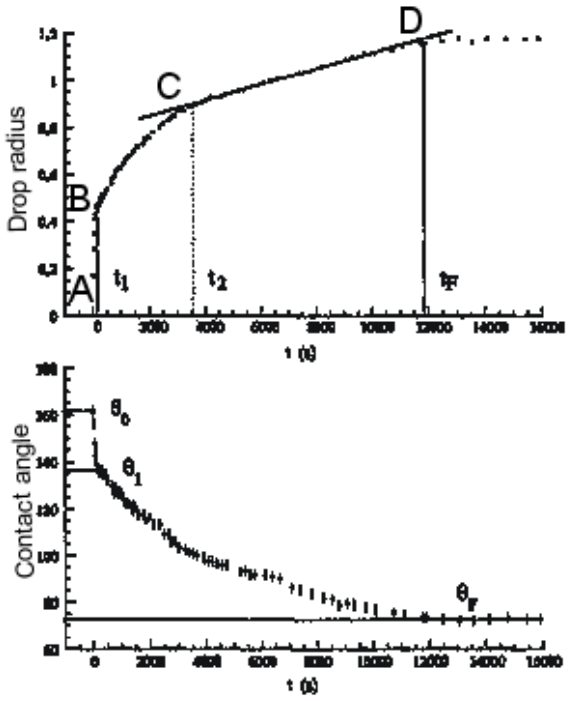

Figure 2.6. Spreading kinetics of liquid aluminium on vitreous carbon substrate/29/

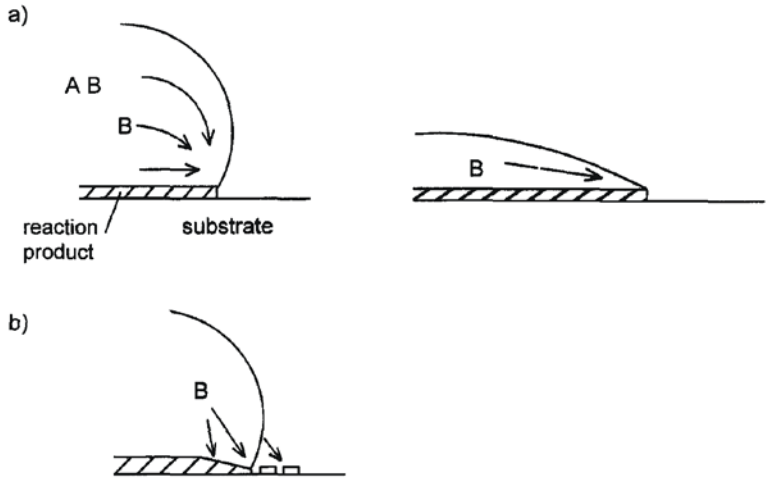

Figure 2.7. Diffusion controlled spreading presented by Mortensen et al /22/. Part a) describes the idea of the model; the triple line velocity decreases with time due to the reduction in diffusion field. Part b) of the figure is more realistic illustration of the reaction in the triple line area /32/.

The existence of the decreasing rate of quasi-linear spreading has been later verified for systems Ag-Cu-Ti on ZrO_2 and ZrO_2-Al_2O_3 ceramics /33/, AlSi alloys on carbon /34/, Cu-Cr on carbon /35/, Si on Si_3N_4 and BN /36/ and for Ni-base alloys with Ti on AlN /37/.

2.4. The influence of alloying elements and oxygen

2.4.1. The influence of alloying elements on wetting and reactivity

The behaviour of a non-wetting melt on a substrate can be changed by adding a specific alloying element. There are both reactive and non-reactive alloying elements with respect to the system. In the non-reactive case no new phases are formed at the interface, but the contact angle can decrease and adhesion can occur. In the reactive case a reaction layer can be found between the liquid and the substrate and the contact angle can decrease even further. These cases are studied here separately.

In *non-reactive case* there are three different ways how an alloying element can influence the wetting and adhesion between the liquid and Al_2O_3. Al_2O_3 has been taken here as an example because it is the most studied ceramic in this field. In an alloy drop consisting of two non-wetting metals there can be only van der Waals interactions at the interface between the liquid and the oxide. These van der Waals interactions are generally solely responsible for the possible adhesion in this case. In this kind of system σ_{LV} is nearly proportional to W_a. Examples of this kind of elements are Ni, Fe and Cu.

In the second case alloying elements interact chemically with the Al_2O_3, but no new oxides are formed. Examples of these elements are Al and Si. In this case wetting and adhesion are improved with respect to matrix metal. The improvement in wetting is due to the increased surface energy σ_{SL} at the melt-ceramic interface. The nature of these reactions is not fully understood, but it has been explained by Al and Si vapours which influence the oxide stability.

In the third kind of non-reactive system the alloying elements adsorb strongly to the liquid-ceramic interface and to the liquid surface. One example of this kind of system is Sn-Al alloy on Al_2O_3 substrate. Here the improvement of wetting is due to two different effects: the decrease of drop surface energy by Sn addition and the decrease of substrate-drop interfacial surface energy by Al addition. Minimum contact angle can be found with proper proportions of these elements. /38/

In the *reactive case* new compounds are formed at the liquid-ceramic interface. In a system with reactive solute B – oxide substrate, the reaction can be new oxide formation by the reduction of less stable substrate. This reaction consists of the dissolution of the substrate oxide and the precipitation of a new oxide to the interface. The interaction between oxygen and solute B is described with Wagner's interaction parameter ε_O^B. It is defined with the following model by Jacob and Alcock /39/:

$$\varepsilon_O^B = -n\left[\left(\frac{\gamma_{O(A)}^{\infty}}{\gamma_{O(B)}^{\infty}}\right)^{1/n}(\gamma_B^{\infty})^{\alpha} - 1\right] \qquad (14)$$

In equation (14) n =4 and α=1/2 as a good estimate for several studied alloys A-B. The γ:s are the activity coefficient of pure element B and the activity coefficients of oxygen in infinite dilution in A and B. If $\varepsilon_O^B < 0$ there are strong chemical interactions between solute B and oxide and the dissolution of oxide will occur, but no new phase is formed unless $\varepsilon_O^B << 0$. An example of the difference in the behaviour is presented in figure 2.8. Here either Cr or Ti is added to non-reactive Ni drop, the interaction parameters being ε_O^{Ti} = -100 and ε_O^{Cr} = -25, respectively.

Reaction layer formation does not guarantee good wetting. The degree of wetting improvement is defined by the nature of the formed new layer. If the replacing oxide (or nitride) is of similar covalent nature than the original substrate, the decrease of contact angle is not significant. On the other hand, if the formed layer has a more metallic nature, the reduction of contact angle is significant. /40/

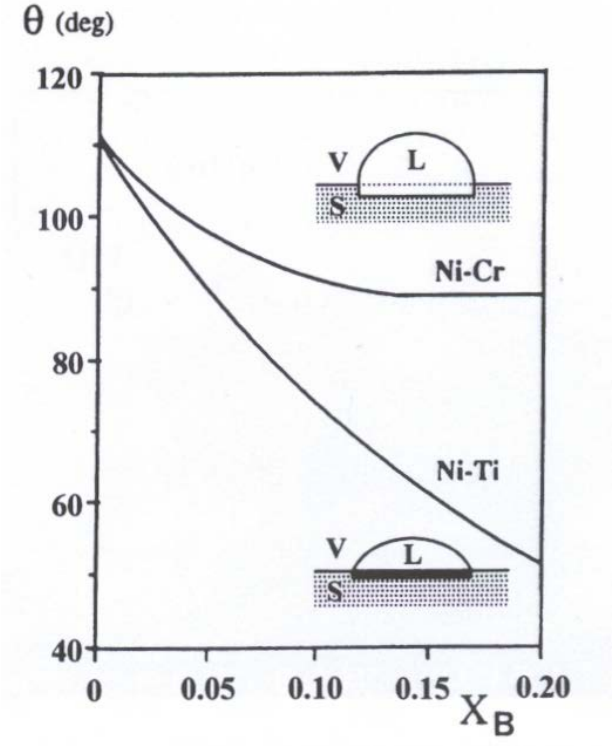

Figure 2.8. Ni-Cr and Ni-Ti contact angles on Al_2O_3 as presented by Eustathopoulos /41/ to show the different influences of between Ti and Cr additions on wetting.

2.4.2. Influence of oxygen on wetting and reactivity

Oxides are thermodynamically very stable compounds in most environments, which result from the reactive nature of oxygen. In our study oxygen has an influence on both wetting and adherence. Many of the oxygen-related phenomena depend on the oxygen partial pressure which defines the equilibrium state in each system. Different ranges of a metal M and Al_2O_3 interaction exist depending on oxygen partial pressure (fig 2.9) /42/.

There are three different equilibrium areas between stable Al_2O_3 and stable M oxide as a function of oxygen partial pressure /42/. Below $P_{O2}^{d(Al2O3)}$ Al_2O_3 is no longer stable. In the reactive area Al_2O_3 will dissolve into the liquid from the substrate increasing Al and O -contents in the melt. In the non-reactive area the oxygen concentration

increases in the liquid, which can cause oxygen adsorption to some interfaces possibly improving the wetting of Al_2O_3 by metal M. The third area is the range of possible mixed oxide Al-M-O formation. Above $P_{O2}^{ox(M)}$ M oxide is the only stable oxide in the system. The influence of dissolved oxygen and oxide film formation are treated separately below.

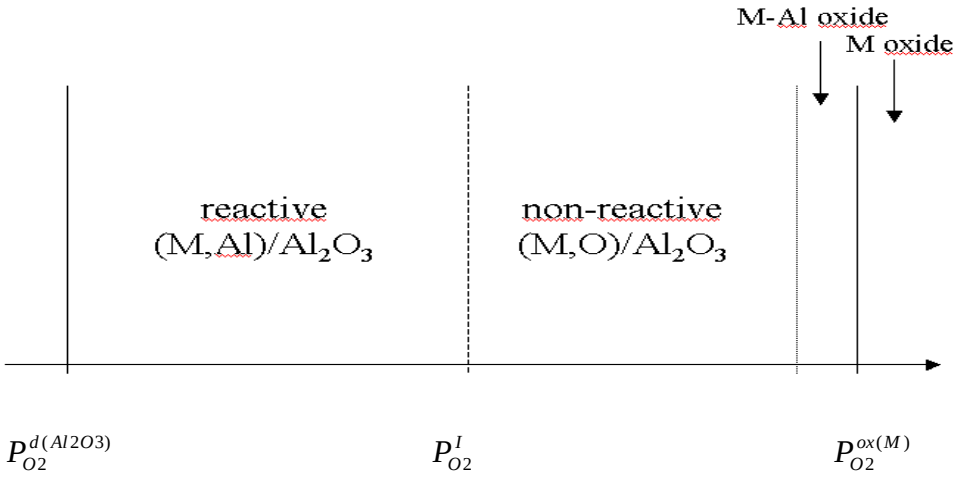

Figure 2.9. The influence of oxygen partial pressure on the reactivity of metal M, Al and O system. In the reactive area Al_2O_3 dissolves in the liquid M, but no new oxides can form. In the non-reactive area the oxygen content of the liquid increases leading to the right-hand side areas where M-Al- and M oxides will form. On the left-hand side of the reactive area the Al_2O_3 is not stable. /42/

Dissolved oxygen has an influence on σ_{LV} and on σ_{SL} and therefore it has an effect also on wetting and adhesion. This has been explained by several phenomena. Gibbs adsorption equation can be used to analyse the effect of relative adsorption of species in the system:

$$\frac{1}{RT} d(\sigma_{LV}) = -\Gamma_O^M d(\ln a_O) = -\frac{1}{2}\Gamma_O^M d(\ln P_{O2}) \qquad (15)$$

where Γ_O^M = the relative adsorption coefficient of oxygen with respect to metal M. A positive value of adsorption coefficient means the enrichment of metal surface by oxygen as compared to liquid and a negative value vice versa. Γ_O^M can be calculated when the value of σ_{LV} is known as a function of varying P_{O2}. Gibbsian adsorption of oxygen to the interface can change the wetting and adhesion even if no stable oxide layer is formed. The surface tension of copper is decreased with dissolved oxygen as presented in Figure 2.10. It is apparent that already small amounts of oxygen drop the surface tension remarkably.

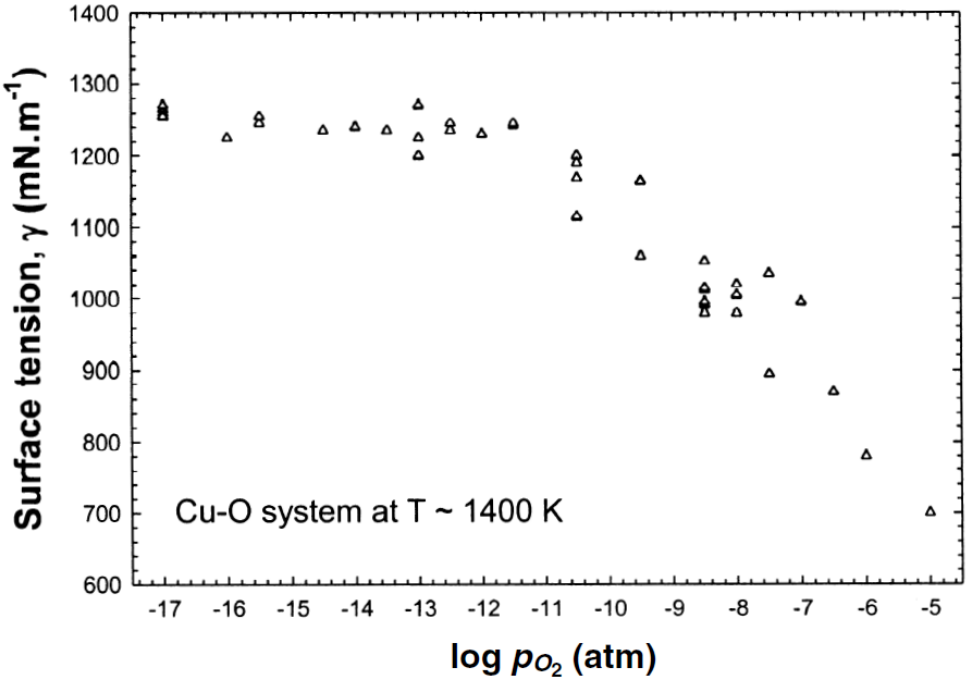

Figure 2.10. The influence of minor additions of oxygen on the surface tension of copper melt at different temperatures /43/.

In some cases there are very rapid changes in the θ - P_{O2} curve. This cannot be explained by Gibbs adsorption, but it has been explained with 2D phase transition. An example of such transition is the complex unstable oxide formation at some P_{O2} value, for example $AgAlO_2$ forming at the Ag – Al_2O_3 interface /44/.

One possible mechanism for solute transport to interfaces has been studied by authors Naidich /45/ and Coudurier et al /46/. In their study dissolved oxygen forms O-metal

clusters with an alloying element. The ionic character of these clusters will cause them to be adsorbed to the interface or optionally to the drop surface. These authors have shown that the oxygen-metal clusters are formed with the most electronegative alloying element atoms in the alloy.

In the work of Coudurier et al /46/ this was proven with the fact that chromium increases the wetting of copper on Al_2O_3 substrate. No formation of new phases at the interface could be found. The developed oxygen-metal cluster model is also compatible with the Gibbs' absorption model as shown in these articles.

Oxide layer formation can occur if the dissolved oxygen content in the melt reaches $P^{ox(M)}_{O2}$. Oxide is formed on the metal surface. Oxide layers will influence the interface formation between the substrate and the melt preventing the wetting. Elimination of the disturbing oxide film can occur either by deoxidation or breaking of the layer. Oxide can also be dissolved into the liquid at a certain combination of temperature and P_{O2}. This happens, for example, with SnO_2 dissolving into molten Sn at low temperatures /47/.

Oxide layers have been produced on purpose in the bonding experiments between Cu and AlN described in /48/ and between Cu and Si_3N_4 in ref. /49/. Both these studies show that thin oxide layers improve the wetting and bonding characteristics as well. The oxygen content of copper is also increased in the experiment to the level where Cu_2O can form. In fact in these experiments the oxide phases are bonded together rather than copper and AlN.

2.5. Wetting and reactivity between aluminium nitride and liquid metals

Aluminium nitride is a covalent compound stable up to high temperatures. Aluminium nitride is an oxidizable material and the bond between oxygen and aluminium is stronger than the bond between aluminium and nitrogen. Bonding energies are –322 kJ/at.g N for AlN and –558 kJ/at.g O for Al_2O_3 /50/, respectively. Therefore the surface of AlN is a complex mixture of nitride, oxide and oxynitride even in high vacuum and at high temperature.

When a liquid drop of metal M which does not form a nitride but dissolves aluminium is placed on the AlN surface the nitride will decompose by the following reaction:

$$\langle AlN \rangle \Leftrightarrow (Al)_M + \frac{1}{2}[N_2] \tag{16}$$

Equilibrium molar fraction value of Al in metal M after the dissociation of AlN was calculated by Eustathopoulos et al /51/. This value can be obtained from the following equation:

$$X_{Al}^{eq} = P_{N2}^{-1/2} \exp\left[\frac{\Delta G^0_{f(AlN)} - \overline{\Delta H}^{\infty}_{Al(M)}}{RT}\right] \tag{17}$$

when $X_{Al}^{eq} << 1$.

In equation (16) P_{N2} is the nitrogen partial pressure for the dissociation of nitride, $\Delta G°_{f(AlN)}$ is the standard Gibbs energy of reaction for AlN formation and $\overline{\Delta H}^{\infty}_{Al(M)}$ is the partial enthalpy of mixing at infinite dilution of Al in solvent M.

Taking $p_{N2} = 10^{-9}$ atm, which is typical for furnaces equipped with oil diffusion pump /52/, the results can be presented in the way shown in Figure 2.11. From this graph it can be seen that the equilibrium amount of aluminium in copper droplet at 1000°C resulting from AlN dissolution is $3*10^{-2}$ in molar fraction. The influence of dissolved aluminium on the surface tension of the droplet metal can become significant. The σ_{LV} values for Cu and CuAl45 at-% are 1,343 mN/m and 1 mN/m respectively, the corresponding contact angles being 131°±2° and 74°±2° /53/

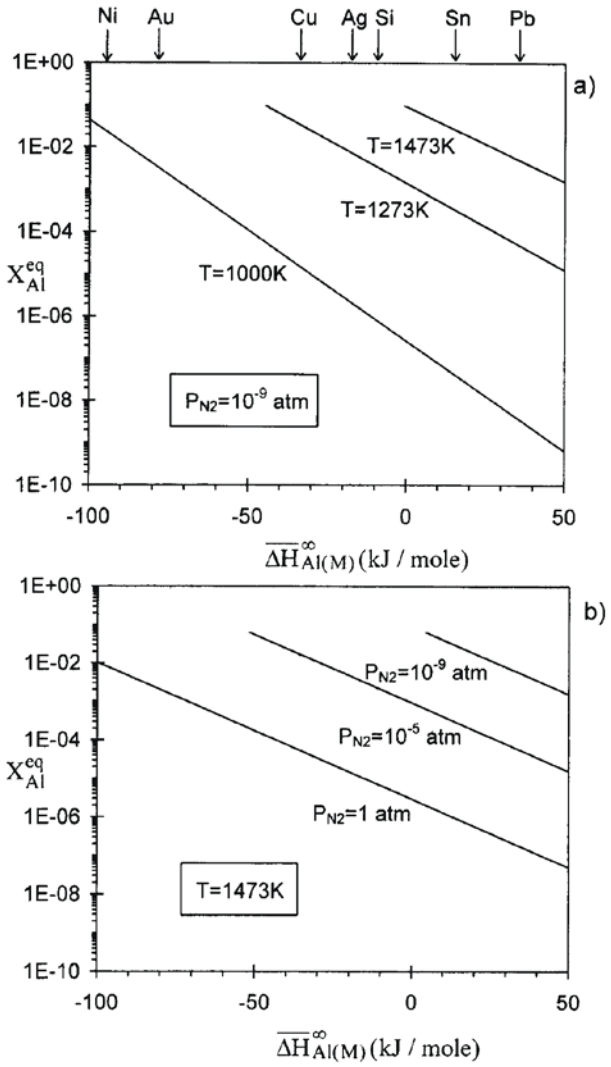

Figure 2.11. Equilibrium molar fraction of aluminium in some metals which do not form stable nitrides at different temperatures (fig 2.11a) or at different nitrogen partial pressures (fig 2.11b). /52/

2.5.1. Wetting and reactivity between AlN and pure metals

AlN wetting by different pure metal melts has been studied quite thoroughly since the 1970's. The measurements have usually been carried out on polycrystalline AlN containing varying amount of secondary phase, usually some per cents of Y_2O_3. The surface roughness and used atmosphere are not always known. A collection of results from high vacuum experiments is presented in Table 2.1. The liquid metal surface

tension values are also given in the same table and finally the work of adhesion has been calculated according to equation (2).

In Table 2.1, it can be seen that only aluminium and silicon wet AlN. From the elements in table 2.1 these two metals have the strongest affinity to nitrogen. Possible reactions which can occur between AlN and liquid metal are the dissolution of AlN into liquid metal and the formation of nitrides or aluminides. For non-wetting metals the strongest interactions occur with nickel, which has been reported to form aluminides with AlN /54/. Iron and cobalt have high W_a with AlN which can be explained by their higher heat of compound formation in /55/

Table 2.1, Wetting of AlN by pure metals in high vacuum

Metal	Surface tension σ_{LV} /55/ (mN/m at their T_M)	Temperature of experiment (°C)	Contact angle (degrees)	Reference	Work of adhesion W_a (mJ/m^2)
Ag	903	1000	134, 135	/54/, /56/	630
Al	914	1000, 1100	53, 53, 60, 113	/54/, /57/, /53/, /58/	550
Au	1140	1100-1250	138-132	/54/	850
Co	1873	1500-1600	138-130	/54/	1390
Cu	1360	1150	120,134,135, 136	/54/, /53/, /60/, /59/	680-980
Fe	1872	1550-1600	135-130	/54/	1320
Ga	718	400-1000	115-105	/54/	300
Ge	621	900-1150	125-118	/54/	360
In	556	200-700	130-120	/54/	360
Ni	1778	1500-1600	114-93	/54/	720
Pb	468	300-800, 750, 420-540	150-140, 131, 154-143	/54/, /58/, /60/	410
Pd	1500	1550	118	/54/	710
Si	865	1500-1600	53-48	/54/	520
Sn	544	250-1150, 900	128-122,142	/54/, /56/	340

Additional joining experiments with the reaction layer identification have been carried out for bonding Ti to AlN /61/, and Mo, Mn, FeSi and Ti to AlN /62/

2.5.2. Wetting and reactivity of AlN by reactive alloys

To enhance wetting of AlN it is possible to add reactive elements to the base metal. The Gibbs' energies of nitride reaction for several elements are given in Table 2.2. From these values it can be anticipated that Zr, Ti and Si will react with AlN to form ZrN, TiN and Si_3N_4 since these nitrides are more stable than AlN according to their Gibbs energy values. Taranets and Naidich /54/ added Cr, V, Nb, Ta and Ti to some non-reactive matrix metals (Sn, Ge or Cu) and found that wetting of AlN increased with these additions. Results for copper matrix are presented in Figure 2-12.

Table 2.2, Gibbs energies of reaction for different nitrides at 1100°C /63/

Nitride	ΔG_f (kJ/mol) /63/
AlN	-167.900
BN	-121.737
Cr_2N, CrN	-26.381, -13.284
NbN	-119.395
Si_3N_4	-290.164
TaN	-143.552
TiN	-208.321
VN	-101.282
ZrN	-237.835

From Figure 2-12 it is obvious that only titanium addition can cause significant wetting of AlN by Cu matrix. Other studies were carried out by Nicholas et al /52/ who added Ti in copper or AgCu28 (w-%) metal alloy and Tomsia and Loehman /57/ who added Ti and Zr in AgCu28 alloy. Results of these studies are summarized in Table 2.3. Studies show that wetting is better in the case of the AgCu28 alloy than in the case of pure copper. It is also evident that titanium increases wetting more efficiently

than zirconium in AgCu28 eutectic alloy. The wetting characteristics of AlN by molten CuZr alloys were not available in literature.

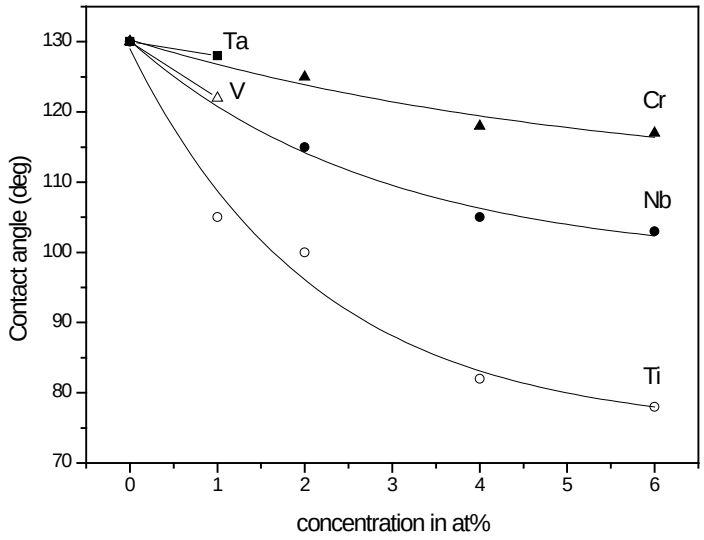

Figure 2.12. Influence of reactive element additions in copper on the wetting of AlN substrate by copper at 1150°C /54/.

Table 2.3. Wetting of AlN by Ti- and Zr-containing Cu-based alloys in high vacuum /57,59/

Alloy (w-%)	Temperature (°C)	Contact angle (deg)	Reference
CuTi5	1150	132	/59/
CuTi7,5	1150	110	/59/
CuTi10	1150	5	/59/
AgCu28Ti2	950	10	/59/
AgCu28Ti1	1000	14	/57/
AgCu28Ti5	1000	3	/57/
AgCu28Zr1	1000, 1100	130, 65	/57/
AgCu28Zr5	1000, 1100	63, 45	/57/

Two different studies have been carried out on the characterization of the reaction layers between AlN and zirconium containing alloys. Nakao et al /64/ found that the only reaction product was ZrN but He et al /65/ found the formation of aluminides

($ZrAl_3$, and $ZrAl_2$) instead of ZrN. Main difference in the tests was the temperature. He made his study by depositing active metal layers and annealing interfaces in steps from 200°C to 800°C for several hours. Nakao's study on the other hand is more similar to conditions in the sessile drop test, i.e., test with molten metals for some seconds at 900°C to 1000°C. Koltsov et al studied the wetting and reactivity of AgZr alloys on AlN. /66/ The obtained contact angle θ_f with AgZr3 alloy was 20°-25° and the analyzed reaction product was ZrN_{1-y} with some non-stoichiometry in composition.

2.5. Wetting and reactivity between silicon nitride and liquid metals

The literature study on Si_3N_4 wetting and reactivity studies reveals that experiments have been carried out with both polycrystalline silicon nitride and with CVD coated thin layers. Bulk silicon nitride contains always a binder phase, which is usually composed of oxides. The amount of oxide phase varies between 1 – 15 %.

In a wetting experiment a liquid metal can either be non-reactive or in reactive case it can dissolve silicon according to the following equation

$$\langle Si_3N_4 \rangle \Leftrightarrow 3(Si)_M + 2[N_2] \qquad (18)$$

In equilibrium, at 1100°C, the dissolved amount of silicon in copper is 5 w-% and the dissolved amount of zirconium in copper is 0,2 w-%. The other liberated substance is nitrogen, which also can be dissolved in zirconium by 5w-% but in copper the solubility is negligible. Possible reactions are nitride or silicide formation. Silicide and nitride forming equations are:

$$\langle Si_3N_4 \rangle + (Me)_{Me} \Rightarrow Me - silicide + 2[N_2] \qquad (19)$$

$$\langle Si_3N_4 \rangle + (Me)_{Me} \Rightarrow Me - nitride + 3(Si)_{Me} \qquad (20)$$

2.5.1. Wetting and reactivity between Si_3N_4 and pure metals

Table 2.4 shows the wetting results for pure metals and the related work of adhesion as calculated with formula (3). All the given results are from experiments carried out in high vacuum. Study with silicon was made in different atmospheres and the result in Table 2.4 corresponds with the results obtained with other metals at similar oxygen partial pressure. Similarly to the results for AlN, wetting was achieved only with aluminium and silicon.

Table 2.4. Contact angles of various pure metals on Si_3N_4, as measured in high vacuum and at the given temperature.

Metal	Surface tension σ_{LV} /55/ (mN/m at their T_M)	Temperature of experiment (°C)	Contact angle (degrees)	Reference	Work of adhesion W_a (mJ/m^2)
Ag	903	1100	155,132	/67/, /68/	300
Al	914	1100	58,48,68,	/67/, /68/, /56/	1530
Au	1140	1100	157	/67/	90
Cu	1360	1100, 1150(36)	131,128,135, 111-126,142,	/67/, /68/, /59/, /69/, /70/	680
Si	865	1450	48 ($p_{O2}=10^{-19}$), 49	/71/, /52/	1440
Sn	544	1100	144,153,	/67/, /68/, /69/	100

2.5.2. Wetting and reactivity of Si_3N_4 by reactive alloys

In general same kind of alloys have been used to enhance wetting on silicon nitride as are used with AlN. In the literature the matrix metal is either copper or silver-copper

alloy, and the additives are Ti, Zr, Cr, Mn or Si. The results from these studies are given in Table 2.5.

Table 2.5. Wetting of Si_3N_4 by Cu and AgCu alloys with reactive additions

Alloy (w-%)	Temperature (°C)	Contact angle (deg)	Reference
CuTi2	1150	130	/59/
CuTi3	1100	82	/67/
CuTi5	1150	23	/59/
CuTi10	1150	8	/59/
CuTi20	1100	8 (110min)	/70/
CuTi30	1100	8 (5min)	/70/
CuTi38	1030	2	/72/
CuMn35	1000	95	/67/
CuZr30	1100	60 (60min)	/70/
CuZr40	1100	5 (60min)	/70/
CuCr1, CuCr3	1150	90	/73/
CuSi3.5Cr1.8	1150	100	/73/
AgCu28Ti2	950	8	/59/
AgCu28Ti2	1000	17	/67/
AgCu28Si5	1100	106	/67/
AgCu27Ti1,5	1150	$\rightarrow 0$	/69/
AgCu34Ti4,5	1150	$\rightarrow 0$	/69/

From these results it can be seen that to achieve perfect wetting it is necessary to add at least 10 w-% of titanium to copper, but only 1,5 w-% of titanium to silver-copper alloy. Chromium, silicon or manganese additions on the other hand do not cause wetting, but only some decrease of contact angle in comparison with pure copper. Zirconium additions of 30 w-% decreased the contact angle down to 60° and 40 w-% of Zr was needed to achieve complete wetting of silicon nitride.

In the literature reactivity between Si_3N_4 and copper alloys containing reactive elements has been reported and both nitrides and silicides have been found. Nicholas et al /52/ reported the formation of both TiN and titanium silicides with CuTi alloys and

Tomsia et al also reported both titanium silicides and TiN with AgCuTi alloy. Naka and Okamoto /70/ report the formation of TiN, ε-$Cu_{15}Si_4$ and η'-(Cu, Si) at the interface in contact with CuTi alloys and ZrN, Zr_5Si_3, Zr_3Si_2 and η'-(Cu, Si) in contact with CuZr alloys.

For chromium containing Cu-alloys Xiao and Derby /73/ found the formation of Cr_2N at the interface with CuCr systems, but with silicon additions to this system, the formation of Cr_2N was suppressed. Nakao et al /64/ studied the interfaces of Si_3N_4 - CuCr5 and Si_3N_4 – CuZr10 systems. With chromium additions the reaction product layer was found to contain Cr_2N, CrN and $CrSi_2$ and with zirconium additions ZrN and Zr_5Si_3.

Ljungberg and Warren /50/ found a two-layer structure at the interface in the system AgCuTi-Si_3N_4. It contained both TiN and Si_3Ti_5. Brazing studies for the same system with Mo and SiC additives to the Ag-Cu-Ti brazing alloy have been carried out by He et al (Mo) /74/ and Zhang et al (SiC) /75/. Both studies have been able to improve the bonding properties of Si_3N_4/Si_3N_4 joints with their additives. Olesinska et al /62/ studied the reactivity when brazing Si_3N_4/Si_3N_4 joints by Cu_2O-Mn-Ti system and obtained good joint properties.

Chapter 3. Goal of the study

The goal of the study is to understand the wetting behaviour of the selected ceramic materials, AlN and Si_3N_4, with the metal alloys CuZr, CuCr and AgZr. Nitride ceramics are not that common in use, but their excellent properties in high temperature applications make them interesting materials for several applications. In the molten metal handling applications good thermal conductivity and good resistance for thermal shock are required. Also basic requirement is a controllable interaction between these reactive metal alloys with the ceramic substrate. Same phenomena determine the quality of permanent bonding between these materials.

In order to understand the interaction, experiments will be carried out to determine wetting and reactivity characteristics for each metal-alloy/ceramic combination. Ex-

periments will be carried out in the best possible furnace installation available. The influence of the furnace atmosphere will be considered and the comparison with more industrial atmospheres will be carried out. Wetting sets up the limits for the usability of these ceramics in these applications. The reactivity of these metal-alloy/ceramic couples is thermodynamically calculated and it is suggested that the best possible material interaction is gained when wetting takes place. With wetting, the reaction layer can form rapidly and form a protective layer against further reaction layer growth. The reaction layer properties will define how well the formed bond can last a mechanical loading. If the reaction layer and the bonding are suitable there are no strong restrictions in the usability of these materials.

Chapter 4. Experimental procedure and materials

4.1. Materials

4.1.1. Aluminium nitride

Aluminium nitride (AlN) was used as the substrate material in the wetting experiments. Polycrystalline ceramic was used as single crystals are not easily available. AlN was supplied by the French company Céramiques & Composites. AlN is produced by hot isostatic pressing (HIP) of powder, where 3 to 5 w-% of yttrium oxide (Y_2O_3) is added as a sintering aid. The final achieved density is 98 % of the theoretical density of AlN.

AlN does not exist as such in nature, but it can be synthesised artificially either as powder, monocrystals or thin films. It decomposes at 2800 °C. Oxygen dissolves to AlN (with maximum solubility of 0,15 at%) and the surface of AlN is easily oxidised in air. Pure AlN cannot be manufactured as a compact macroscopic material and therefore sintering aids such as Y_2O_3 and CaC_2 are added to AlN matrix.

Figure 4.1. shows a scanning electron microscope image of the substrate material. Dark matrix phase consists of the AlN grains and the secondary white phase is the

binder phase. This phase is a mixture of Y and Al oxides; it is commonly called YAG and its composition is close to $Y_3Al_5O_{12}$ /76/.

Sample preparation and surface roughness measurements

The as-received test samples were small 13 mm diameter cylinders with the height of about 1,4 mm. In order to achieve acceptable accuracy in these kinds of wetting measurements the often-used minimum requirement for substrate surface smoothness is 0,1μm and the local sample tilting less than 2°/77/.

First the samples were ground with SiC paper down to mesh size 1000 to get a planar surface. Then different grades of diamond pastes were used in automatic polishing procedure with the following particle sizes and polishing procedure durations:

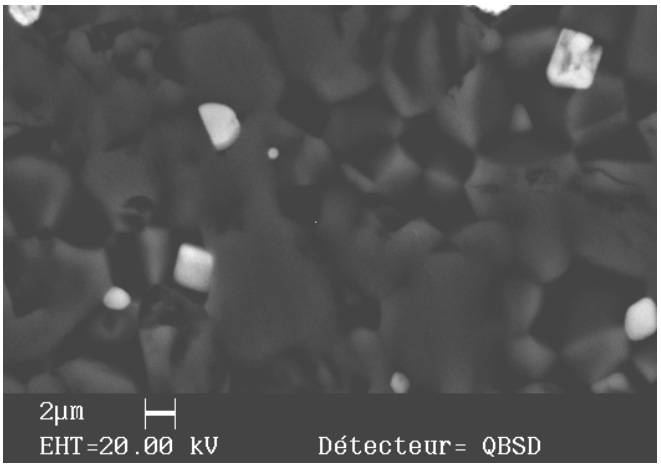

Figure 4.1. SEM image of polished and chemically etched AlN test sample surface.

30 μm paste for 30 minutes
15 μm paste for 30 minutes
6 μm paste for 60 minutes
3 μm paste for 4 hours
1 μm paste for 4 hours

The polishing response of the matrix and harder binder phase of the ceramic material were different. The density and porosity of original ceramic also influenced the surface quality. Therefore it was not possible to obtain a pore-free surface. Figure 4.2 shows an optical microscope image of the polished AlN surface. After polishing the surface roughness was measured with optical and mechanical profilometers. The measured value was R_a, which is the average surface roughness of the material, i.e., the average deviation from the median plane of the profile.

Optical profilometer scans a surface area of about 194 μm x 194 μm at a time, while with the mechanical profilometer it is possible to measure larger area of surface during one measurement and therefore to get more representative results. Figure 4.3 shows an optically acquired profile. Table 4.1 contains the results of both kinds of the profilometer measurements. According to the results the used sample preparation procedure fulfills the prescribed requirements for surface quality.

Table 4.1. Surface roughness of AlN after the used sample preparation procedure.

	R_a (nm)
Optical profilometer	40 – 60
Mechanical profilometer	70 – 90

Due to the rapid oxidation of AlN surface, the substrate was etched just before experiment with a procedure specially designed for this material by Baffie /78/. He exposed AlN to different acids and studied the results with the surface analysis methods (SIMS (Secondary ion mass spectroscopy) and XPS (x-ray photoelectron spectroscopy)). He found that before etching there was a reaction product layer on the AlN substrate; the layer contained phases AlOOH, $Al(OH)_3$ and γ-Al_2O_3.

The used etching procedure was a 40% HF (hydrofluoric acid) treatment at room temperature for 10 minutes, followed by washing with distilled water and drying with purified air. This treatment was found to be the most effective for removing oxidised and hydrated layers from AlN surface.

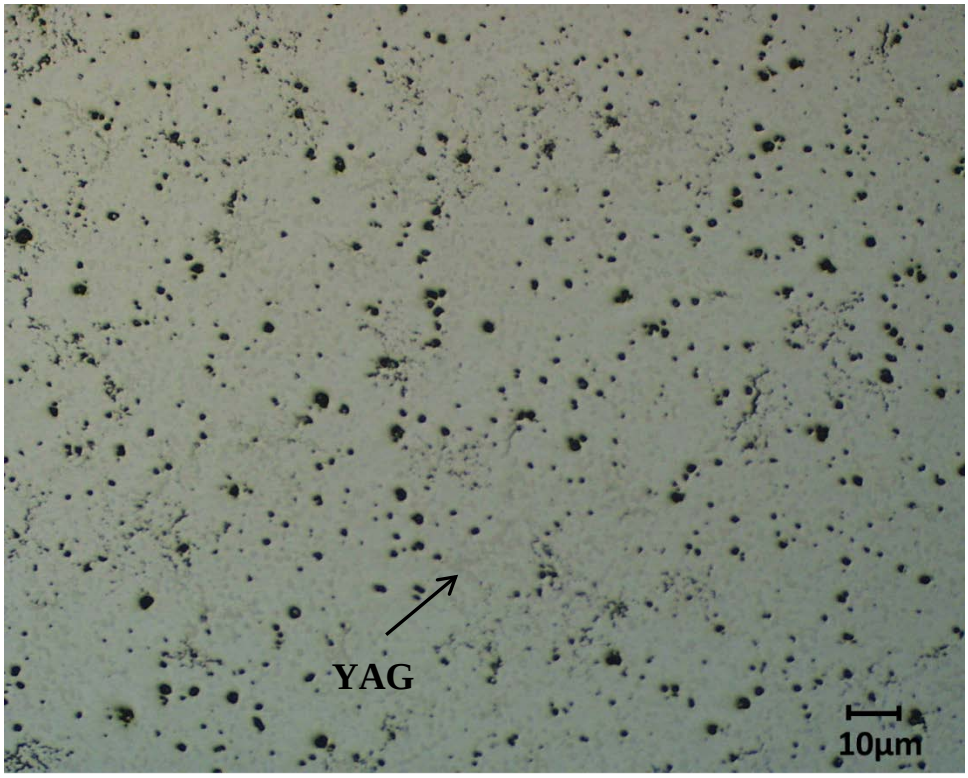

Figure 4.2. Optical image of the polished AlN surface. It is possible to see the slightly darker YAG binder phase and porosity.

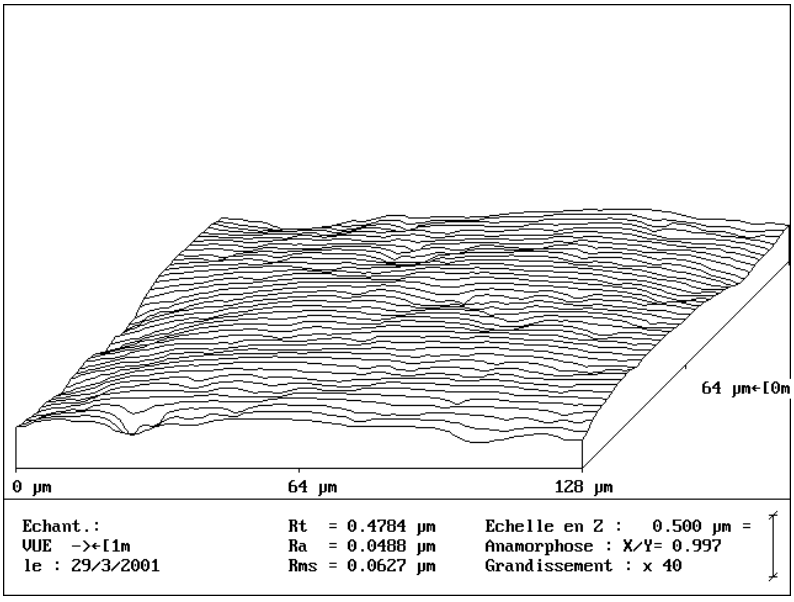

Figure 4.3. Surface roughness of polished AlN as measured with an optical profilometer.

4.1.3. Silicon nitride

Silicon nitride Si_3N_4 was supplied by Ceramic Technologies. It is manufactured by sintering with Al_2O_3 and Y_2O_3 additives used as sintering aids. The amount of the oxide binder phase is 2 – 3 w-% .

Figure 4.4. shows a SEM image of Si_3N_4. Here the dark phase is the matrix ceramic and the lighter phase is the Al_2O_3/Y_2O_3 binder mixture.

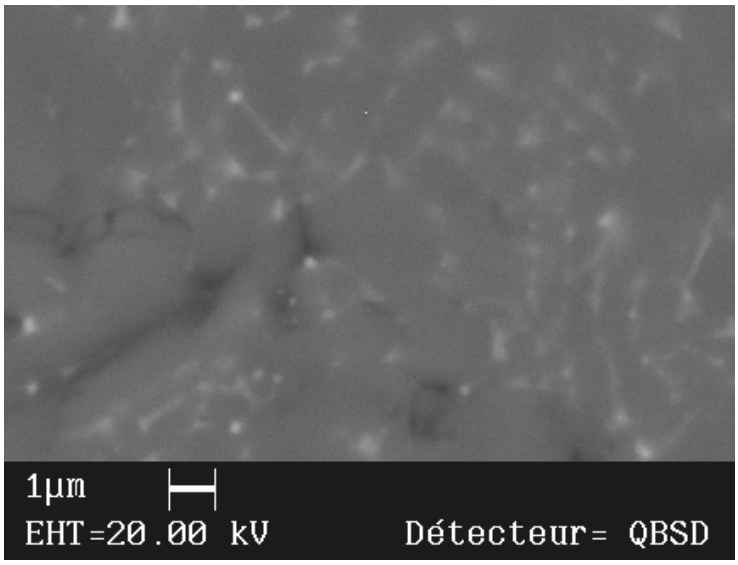

Figure 4.4. SEM image of the studied Si_3N_4 ceramic

The surface of silicon nitride is readily oxidized at room temperature to form stable SiO_2 layer. Another layer of $Si_xN_yO_z$ has been reported to form between the original nitride surface and formed oxide layer by Maguire and Augustus /79/. Layer has been later identified as stable Si_2N_2O and its thermodynamics has been studied, for example, by Rocabois et al /80/. Direct reduction of solid SiO_2 layer would need the oxygen partial pressure smaller than 10^{-26} Pa according to Ellingham diagram in, for example, /81/.

In order to have a pure Si_3N_4 layer in the wetting test at 1100 °C the atmosphere should have a definite pO_2/pN_2 ratio, which can be derived from figure 4.5. Since the

measured oxygen partial pressure for our installation was 10^{-12} Pa /82/, the partial pressure of nitrogen should be more than 10^{-17} Pa according to Du et al /83/. The thermodynamic stability diagram for SiO_2, Si_2N_2O and Si_3N_4 is represented in Figure 4.5.

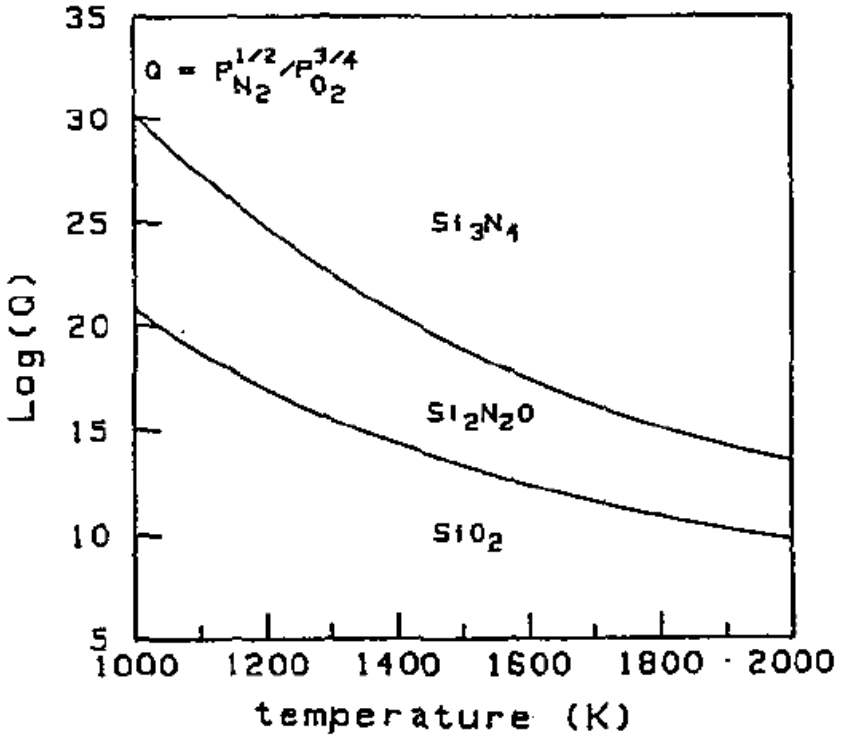

Figure 4.5. The thermodynamic stability areas for SiO_2, Si_2N_2O and Si_3N_4 as a function of log (O) and temperature /83/.

The oxidation of Si_3N_4 surfaces can occur either by passive or active oxidation mechanism /84/. The passive oxidation will form stable SiO_2 layer to the surface and the formation of volatile SiO gaseous species takes place in the active oxidation of Si_3N_4 surfaces at low oxygen partial pressures ($<10^{-1}$Pa according to figure 4.6). The oxygen partial pressure-dependence of oxidation mechanism is represented in Figure 4.6 as a function of temperature.

In an experiment made with tin the removal of Si_2N_2O was noted to occur in the range of 900°C - 1100°C /80/. This was observed from the fact that at 900 °C the experiments on both Si_2N_2O and Si_3N_4 gave similar contact angle values, but at higher temperatures the difference became significant.

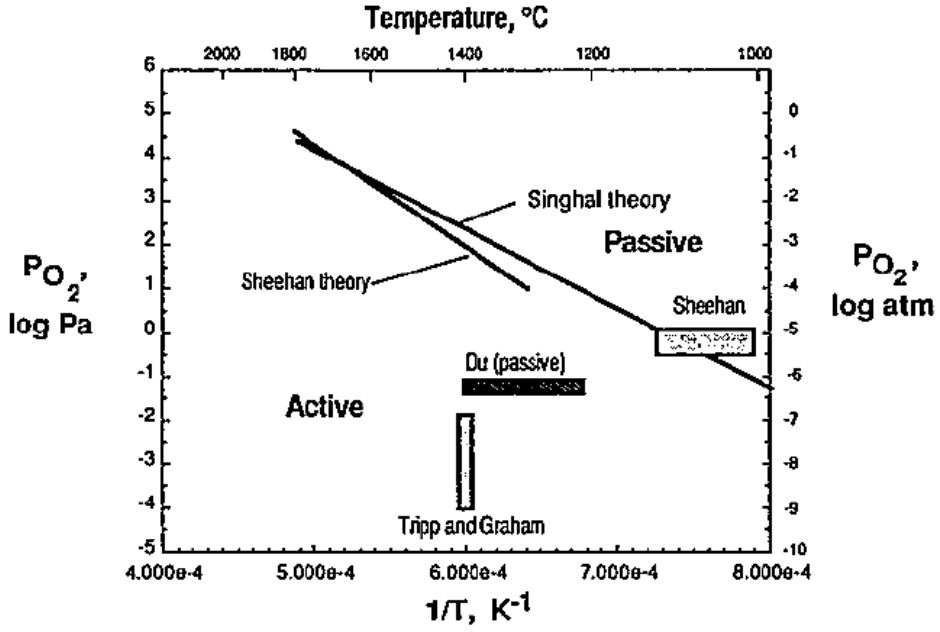

Figure 4.6. The transition from active-to-passive oxidation mechanism as a function of temperature according to different theories /84/.

From all the facts presented above it can be concluded that the surface of Si_3N_4 can in our working environment be free from both SiO_2 and Si_2N_2O. Traces from these compounds can be anyway found due to un-equilibrated reactions.

Sample preparation and surface roughness

Si_3N_4 was received as 3 mm thick plates from which the 10 mm x 10 mm samples were cut with diamond saw. Si_3N_4 is harder material than AlN and the binder phase is evenly distributed between the Si_3N_4 grains. Polishing was carried out with series of diamond pastes with following particle sizes and process durations:

45 μm for 5 min
30 μm for 5 min
15 μm for 10 min
6 μm for 15 min
3 μm for 15 min

The profile of substrate surface as measured with an optical profilometer is presented in Figure 4.7. The surface was much more homogeneous than the surface of AlN. Consequently there was no need to measure the surface roughness with a mechanical profilometer, but for several optical profile measurements an average value was calculated. The R_a value of Si_3N_4 was 10 – 20 nm.

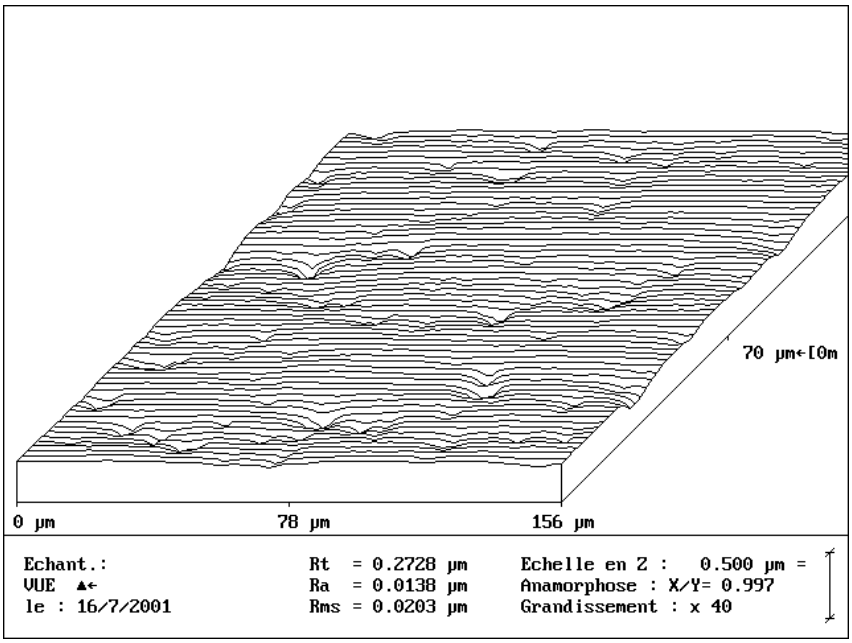

Figure 4.7. Measurement of surface roughness of polished Si_3N_4 with optical profilometer.

4.1.2. Metal alloys and their sample preparation

The used alloys were either prefabricated or they were formed in-situ from pure substances. In the in-situ fabrication method the alloying metal piece of proper size is put on the top of the base metal in the sessile drop experiment so that during melting the alloy is formed. Table 4.2 gives the list of used metals and their suppliers.

Table 4.2. Metals used in experiments

Metal	Purity	Supplier
Cu	99,99	Outokumpu
Ag	99,99	
CuZr-alloys	99,5	Outokumpu
AgZr-alloys	99,5	
Zr	99,5	Cezus
Cr	99,8	Delachaux

The sample preparation was carried out just before starting the experiment. The outer layer, sometimes oxidised was first removed mechanically from all samples. After weighing the samples were washed with ultrasound in acetone.

4.2. Experimental procedure

The basic principle of the contact angle measurements by sessile drop method is presented in Figure 4.4. The measured parameters for evaluating the wetting are the left and right-hand contact angles (θ_l and θ_r) at triple line, the radius (r) of the drop at the triple line and the height (h) of the drop. The experiment is recorded until the equilibrium is reached, and afterwards these parameters are measured from the spreading stages of the drop on the substrate. The final contact angle is calculated as the mean value of the left and right-hand angles.

The contact angle can also be calculated from the measured radius and drop height data by using the equation 21. The equation is valid when the drop is spherical and not deformed by gravity; this is the case if the drop mass is smaller than approximately 100 mg:

$$\theta = 2\arctan\frac{h}{r} \qquad (21)$$

By comparing the two measured values, it can be estimated whether the drop is symmetrical or not. The difference in these values results from the irregularities in the shape of the drop and in the surface topography of the substrate. To ensure that the measured contact angle is of advancing type it should be confirmed that the radius of the drop increases or stays the same and height decreases or stays the same as a function of time during the experiment. In the case the drop is pinned these dimensions will stay the same.

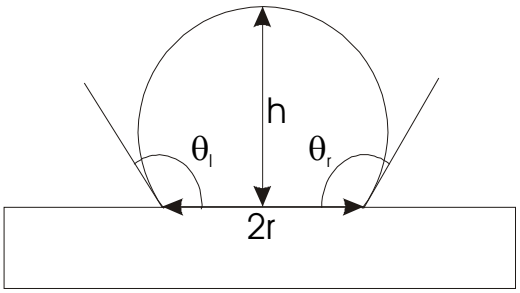

Figure 4.4. The measured geometrical entities during the sessile drop experiment

During the experiment the metal evaporates and the influence of decreasing volume on the contact angle must be taken into account. The volume of a drop can be calculated with the following formula:

$$V = \pi \frac{h^3}{6} + \pi \frac{hr^2}{2} \qquad (22)$$

With volatile metals the experiments should be carried out in a shielding inert gas environment to minimise the evaporation. The amount of volume loss should remain smaller than 10 % for the obtained contact angles to stay real. The variation of the volume can also be due to the asymmetry of the drop, which is often the case in the beginning of an experiment.

4.3. Installation

4.3.1. Furnaces

The experiments were carried out by the sessile drop method in high vacuum. Three different furnaces were used: one with alumina tube and two metallic furnaces. The principles of all of these installations are shown in Figures 4.5, 4.6 and 4.7.

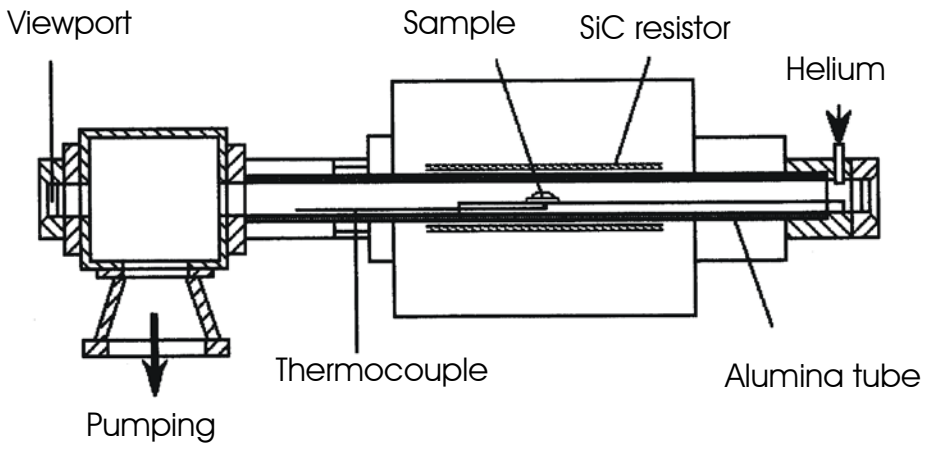

Figure 4.5. The furnace with an alumina tube

The furnace with an alumina tube is presented in Figure 4.5. It consists of an Al_2O_3 tube which is externally heated with SiC resistor and has a block at the end of the tube, which allows the installation of a vacuum pump system. Tube is closed at both ends with view ports, which makes it possible to see through the tube. There is also an inlet for the shielding gas and platinum/rhodium thermocouple which is placed below the sample holder. The accuracy of the temperature measurement is ± 10°C. Maximum temperature with this installation is 1500 °C.

Pumping facility contains primary and secondary pumps. Both of these pumps have also a liquid nitrogen trap. The highest vacuum obtained with this system is of the order of $1 \cdot 10^{-6}$ mbar.

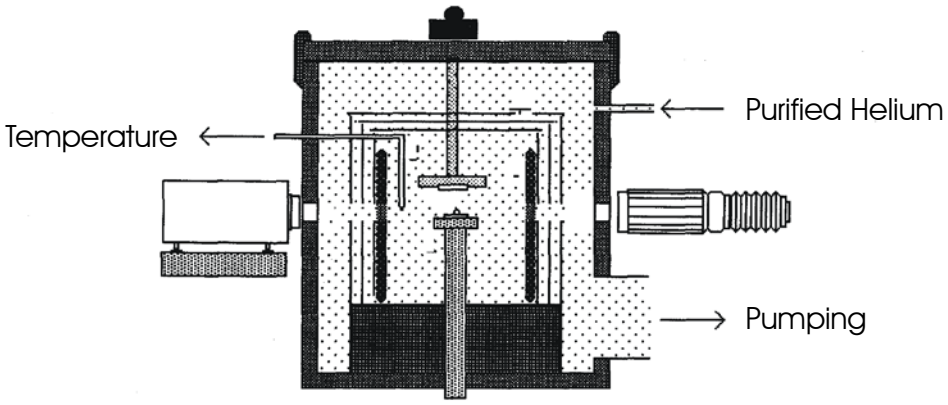

Figure 4.6. The vertical metal furnace used in this study.

Both metal furnaces are placed inside a water-cooled double-walled vacuum chamber made from stainless steel. Similar pumping system as in the furnace with alumina tube is also connected to these furnaces, and it is also possible to work under inert gas atmosphere. There are two aligned holes in the chamber to enable the viewing of the sample.

The vertical metal furnace (Figure 4.6.) is heated with a molybdenum resistor, which is surrounded by a five-layer thermal insulation. Three inner layers are made from molybdenum and two outer layers are made from stainless steel. The sample is placed in the furnace centre onto a sample holder made from Al_2O_3. The maximum working temperature is ~ 1500 °C and the highest vacuum obtainable at high temperatures is $3 \cdot 10^{-6}$ mbar.

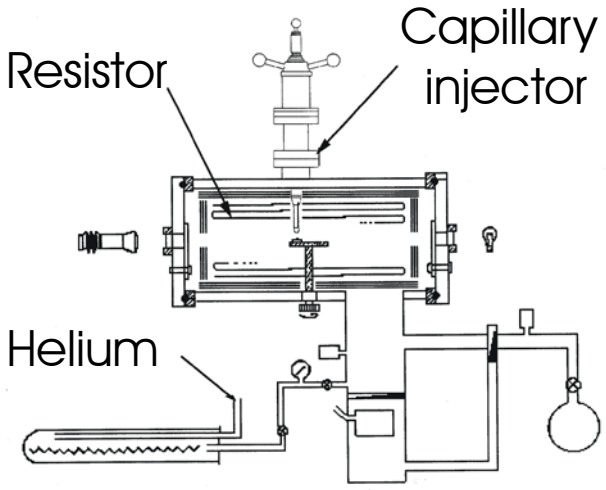

Figure 4.7. The horizontal metal furnace used in the study.

The horizontal metal furnace (Figure 4.7) is similar to the vertical furnace besides some small details. The sample holder is rotating and it is possible to inject molten metal onto the substrate with a capillary syringe. In this installation all the joints are sealed with copper gaskets; consequently the vacuum here is one order of magnitude better than in the previous furnaces. The maximum working temperature is 1500 °C and the vacuum at 1150 °C is of the order of $3 \cdot 10^{-7}$ mbar.

4.3.2. Liquid drop profile acquisition

The contact angle values and the dimensions of the generated drop are recorded continuously with a CCD camera and a video recorder. Behind the drop there is a light source. CCD camera and the light source are aligned with the holes and the sample in the chamber. The camera takes 24 frames per second, so the time resolution is about 40 ms.

After experiment the contact angle, the height and the radius of the drop at the triple line are measured either with a computer using some drawing software or optionally with a special program designed to calculate the exact values by using either spherical or elliptical approximation of the drop shape obtained from the image of the drop. The

accuracy of this kind of measurement is 1% for the linear dimensions (r and h) and ± 2° for the contact angles /85/.

4.4. Carrying out the experiment

The prepared substrate - metal pair is put onto the sample holder as soon as possible after the weighing and final cleaning. The horizontality of the sample holder is adjusted and controlled with a level and the chamber is closed and evacuated. To enhance the desorption of gas molecules, the atmosphere is purged with purified helium gas three times (two times at ~ $2 \cdot 10^{-2}$ mbar, and once more at ~ $5 \cdot 10^{-6}$ mbar) during pumping. When the vacuum is good enough (between $2 \cdot 10^{-6}$ and $2 \cdot 10^{-7}$ mbar, depending on installation) heating is started.

The thermocouple is located as close to the sample as possible so that the temperature can be measured as accurately as possible. The first experiment is carried out with some pure metal (here copper) to verify the real temperature of the sample. Heating is carried out as fast as possible by retaining the vacuum, which should stay between $3 \cdot 10^{-6}$ and $4 \cdot 10^{-7}$ mbar, depending on installation.

4.5. Characterisation

After the experiment the droplet solidifies during cooling with the furnace. It is photographed to verify the symmetry and weighed to calculate the amount of evaporation. If there is a reaction layer at the interface its thermal expansion coefficient usually differs from that of the substrate and during cooling the droplet-substrate pair will crack to form a specially shaped fracture. The cross section of the crack profile will resemble one of the cases in Figure 4.8.

The fracture can be either cohesive, adhesive or a mixture of these. By characterising this fracture type it is possible to compare the strength of interfacial bonding against the internal integrity of the substrate ceramic. Finally the samples are cut carefully into two halves and polished for the analysis of the interfaces with SEM.

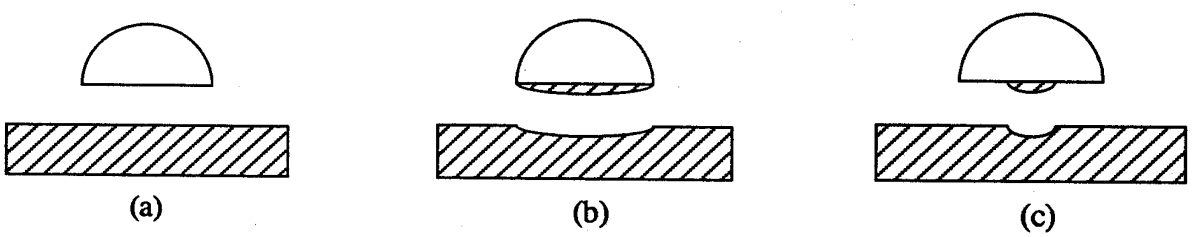

Figure 4.8. Different cases of droplet fracture: a) adhesive, b) cohesive and c) mixture of the two.

Chapter 5. Thermodynamical calculations

With thermodynamics it is possible to predict which reactions will be the most probable ones at the formed interfaces of wetting experiments. Data in phase diagrams and literature are used to compare the stabilities of different possible reaction products formed at the interface. Calculations for probable reactions are carried out to determine the driving force of each reaction. With the obtained value it is also possible to calculate the theoretical reaction layer thickness formed at the interface. The way these calculations are made is presented in the Appendix. This calculation is in no way comprehensive, but just a guiding one for comparison with the experimental findings and for further discussion on the controlling mechanisms in the reactive wetting.

Calculations are made for one reaction considered as the most probable one for each experiment. Probable reactions are predicted from the phase diagrams. All these calculations can be found in Appendix. Table 5.1 presents the evaluated reactions and their reaction energies at the temperature of each experiment. The theoretical reaction layer thicknesses are also presented in Table 5.1.

Table 5.1 Calculation results for reaction energies and reaction layer thicknesses

Reaction	ΔG_M [kJ/mol]	T[°C]	Thickness e [μm]
$(Zr)_{Cu} + AlN \leftrightarrow ZrN + (Al)_{Cu}$	-99567	1150	25
$2(Cr)_{Cu} + AlN \leftrightarrow Cr_2N + (Al)_{Cu}$	-53568	1100	3,7
$(Zr)_{Ag} + AlN \leftrightarrow ZrN + (Al)_{Ag}$	-94680	980	32
$4(Zr)_{Cu} + Si_3N_4 \leftrightarrow 4ZrN + 3(Si)_{Cu}$	63240	1150	0,3
$8(Cr)_{Cu} + Si_3N_4 \leftrightarrow 4Cr_2N + 3(Si)_{Cu}$	242388	1100	$1*10^{-7}$
$4(Zr)_{Ag} + Si_3N_4 \leftrightarrow 4ZrN + 3(Si)_{Ag}$	79965	980	$1,5*10^{-2}$

Chapter 6. Results and discussion

6.1. Experiments on Aluminium Nitride

6.1.1. Wetting and reactivity between AlN and copper

Experiments with unalloyed oxygen free copper were carried out using two different furnaces, the alumina tube furnace and the vertical metal furnace. This was carried out for revealing the reproducibility of the results with these two different systems. The temperature shown by thermocouples was calibrated by observing the melting temperature of pure copper, which is known to be 1084°C. In both experiments about 50 mg mass of copper was placed in the centre of a polished and etched AlN substrate.

With pure copper there is no time-dependent variation in the contact angle. The final contact angle values measured in both experiments are presented in Table 6.1. The results show that the results are reproducible for this system in the used two furnaces. Results are also in good agreement with the values obtained from literature, which are

presented in Table 2.1. This confirms the correctness of our results, as far as it depends on the quality of used equipment and the experimental arrangements.

Table 6.1 Results of the contact angle measurements on AlN / Cu system in different furnaces. The actual temperature and the pressure during the experiment are shown in the table.

Furnace	Temperature (°C)	Pressure (mbar)	θ_F (°)
Alumina tube	1100	$8 \cdot 10^{-7}$	129 ± 2
Metal	1100	$1 \cdot 10^{-6}$	127 ± 2

Slight adherence of the solidified droplet to the AlN substrate made us to suspect some kind of interaction between AlN and pure copper, even though several articles /52/, /57/, /59/, state that there is no reactivity between these materials. Results in an article by Ohuchi and Kohyama /86/ suggest that some kind of electronic structure change does take place at the interface. This could be the reason for the observed adherence in our case.

6.1.2. AlN – CuZr system

In the first experiments with alloyed copper the aim was to study the reproducibility of results with different installations. Zirconium is known to be very reactive with oxygen and the reactivity is assumed to disturb our experiments in some amount. With the CuZr1 (w-%) alloy different methods for alloy fabrication were studied and with the CuZr5 (w-%) alloy the aim was to test different installations. Different installations have different test conditions and this is likely to influence the results.

From the Cu – Zr binary phase diagram in Figure 6.1 it is noted that the maximum solubility of Zr into Cu is smaller than 0,1 w-%. With larger Zr additions the alloy can be regarded as a mixture of zirconium saturated copper and the eutectic phase Cu_5Zr. These two phases can be expected to form during the solidification after the wetting

experiment. Binary intermetallics between Al and Cu can be excluded as copper dissolves 19,5 at-% aluminium even at room temperature /87/ and it is not likely that the content of aluminium in liquid would exceed this value.

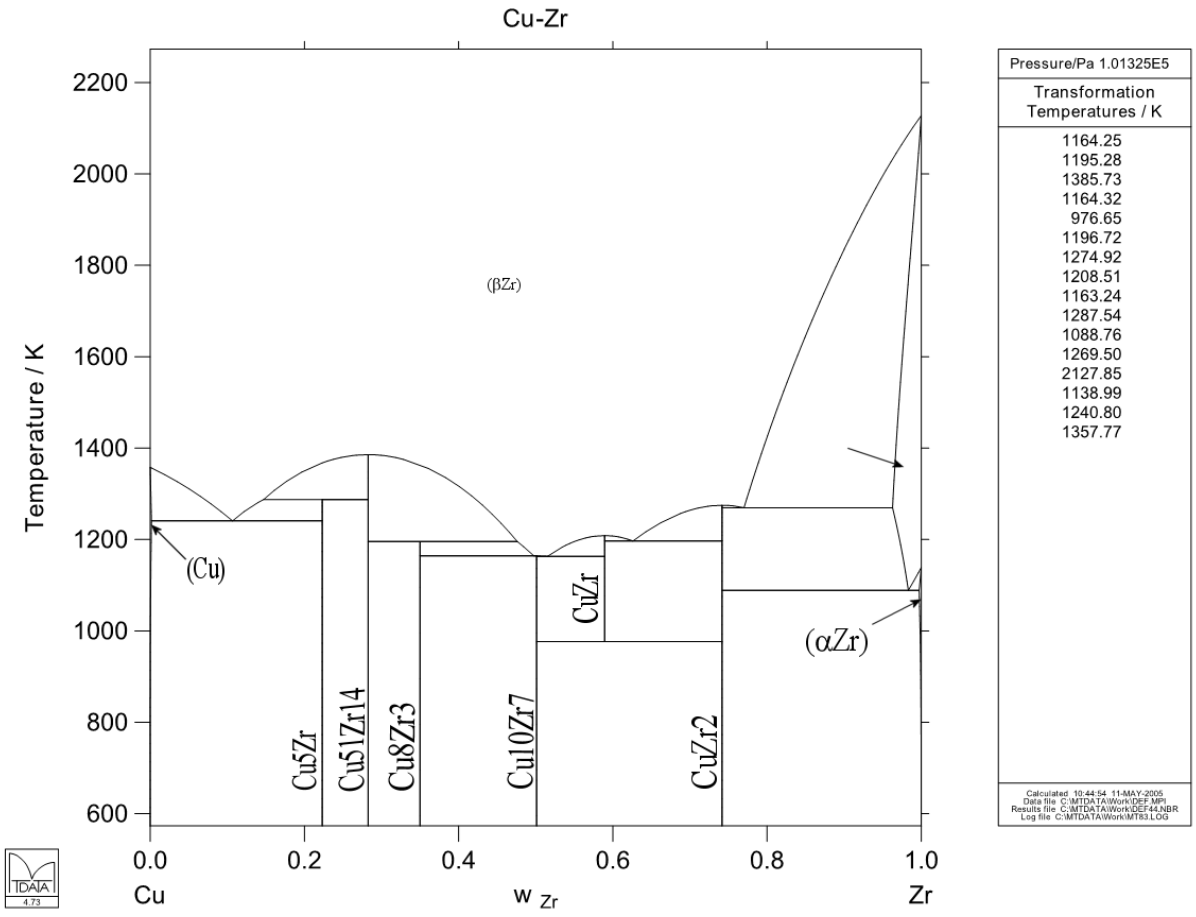

Figure 6.1. Binary phase diagram of the Cu – Zr system. /88/

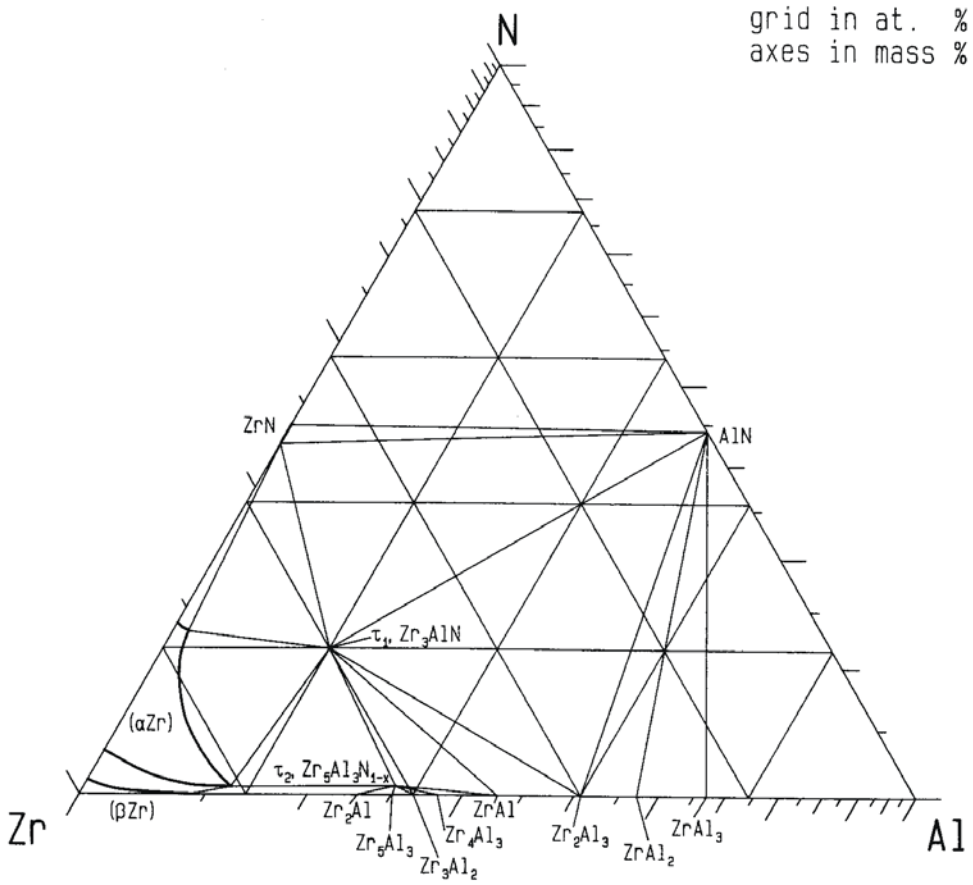

Figure 6.2 The ternary phase diagram of the Al-N-Zr system at 1000°C. /93/

In the ternary phase diagram in Figure 6.2 there are two basic nitrides AlN and ZrN and two more complex mixed nitrides present at 1000°C. From the composition point of view these complex nitrides can be formed. Therefore the possible reactions at the interface are the precipitation of Al_xZr_y intermetallics or the formation of Zr_xAl_yN or ZrN phases. ZrN is actually a compound which has a domain of non-stoichiometry. Gribaude et al report the y in $ZrN_{(1-y)}$ to vary from 0 to 0,12 at 1000°C /89/. In addition, for a Zr- containing alloy in thermodynamic equilibrium with $ZrN_{(1-y)}$ at a given temperature, the value y depends on the thermodynamic activity of Zr so that y increases with a_{Zr}, as discussed for Ti in ref /90/.

Wetting between AlN and CuZr1 (w-%) alloy

The first experiments on alloyed copper were carried out by adding one weight percent of zirconium to pure copper. The alloy can be prepared prior to the experiment or in-situ during the experiment. The influence of alloy preparation method was studied by comparing the results of two otherwise identical experiments.

In-situ alloy fabrication was carried out by placing the alloying material, in this case zirconium, to a small hole drilled on the top of the copper cylinder. The alloy formation stages are shown in Figure 6.3.

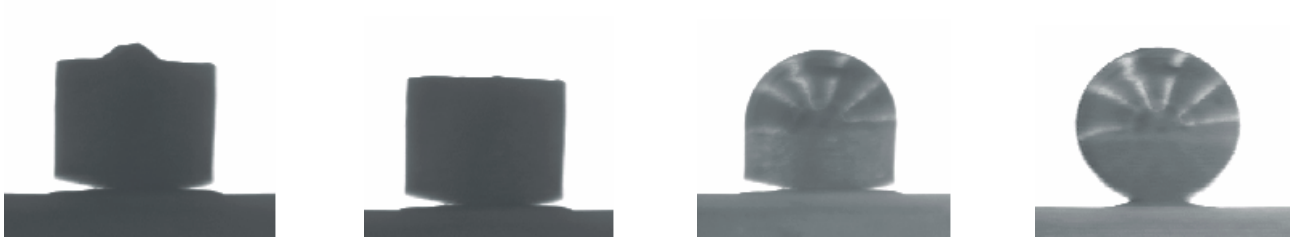

Figure 6.3 In-situ formation of the CuZr alloy during the wetting experiment. Melting starts locally from the top of the metal cylinder at 910°C and then propagates with increasing temperature towards the complete melting at 1078°C.

The contact angle versus time curves, resulting from experiments carried out by using both of these methods, are shown in Figure 6.6. It can be seen that the contact angle behaves in a very different manner depending on the alloy fabrication method. With prefabricated alloy the drop is asymmetric throughout the experiment and no change in contact angle is seen even when the temperature is increased from 1100 °C to 1150 °C. This is due to a continuous layer of oxide formed around the molten drop that blocks all the reactions at the triple line.

Evidence on the presence of this oxide can be seen both during the experiment (Figure 6.4.) and in studies carried out with scanning electron microscope (SEM) after the experiment (Figure 6.5). Figure 6.4 shows the presence of solid particles on the drop

surface. Figure 6.5 taken from the triple line shows that a powder-like phase (ZrO_2) is located in front of a Zr-containing phase. The Zr –containing eutectic phase seems to wet locally the AlN surface and the oxide seems to block the metal from propagating further.

With alloys prepared in-situ the results of wetting experiments are different. The initial value of contact angle is 156°± 2° and a sharp decrease in the contact angle value occurs at 500 seconds after the drop formation. The final equilibrium angle is 116° ± 2°. The sharp decrease is supposed to be resulting from the dissolution of the oxide layer and therefore the equilibrium contact angle represents the real wetting situation.

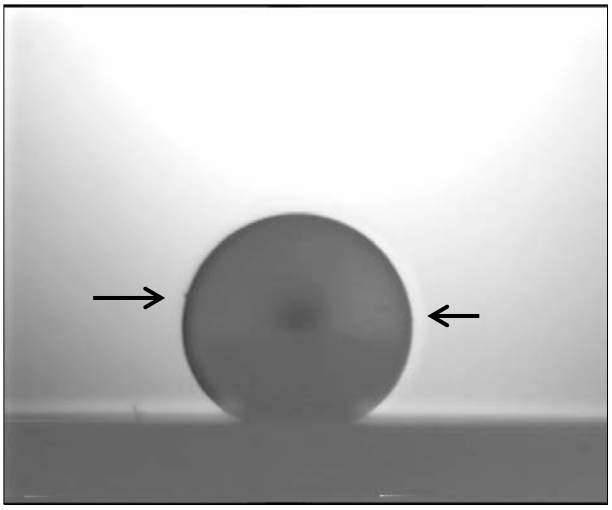

Figure 6.4. Solid particles can be seen on the CuZr1 (w-%) drop surface during the experiment. Oxide particles are pointed out with arrows.

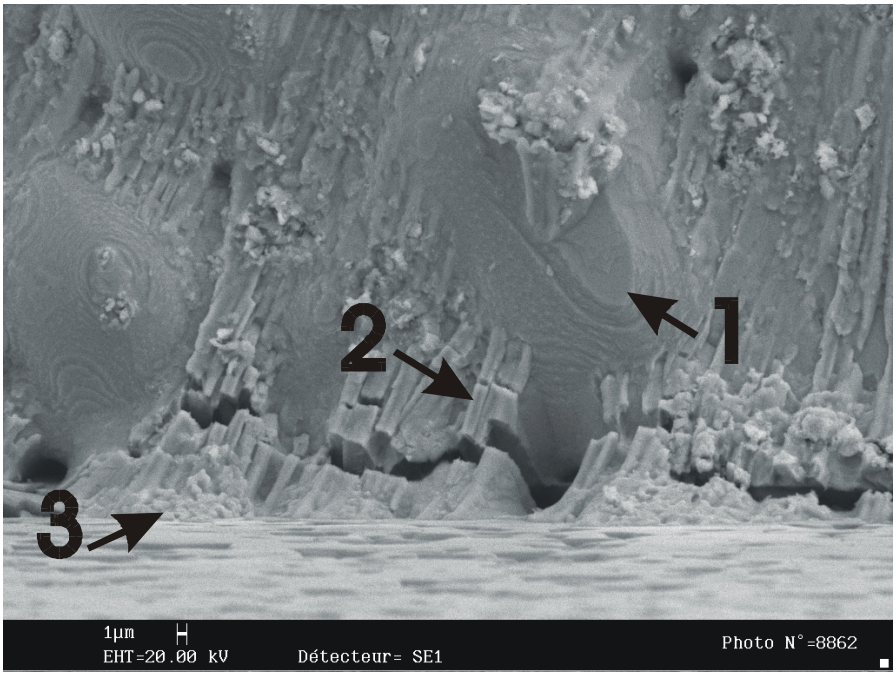

Figure 6.5. SEM picture taken after the CuZr1/AlN wetting experiment from the triple line. The surface in front is the AlN ceramic surface. The numbered phases are 1) pure copper, 2) Cu_5Zr eutectic, 3) ZrO_2.

The difference between the two experiments is assumed to result from the significant difference in the amount of oxygen present in the metal sample. The sample can be completely covered with zirconium oxide (ZrO_2) layer in the case of prefabricated CuZr1. In the in-situ alloy fabrication experiment only the small piece of pure zirconium on top of the copper cylinder is covered with ZrO_2. When the temperature is increased during the experiment, the eutectic formation starts at 910 °C as can be seen from the binary phase diagram of copper – zirconium system shown in Figure 6.1.

The Cu-Zr eutectic formation is assumed to bring enough mechanical perturbation into the surrounding surface for breaking locally the ZrO_2 layer from the surface of zirconium. High amount of oxide on the alloy drop surface has a strong blocking effect on the spreading of the liquid on substrate. To obtain spreading in the sessile drop experiments with the prefabricated alloy the ZrO_2-layer on the surface would have to be reduced away, dissolved or broken in some other way. To reduce the oxide at this temperature the oxygen partial pressure in the system would have to be smaller than $5*10^{-29}$ Pa for the 1 w-% amount of Zr in the prefabricated alloy. So small partial pressure of oxygen is not achievable in these installations where the working pressure is in the range of 10^{-4} to 10^{-5}Pa.

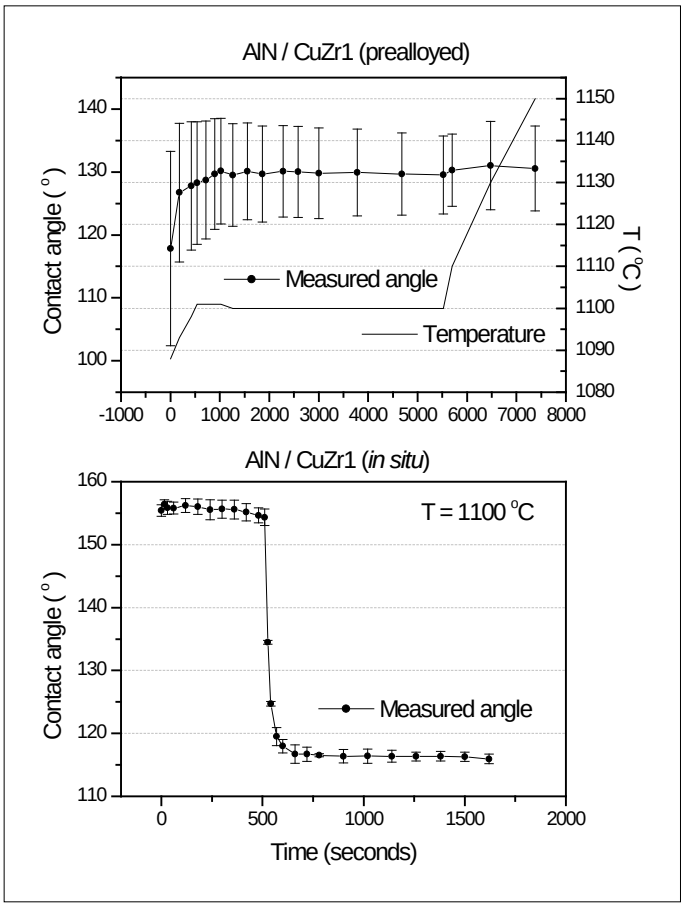

Figure 6.6. The difference in the wetting (contact angle vs. time) behaviour of CuZr1 (w-%) alloy on AlN substrate caused by the different fabrication methods of the CuZr1 (w-%) alloy. In the upper figure the alloy is prefabricated before the experiment, whereas in the lower figure the alloy is fabricated in-situ during the experiment.

The selected alloy fabrication method for the actual experiments was the in-situ method. The results from the AlN substrate – CuZr1 (w-%) wetting experiment carried out at 1100 °C and in $3 \cdot 10^{-7}$ mbar vacuum using the metal furnace are presented in Figure 6.7. After the spreading the contact angle θ value tends slowly towards a steady contact angle $\theta_F = 115°$. Loss of the drop mass during experiment was ~ 3 %, which is acceptable concerning the accuracy of the results. The 500 seconds plateau value in the contact angle after melting is most likely the time required for the oxide layer disintegration. After that time the surface oxide layer is broken at least partially and the

liquid can spread. The possible formation of new phases will be discussed in the Characterisation part in Chapter 6.1.2.

The volume of the drop seems to vary very irregularly in the beginning of the experiment. This is due to the pinning of the drop until the rapid spreading. In the non-wetting phase of the experiment surface defects and oxides on the drop surface have a strong influence on the contact angle. After the spreading the volume is stabilised and closer to the real volume. From this volume value after stabilisation it is possible to calculate how much the liquid metal is vaporising during the experiment. To maintain the advancing triple line front, the evaporation should be less than 10 % of the volume. From the volume curve it is noted that the volume loss is less than 10 % in the experiment and from that point of view the experiment and its results should be correct.

a)

b)

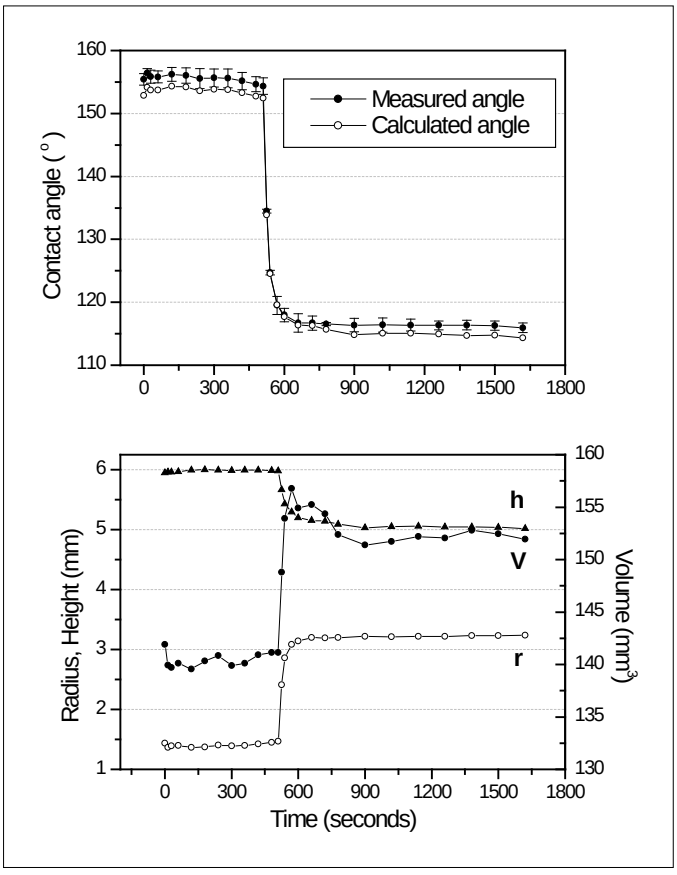

Figure 6.7. Results from the wetting experiment with CuZr1 (w-%) alloy on the AlN substrate. Temperature is 1100°C and the vacuum level is $3 \cdot 10^{-7}$ mbar. Fig. 6.7a) shows the contact angle vs. time behaviour, whereas Fig. 6.7b) shows the drop height, volume and radius as function of time after melting.

Wetting between AlN and CuZr5 (w-%) alloy

Next experiment was carried out with the Cu – 5 w-% of Zr alloy. When considering the results from the previous experiments with the Cu – 1 w-% of Zr alloy all the next experiments were decided to be carried out with the in-situ alloy fabrication method. One purpose was to test different furnaces and to evaluate the reproducibility of the results. Therefore the AlN – CuZr5 (w-%) wetting test was carried out using all three different furnace installations. The final contact angles obtained in these experiments are presented in Table 6.2 and in Figures 6.8. and 6.9.

Table 6.2. The results from AlN – CuZr5 wetting experiments carried out by using different furnace installations. The actual temperatures and pressures during the experiments are shown in the table.

Furnace	Temperature (°C)	Pressure (mbar)	θ_F (°)
Alumina	1100	$1 \cdot 10^{-6}$	110 ± 2
Vertical metal furnace	1100 (1150)	$3 \cdot 10^{-6}$	105 ± 2 (104 ± 2)
Horizontal metal furnace	1170	$5 \cdot 10^{-7}$	107 ± 2

The difference between the alumina tube and metal furnaces is in the atmosphere. The efficiency of vacuum pumping system and the purity of working environment seem to be the critical aspects when working with alloys containing zirconium due to the high reactivity of Zr with any oxygen source in the system. Therefore the (almost an order of magnitude) higher pressure and maybe some impurities coming from the alumina tube itself influence the results and the droplet spreading requires much longer time than in working with metal furnaces as seen in Figure 6.7. The difference

a)

b)

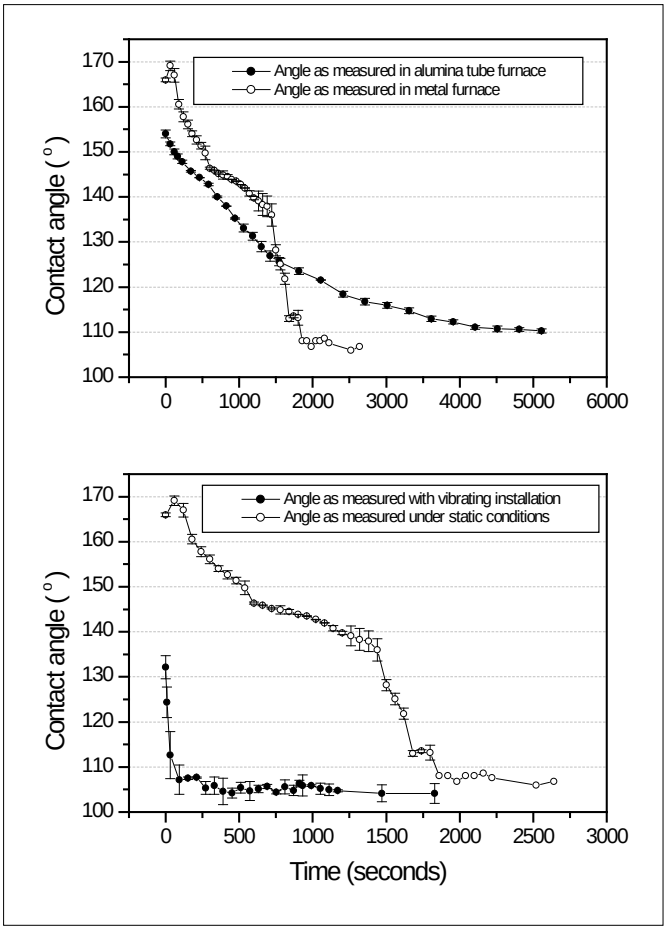

Figure 6.8. The contact angle vs. time curves for the CuZr5 (w-%) – AlN system in different furnaces (fig. 6.8a) and in metal furnace with vibrating and static sample holder installations (fig. 6.8b).

in the vacuum between the two metal furnaces results from different atmosphere of the chambers. The vertical furnace has worse sealing than the horizontal furnace. Therefore the best possible vacuum cannot be reached with the vertical metal furnace.

When comparing the results from two different metal furnaces, a clear difference can be seen in the wetting kinetics in these two installations. The unintended mechanical vibrations occurring in the vertical furnace formed an obvious reason for this. This mechanical instability caused the ZrO_2-layer to break rapidly and the final contact angle value was reached in a short time. The value of the angle is probably also influ-

enced by these high frequency vibrations. Therefore it is not possible to state whether the final contact angle corresponds to the equilibrium situation or whether it is smaller than the corrected value due to the unintended vibrations.

The best installation to work with was the horizontal metal furnace, where also the lowest pressure values could be achieved. The final wetting results obtained with AlN substrate and CuZr5 (w-%) alloy show continuously changing contact angle throughout the experiment. Now the time required for the final stage of spreading of the drop was three times longer than in the case of CuZr1 (w-%) alloy. Temperature was increased finally to 1170°C to speed up the reactions. This higher temperature can decrease the final contact angle value by a few degrees as compared to the value which would be obtained at 1100°C.

It is also possible that the reactions between the substrate and the zirconium control the spreading rate instead of sudden oxide layer disintegration. As discussed in Chapter 2.3.2, the final interfacial composition controls the obtained contact angle rather than the intensity of reactions. Therefore the final wetting angle value is very close to the value obtained with the CuZr1 (w-%) alloy. This is due to the fact that the composition of the interface is very similar in both cases as will be shown later by characterisation.

a)

b)

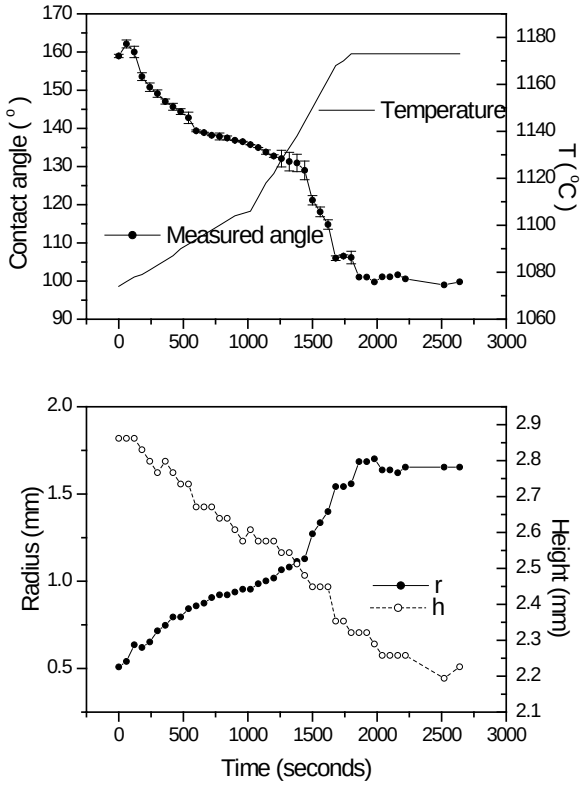

Figure 6.9. Wetting test results for AlN - CuZr5 (w-%) system: a) contact angle vs. time and temperature, b) droplet height and radius as a function of time.

Wetting between AlN and CuZr0,1 (w-%) and CuZr10 (w-%) alloys

These experiments were carried out for studying the influence of the alloying element content on the wetting. Because zirconium is a reactive element in this otherwise inert system, it is expected to enhance the wetting in general and with positive dependence. This means that when Zr-concentration increases, better wetting is achieved, as was the case in the system AlN – CuAgZr studied by Tomsia /69/. Interfacial reaction product is similar in all experiments with varying Zr – contents as will be shown in the characterisation of the interface. The interfacial characteristics are only changing with the reaction time. The concentration and activity of Zr can account for the decrease in contact angle from CuZr1 (w-%) to CuZr5 (w-%).

This correlation between Zr-concentration and wetting seems to be true for the one and five percent Zr additions, but not for the 0,1 w-% and 10 w-% additions studied here. The obtained final contact angle values are represented in Table 6.3.

Table 6.3. The wetting results in the AlN – CuZr (w-%) system obtained with different zirconium contents in the alloy.

Materials (w-%)	Temperature (°C)	Pressure (mbar)	θ_F (°)
Cu	1100	$1 \cdot 10^{-6}$	127±2
CuZr0,1	1100	$4 \cdot 10^{-7}$	159±2
CuZr1	1100	$3 \cdot 10^{-7}$	116±2
CuZr5	1170	$5 \cdot 10^{-7}$	107±2
CuZr10	1100 (1200)	$1 \cdot 10^{-6}$	155±2 (137±2)

It is noticeable that with 0,1 % and 10 % of Zr in the CuZr alloy the contact angle value is larger than the value with pure copper. This is possibly due to the interaction of oxygen with zirconium. With 10 % of zirconium, the formed ZrO_2 - layer is so thick that in the used installation it is not possible to break it and it blocks the spreading of the drop. There was only slight increase in the drop radius value as function of time and the decrease in contact angle value was about 10° during the spreading in the one-hour experiment. Increasing temperature to 1200°C increases the thermal energy of the system and allows the slight disintegration of the oxide layer and therefore the decrease of the wetting angle.

Reactive wetting

Common way of analyzing reactive wetting is to study the droplet spreading rates from the wetting curves as well as the shape of the spreading curve. The spreading behavior characteristics are measured from previous Figures 6.7 and 6.9 are presented in Table 6.4. At the Zr compositions of 0,1% and 10% practically no changes in the

drop shape occurred. Therefore the discussion here applies only to CuZr1(w-%) and CuZr5 (w-%).

Table 6.4. Spreading behavior characteristics of CuZr1 (w-%) and CuZr5 (w-%) on AlN in the wetting experiments.

	1st stage dR/dt	duration	2nd stage	Duration	3rd stage	Duration
	mm/s	s	mm/s	s	mm/s	S
CuZr1 (w-%)	≈0	520	0,02	80		
CuZr5 (w-%)	$2{,}8\text{x}10^{-4}$	660	$1{,}7\text{x}10^{-4}$	720	$4{,}9\text{x}10^{-4}$	600

Even though the same installation was used, a quantitative comparison between these systems is not possible due to the fact that the experiments were carried out at different temperatures. The spreading is very different in 1 w-% Zr and 5 w-% Zr. With CuZr1 there is only one abrupt change in the spreading curve. Before and after the actual spreading there are no gradual changes in the drop shape which would indicate some kind of reaction taking place. In Figure 6.7 it can be seen that with CuZr1 (w-%) the initial contact angle (~140°) stays constant for about 10 minutes and then the spreading to final contact angle value occurs during 80 s. There is no evidence in the spreading curve on the reactivity as a function of time.

With CuZr5 (w-%) in Figure 6.9 there are three changes in the spreading rate. All the stages are quite similar; there is a gradual increase in the radius and a decrease in the wetting angle. Only the rates vary slightly in different stages. Linear regimes in this curve indicate a new interfacial compound formation and the dependence of triple line spreading on time depends on that. Any significant decrease in the triple line moving rate is not revealed but the rates are of the same order of magnitude throughout the spreading curve. In general the reactive spreading can be controlled either by the diffusion rate of reactive species or it can be controlled by the kinetics of the chemical reaction itself /40/. Conclusions on the spreading mechanisms are made after the interface characterisation in the next chapter.

Characterisation of the AlN – CuZr interfaces after wetting experiments

Figure 6.10 shows a SEM - image of the interface in the AlN – CuZr5 (w-%) system. In the lower part of the figure is the AlN ceramic substrate and the upper part is the CuZr5 (w-%) alloy formed by solidification after the experiment. The light coloured phase (number 5 in the figure) is the binder phase YAG, composed of Y and Al oxides, and the dark phase is the AlN matrix (4). Two different phases in the metal alloy are the copper phase (1) with dissolved Zr content of 0,10 w-%, and the eutectic (Cu) + Cu_5Zr – phase mixture (2). Reactions seem to take place at the interface where the alloy is reacting with the dissolving substrate ceramic and its binder phase (3). Binder phase effects seem to be local and therefore it can be assumed that they do no significantly change the overall wetting or reactivity between the base ceramic and metal alloy.

The higher magnification image of CuZr5 (w-%) on AlN in Figure 6.11 shows that there is a discontinuous reaction layer (phase 3 in the figure) at the interface. EDS analysis is not quantitatively accurate as the EDS beam diameter is larger than 1μm and the thickness of this layer after one hour experiment is at maximum 500 nm. Anyway, the elemental analysis carried out for identifying this phase revealed that the phase is rich in Al, Zr and N. From the phase diagram in Fig 6.2 it is noted that the phase Zr_3AlN does exist in suitable composition range. In the same diagram it can also be noted that (Zr,Al)N exists in the whole range between pure AlN to ZrN and therefore all Al-Zr compositions can be found for this nitride. In the experiment of six hours the thickness of this layer had increased at some points to 1200 nm and it was found that the thick layer consisted of ZrN and only about 5 w-% Al was remaining in the analysis. Comparison to theoretical equilibrium thickness of reaction layer (125μm) shows that the interface after 6 h experiment remains far from equilibrium.

The interface of CuZr1 (w-%) on AlN is shown in Figure 6.12. The best possible compositional evaluation is that there is a continuous adsorption layer of Zr + O in the interface which enhances the wetting. No remarkable new phases are found. It is also possible that the AlN surface has started reacting to form (Al,Zr)N. Oxygen is also found in these areas. For CuZr10 (w-%) there is a similar Zr-rich phase found at the

interface even though the droplet spreading never took place. In these analyses oxygen is not as predominant but the contents of Zr-Al-N-O are 17-36-32-8 showing that Zr is reacting with AlN but not to the extent where ZrN would start to dominate. This could have been changed in a long duration experiment.

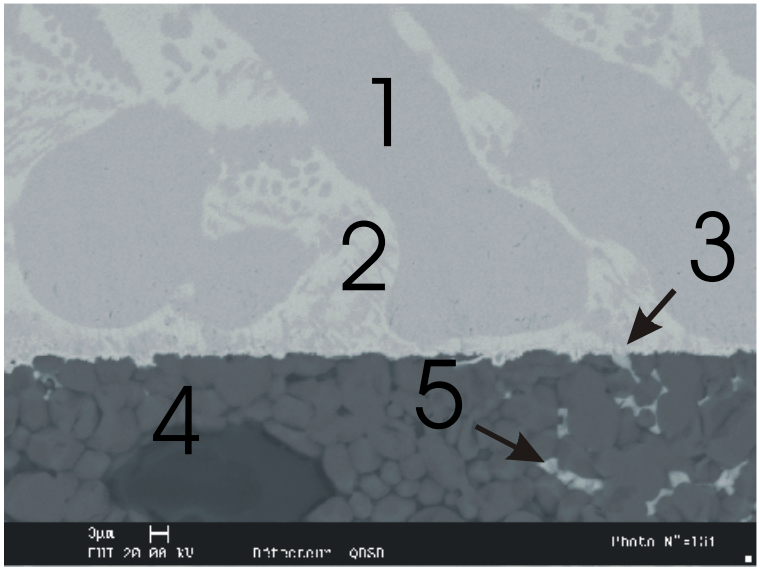

Figure 6.10. SEM-image (backscattering) of the substrate – alloy interface in the system AlN – CuZr5 (w-%) after wetting experiment. Phases: 1) Cu, 2) Cu_5Zr+ Cu(Zr), 3) Y_2O_3 reacting with Zr, 4) AlN matrix and 5) YAG binder phase consisting of yttrium – and aluminium oxides.

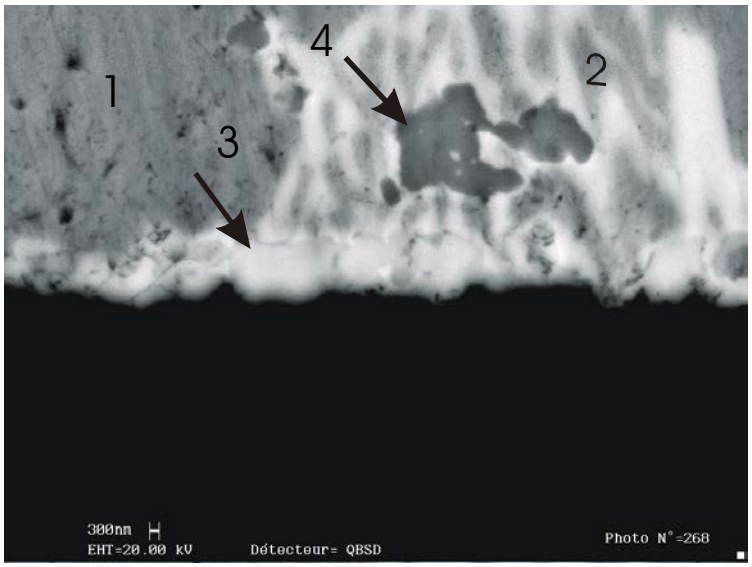

Figure 6.11. A higher magnification SEM – image (BS) of the interface in the system AlN – CuZr5 (w-%) after wetting experiment for six hours. Phases: 1) Cu, 2) Cu_5Zr, 3) ZrN and 4) almost pure Zr particle.

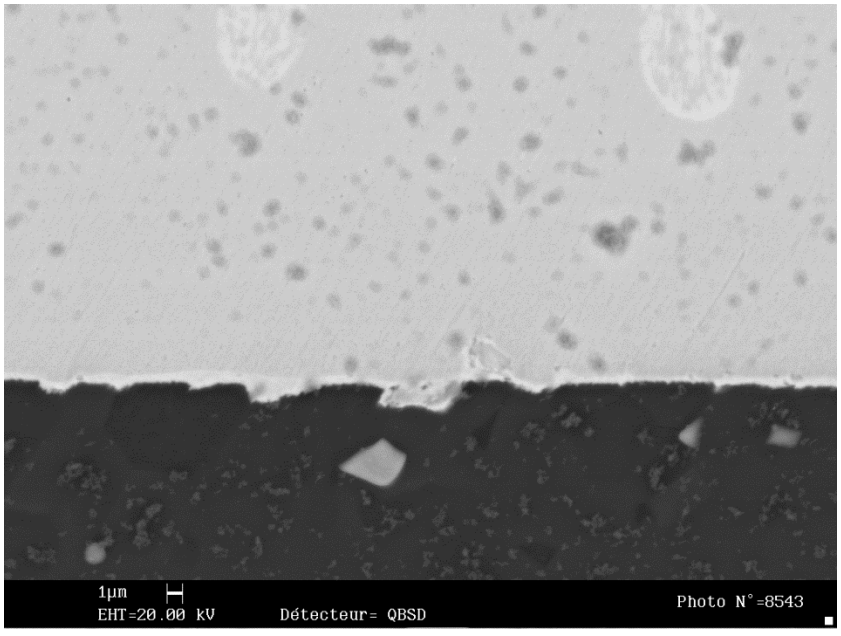

Figure 6.12. SEM image of CuZr1 (w-%) on AlN after wetting experiment. The visible Zr adsorption layer thickness is 200-300 nm.

ZrO_2 was found on the drop surface and at some parts of the triple line as shown in Figures 6.3. and 6.4. Since the reduction of ZrO_2 is not possible due to its high stability in the experimental conditions, the total amount of that phase must be the same throughout the experiment with the possible small increase coming from the atmosphere and from the ceramic binder phase. The analysis of ZrN layer found at the droplet – substrate interface contains varying amounts of oxygen. Oxygen can be dissolved in the ZrN or it can be in the form of oxynitrides or oxides depending on the N-O ratio. The ternary phase diagram of Zr-O-N system is shown in Figure 6.13. Three different oxynitrides, Zr_2ON_2 (γ), $Zr_7O_8N_4$ (β) and $Zr_7O_{11}N_2$ (β'), are reported by authors in refs. /91/ and /92/. From these only the β-phase is stable at 1200°C. As the used analysis method was not capable of detecting separate phases, it is assumed that the analysed oxygen is dissolved into ZrN. The phase diagram in Fig. 6.13. is in accordance with this interpretation.

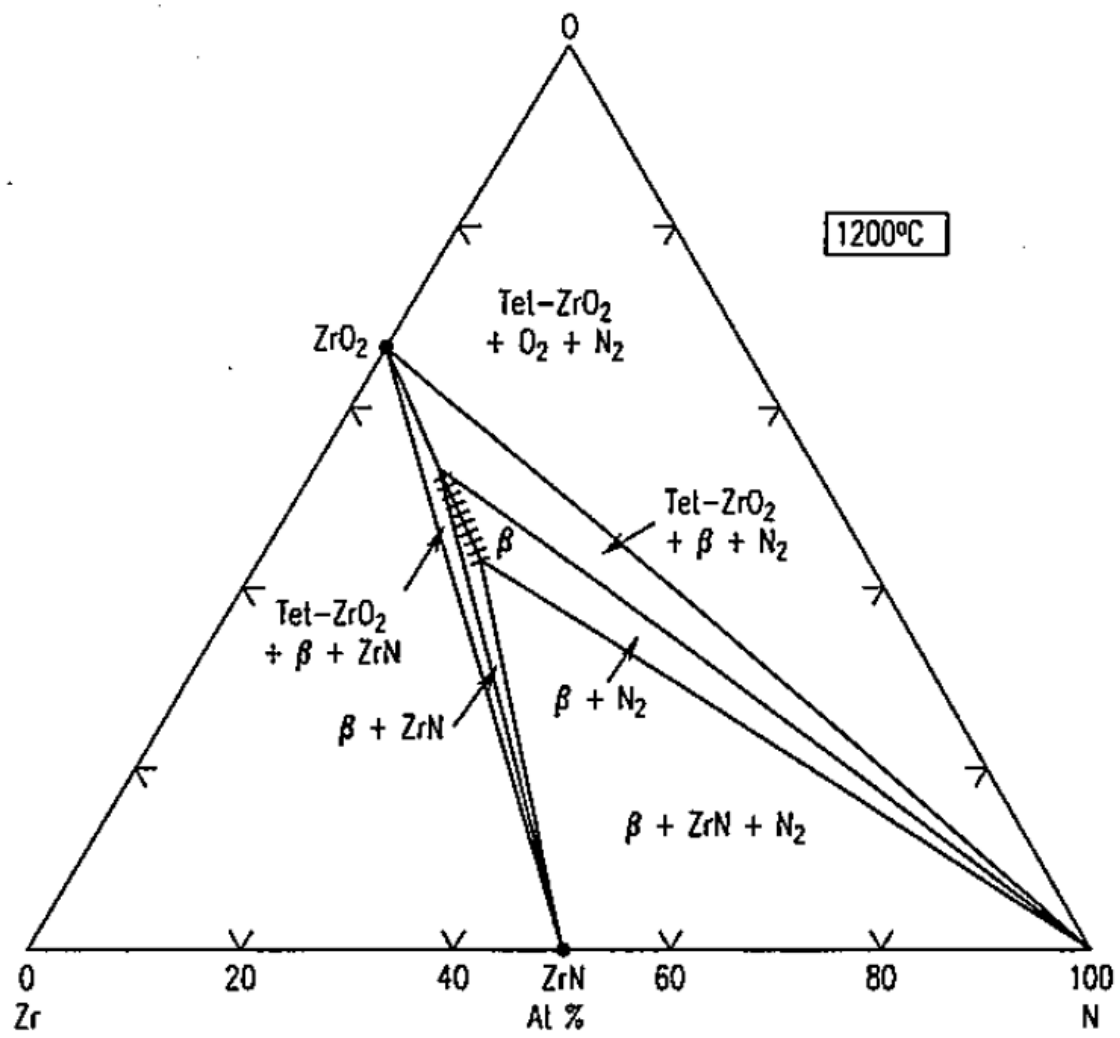

Figure 6.13. The ternary phase diagram of the Zr-O-N system /93/.

One way for identifying the components of this structure is to produce elemental distribution maps from selected areas. This kind of map is shown in Figure 6.14. From the map it is obvious from the higher intensity that there is a Zr-rich adsorption layer in the interface and this layer has a higher Zr-concentration than the eutectic phase (17 w-%) formed during the solidification. This Zr-rich layer has to be generated during the experiment when the zirconium was dissolved evenly to melt and could easily adsorb to the interface. In many analyses also significant amounts of oxygen are found in this layer. This could indicate the oxide clusters assisting in the adsorption as was mentioned in references /45,46/. On the other hand the elementary distribution map of oxygen does not fully support this assumption.

In the centre of the image in Fig 6.14 there is an area where the binder phase of the ceramic AlN substrate interacts with the alloy. This area contains oxygen, yttrium and zirconium, but neither aluminium nor significant amounts of nitrogen. It can be assumed that in this area zirconium reacts with Y_2O_3 and forms ZrO_2 since ZrO_2 is thermodynamically more stable compound in these conditions. From the aluminium distribution map in Fig 6.14 it can be seen that the aluminium dissolved from matrix during the formation of ZrN is not clearly visible in the metal alloy side; this is due to the high solubility and small concentration of Al in Cu.

After one hour reaction time there is still zirconium retained in the alloy. Some of this can be found as isolated particles which have not been dissolved in the original in-situ alloy making. This is possibly due to restricting oxide layer around metallic Zr. From these reasons the reaction at the interface is either not complete or there are factors that slow down or stop the reaction. One reason for restriction can be the slow diffusion of Zr through the formed interfacial layer. A very low diffusion coefficient of $10^{-19} m^2 s^{-1}$ (at 1243K) is reported for Zr in ZrN in /94/.

The Gibbs energies of reaction of zirconium nitride and zirconium aluminides at the 1100°C temperature are listed in Appendix. There the most stable compound of these nitrides and aluminides is ZrN. ZrN formation is in the long run the only reaction taking place at the interface as is predicted also from the negative Gibbs energy of reac-

tion in Chapter 5. In the interfacial reaction the substrate AlN decomposes and aluminium dissolves to CuZr alloy by the reaction:

$$AlN + Zr_{(Cu)} = ZrN + Al_{(Cu)} \qquad (23)$$

In this study the analysis of the interface in AlN – CuZr system shows no large deviation of the formed $(Zr,Al)N_{(1-y)}$ from the stoichiometric composition. If Zr and Al are combined together and then compared to the nitrogen amount, non-stoichiometry can be found with y values in the range of 0,03-0,04. Coefficient y-values as high as y = 0,12 were not found.

The adherence of the droplet to the substrate is very strong and the shape of fracture reveals the domination of cohesive rather than adhesive forces at the interface. This can be seen by comparing Figures 6.15 and 2.8. This kind of fracture suggests that the formed interfacial layer is more strongly bonded with metallic bonding than the substrate material based on covalent bonds.

The surface tension of zirconium (1480 dyn/cm) is larger than that of copper (1360 dyn/cm). In earlier studies on the influence of alloying on surface tension it was found that an alloying element with a larger surface tension value will generally increase the overall value of the surface tension of the alloy /95/. According to the results in this study the increasing surface energy of solid – liquid interface cannot be the controlling factor since with higher Zr contents the wetting, on the contrary, is enhanced. This can be explained first with the formation of a continuous adsorption layer of Zr and after longer time with the formation of a zirconium nitride layer at the interface. ZrN has more metallic nature than AlN. This is one reason why Zr addition and ZrN formation promotes the wetting and bonding in AlN – CuZr system.

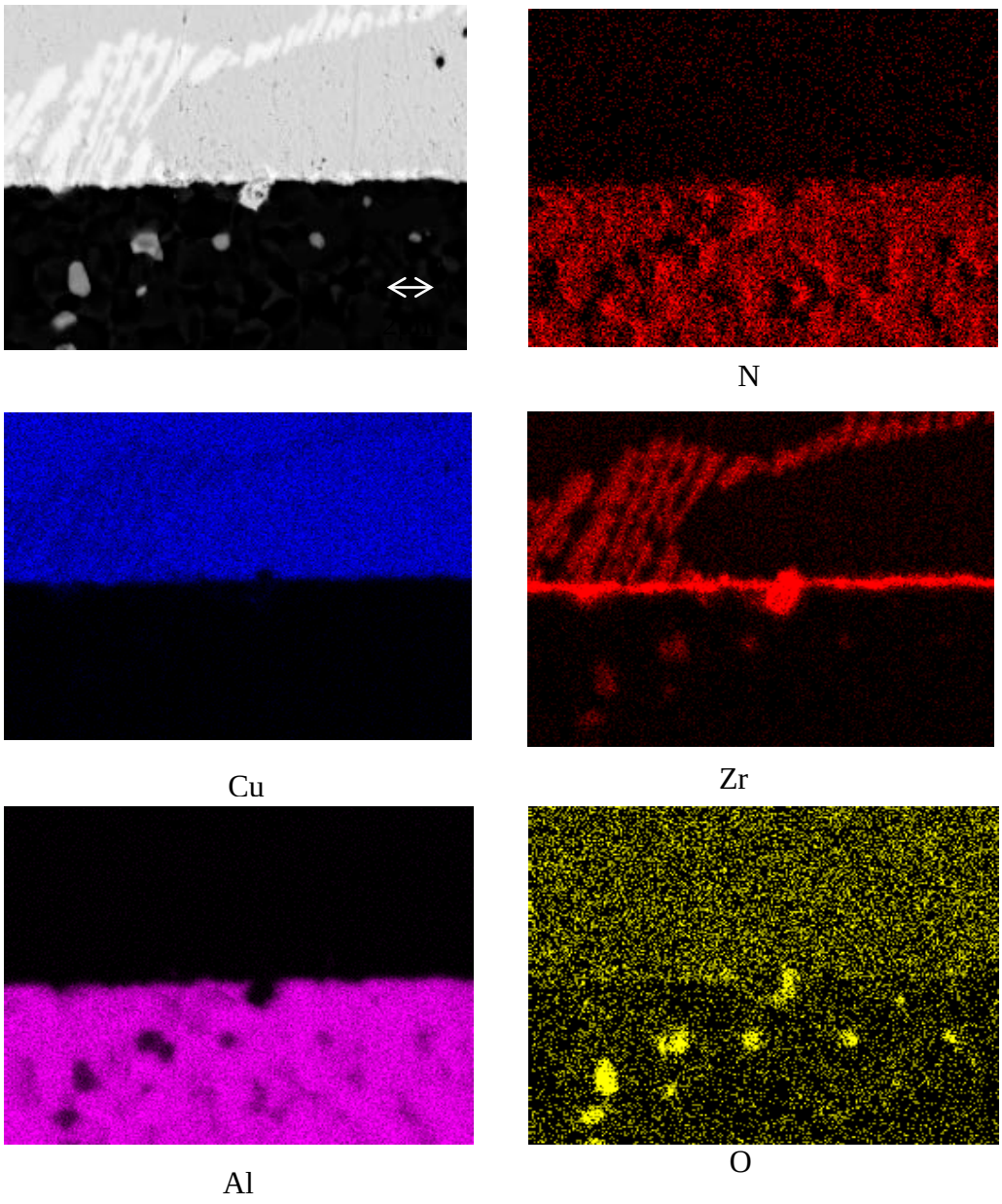

Figure 6.14. SEM-EDS elemental distribution maps of the interface region in the system AlN – CuZr5 (w-%). The first image is the actual SEM – image.

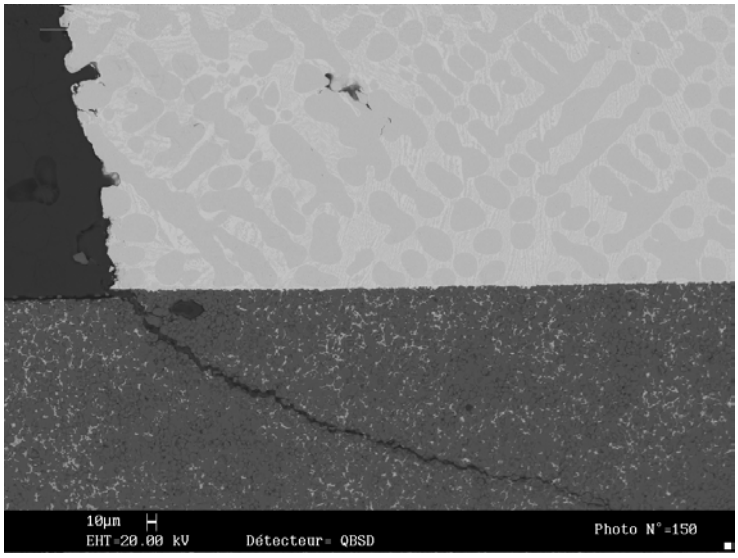

Figure 6.15. The geometry of the post-solidification fracture at the AlN – CuZr5 (w-%) interface.

Conclusions on AlN-CuZr wetting and reactivity

In general alloying can have different influences on wetting. Chemical reactions between the liquid and the substrate in the case of CuZr on AlN could be either the formation of nitrides or aluminides. The reaction product can be either a continuous layer or it can form locally. If the reaction layer is continuous at the interface between the drop and substrate, the wetting between the reaction product and the alloy which has a composition different from the original alloy, will finally control the equilibrium situation.

Therefore it can be stated that zirconium enhances the wetting and decreases the contact angle of copper in the Cu – AlN system. This is due to the formation of interfacial ZrN layer. The initial adsorption of zirconium to the interface lowers the contact angle close to that of ZrN. Due to the lack of measured experimental data in the literature we cannot compare the measured contact angle values in the system AlN – CuZr with previous studies.

Since there is a Zr-rich adsorption layer in the interface which will provide as much Zr to the triple line as needed and on the other hand the Zr diffusion through ZrN is very low it can be stated that the growth of new nitride layer controls the spreading.

The horizontal metal furnace had the best vacuum and purity of working environment and therefore was selected for these experiments. Still the oxygen disturbed the wetting phenomena of the zirconium - containing alloys causing pinning of metal-alloys during spreading. Acceptable values for CuZr1 (w-%) and CuZr5 (w-%) alloys were achieved after sufficient holding time and the droplet was able to spread due to the dissolution or disintegration of the zirconium oxide layer. The values of 116° ± 2° and 107° ± 2° for the alloys CuZr1 (w-%) and CuZr5 (w-%), respectively, represent a non-wetting situation but they are smaller than the values for pure copper. To verify the surface cleanliness of AlN surface and to distinguish whether the amount of Al_2O_3 is significant in the surface an experiment was made with CuZr5 (w-%) alloy on Al_2O_3. Respective contact angle was found to be 77° ± 2°, varying significantly from the values achieved in experiments on AlN.

In the literature results on the addition of Zr into non-reactive metal on AlN are reported /64/ where the formation of only ZrN is detected at the interface. The formation of Al–Zr intermetallics is reported in some articles /65/, where reaction layers resulting from joining experiments are characterized. A review of these articles was presented in Chapter 2.5.2.

6.1.3. AlN – CuCr system

Next experiments were carried out on AlN - CuCr1,5 (w-%) system. Figure 6.16 shows the binary phase diagram of copper and chromium in the copper rich corner. Copper and chromium form a eutectic mixture with the composition of 1,3 w-% of Cr. This compound has a melting point of 1075,6 °C. Cu and Cr do not form any intermetallic compounds and maximum solubility of Cr into Cu is 0,89 at-%.

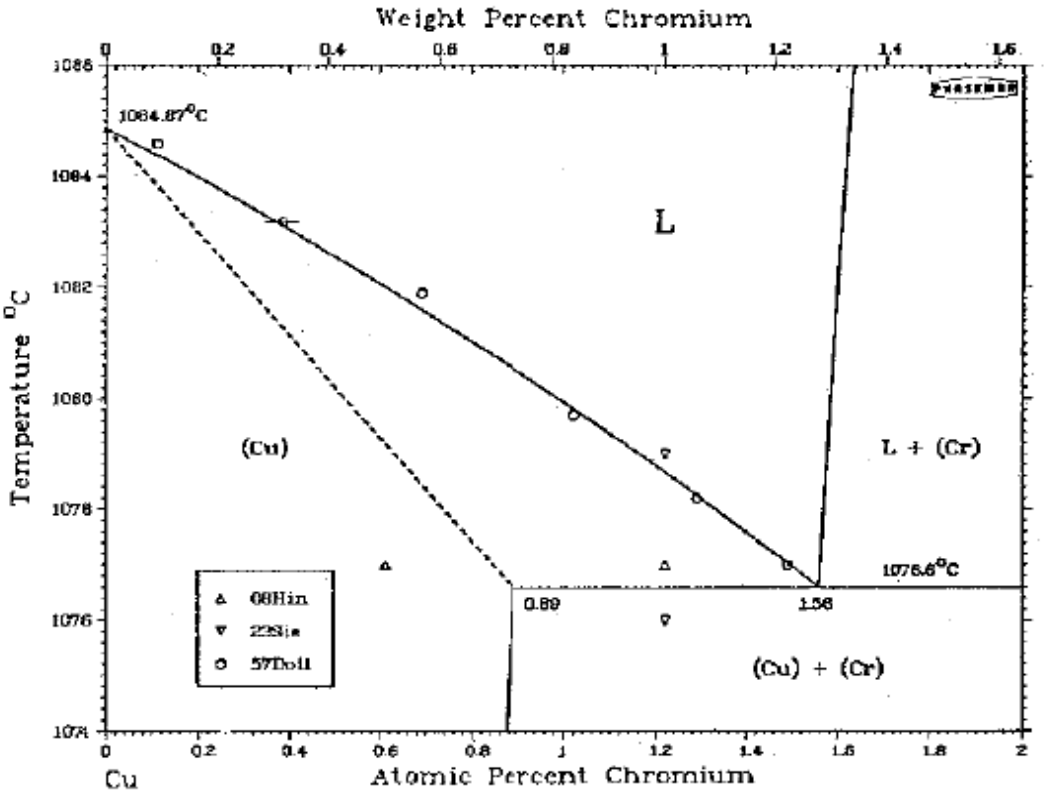

Figure 6.16. The phase diagram of the binary Cu-Cr system /96/

In the system Al-Cr-N there are both chromium nitride, aluminium nitride and some Al_xCr_y compounds according to HSC /63/. In the wetting experiment it is possible that any of these may be formed. The thermodynamic stability of these phases is estimated in Appendix and it predicts the Cr_2N formation in the wetting experiment.

Reactive wetting between AlN and CuCr1,5 (w-%)

The sessile drop wetting experiment was carried out in the horizontal metal furnace at 1100 °C. The CuCr1,5 (w-%) alloy was fabricated in-situ.

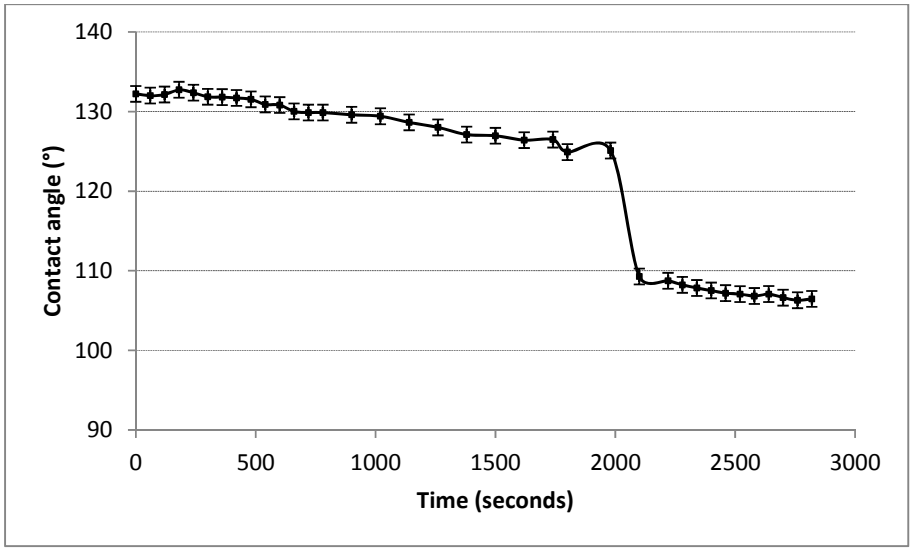

a)

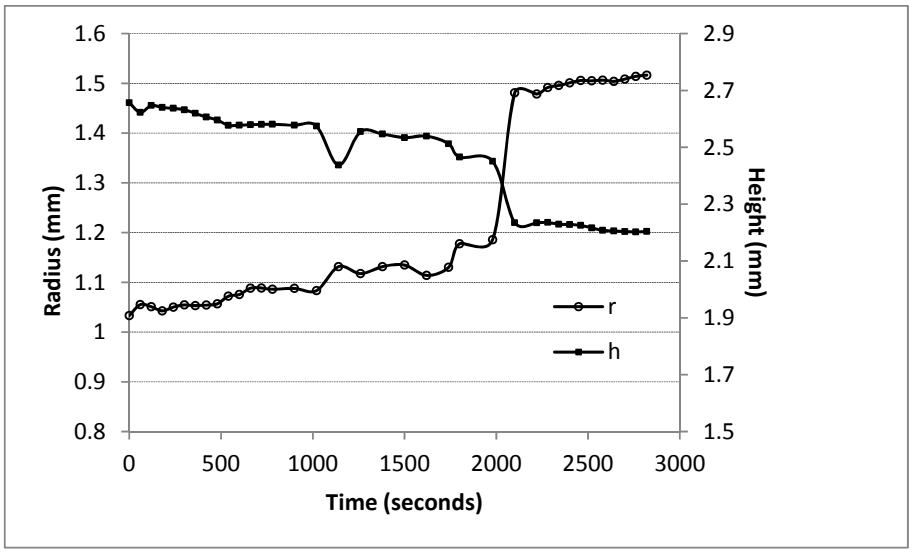

b)

Figure 6.17. Wetting test results for the AlN - CuCr1,5 (w-%) system: a) contact angle vs. time, b) droplet height and radius as a function of time.

Figure 6.17 shows the development of wetting in the AlN - CuCr system. The initial contact angle was 132° ± 2° and a continuous oxide layer was visible at the surface of the molten droplet. For the first 33 minutes the average rate of spreading was 7.6×10^{-5}

mm/s. A sharp decrease of the contact angle to 109° ± 2° occurred after the disintegration of the oxide barrier (the average rate of spreading was $dR/dt = 2.5x10^{-3}$ mm/s). The final contact angle 107° ± 2° was reached at $dR/dt = 4.2x10^{-5}$ mm/s. Without the sudden faster spreading the triple line could have been stated to propagate linearly. This mode of spreading is similar to the CuZr5 (w-%) on AlN-case. Oxide particles migrating on the surface of the molten alloy were observed in the experiment also after the disintegration of the continuous layer.

Chemical reaction-limited reactive spreading occurs in this case. After the sudden drop in the contact angle the propagation of the triple line occurs as dominated by the rate of AlN dissolution and new layer formation to the interface and to the triple line. This can be seen from the variation in the thickness of the reaction layer in following chapter.

Characterisation of AlN – CuCr interface

After the sessile drop experiment the adherence of the solidified drop to the substrate is strong. Formation of a cohesive type crack in the substrate after solidification occurs due to the adherence. This strong bonding is due to the continuous reaction layer which is formed at the interface during the wetting experiment. This interfacial layer can be seen in Figure 6.18.

The thickness of the reaction layer varies coherently with the spreading of the drop. The thickness is about 7 μm at the centre of the drop. In the area close to the triple line the thickness is well below 1μm indicating here the existence of an original adsorption layer before the layer growth. This layer is shown in Figure 6.19. From the cross-section of the interface it can be seen that the reaction advances in both directions, towards the ceramic and towards the alloy. A high-magnification image of the interface is in the Figure 6.20. In comparison with the theoretical equilibrium thickness of reaction layer (3,7μm) the thickness is found out to be very close to the average thickness of the layer after the experiment.

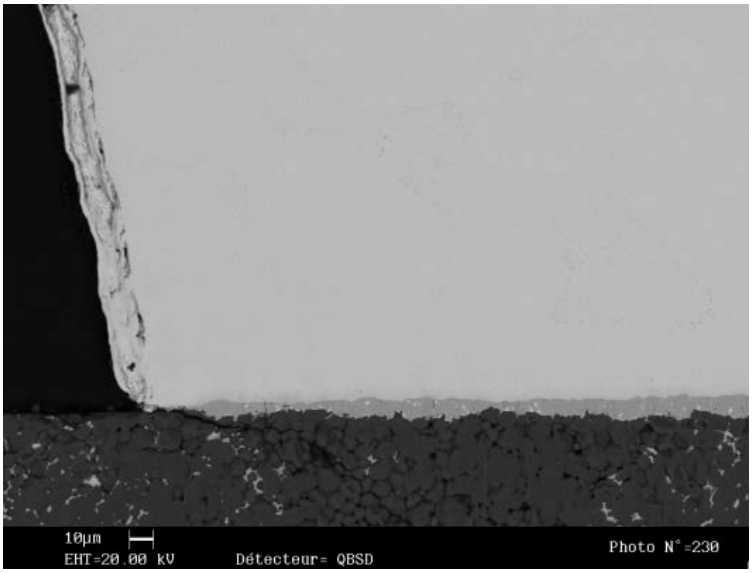

Figure 6.18. Interface and the triple line in the system AlN – CuCr1,5 (w-%) after wetting experiment. The cohesive-type crack is visible starting from the triple line and propagating to the substrate.

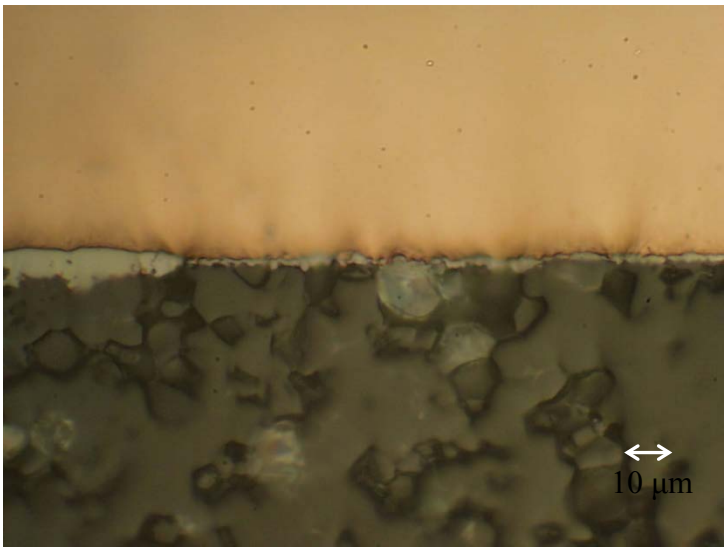

Figure 6.19. Optical microscope image of the interface in CuCr1,5 (w-%) –AlN system. Chromium rich layer is visible throughout the interface although there are large variations in its thickness.

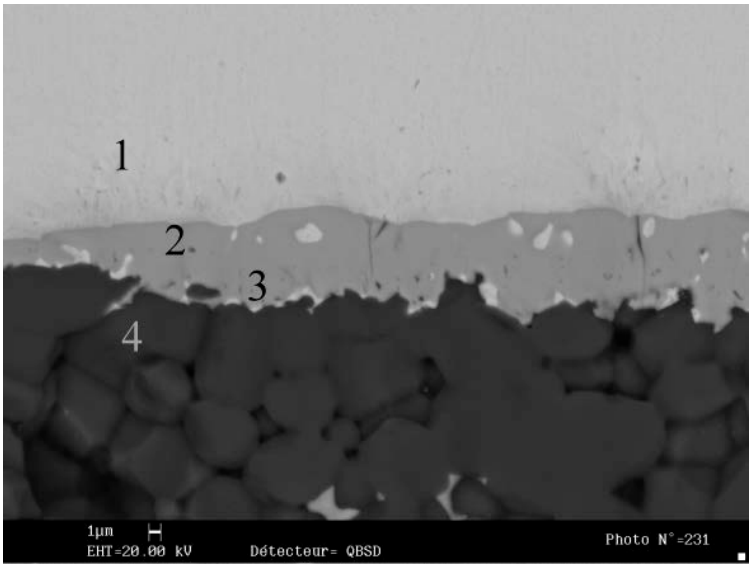

Figure 6.20. A SEM-image of the interface in the system AlN – CuCr1,5 (w-%) after wetting experiment. Phases: 1) CuCr1,5, 2) Cr_2N with CuCr1,5 inclusions, 3) Cr_2N with AlN inclusions and 4) AlN matrix with YAG binder phase.

The original substrate surface can be detected in the middle of the reaction layer since below this line there are some particles of AlN substrate left in the reaction product. The composition of the reaction layer corresponds to Cr_2N. According to EDS analysis the lower part of this Cr_2N layer contains residual AlN inclusions and the upper part contains CuCr alloy inclusions. Also oxygen was detected in major part of the layer. Oxygen content varied from few per cents to 17 at-%. At the point where the oxygen content was 17 at-% the composition of reaction layer corresponds closely to $Cr_3(ON)_2$. Aluminium is not detected in the solidified drop.

This kind of growth of the interface can be possible if the diffusion coefficient of chromium in the formed nitride layer is high. It is reported to be $2{,}46 \times 10^{-12} m^2/s$ at 1064K /97/. In comparison with the diffusion coefficient of Zr in ZrN ($10^{-19} m^2 s^{-1}$ at 1243K) it is noted that the difference is remarkable and in favour of Cr_2N formation.

Even though in Table 2.2 the Gibbs energies of reaction of chromium nitrides are significantly less negative than the Gibbs energy of reaction of AlN, the formation of Cr_2N occurs in the experiment. Since the most stable compound among these nitrides

and aluminides is AlN, the aluminium released from the reacting AlN dissolves into the liquid CuCr alloy. The Cr_2N formation is therefore estimated to be the only reaction taking place at the interface. Chemical analysis from this kind of interface was not found in the literature.

The thickness of the interfacial reaction layer is significantly larger than in the AlN – CuZr system. The maximum thickness of Cr_2N is ten times larger than the thickness of ZrN. The most probable reason for this is the large difference in diffusion rates of chromium and nitrogen in Cr_2N layer. The formed Cr_2N has a metallic nature and therefore wetting is increased by its formation /98/. The surface tension of chromium is 1700 dyn/cm, which is higher than that of copper or zirconium. That could promote wetting even if the other conditions would be neglected.

The wetting experiment on AlN - CuCr system was carried out with 1,5 w-% chromium content. During the experiment an oxide layer was visible on the liquid drop surface. Similarly to zirconium experiments there is a sudden drop in the contact angle value in spreading stage of the liquid which most likely is taking place after disintegration of oxide layer. The measured final contact angle was smaller (113°±2°) than the contact angle of pure copper on AlN (127°±2°) but slightly larger than that for CuZr5 w-% alloy on AlN (107°±2°). Reactive wetting was initiated with Cr adsorption to the interface possibly assisted by oxygen and thereafter the wetting was controlled by the Cr_2N growth. The final wetting angle represents the wetting of Cr_2N by CuCr1,5 w-% alloy.

6.1.4. AlN – AgZr system

The next studied material combination was AlN – AgZr3 w-% alloy. In this study the wetting experiment for AlN – pure Ag system was not carried out, but in earlier studies the contact value for that system has been determined to be 134° /66/, demonstrating that silver does not wet AlN and that the contact angle is larger than the AlN-Cu contact angle.

Matrix material was changed from copper to silver to study whether the alloy base material has any influence on the wetting and reactivity of Zr on AlN. Thermodynamic calculations in the Appendix predict ZrN formation. The literature review in Chapter 2.5.2 proposes that the change is significant. The binary phase diagram of silver – zirconium system is shown in Figure 6.21

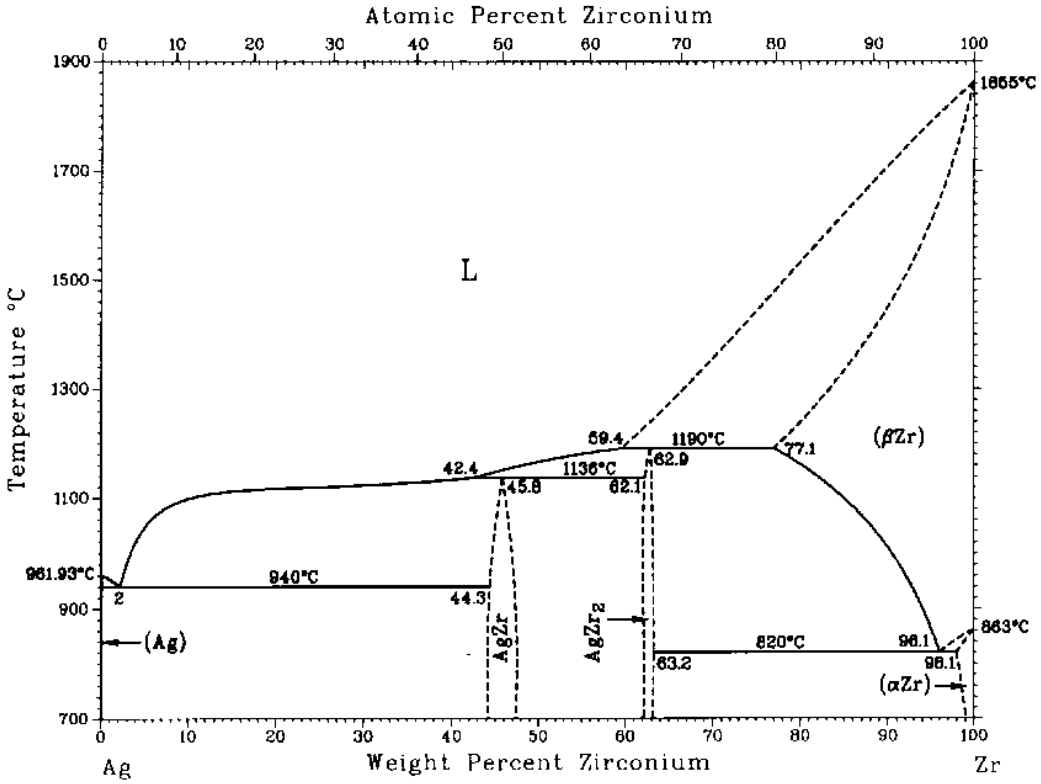

Figure 6.21 Binary phase diagram of Ag-Zr system/99/

The obtained results will be compared with previously reported experiments for varying Zr composition in Ag /66/ and in Cu-Ag /100/ alloy even though different installations used makes it difficult to carry out quantitative comparisons.

Reactive wetting between AlN and AgZr3 (w-%)

The amount of 3 w-% of zirconium was added to silver. Alloy was prefabricated from pure Ag and Zr. Wetting experiment was performed in the alumina tube furnace. The test temperature for AlN – AgZr system was 980°C.

Immediately after the melting of the alloy the initial wetting angle $\theta_f = 58° \pm 2°$ was significantly smaller than in the studied CuZr systems. In first 90 seconds rapid spreading of the droplet occurred with dR/dt = 0.01 mm/s, and there was no sign of disturbing oxide layer. In the second phase of spreading the contact angle decreased down to $15° \pm 2°$ with the spreading rate of $2{,}5 \times 10^{-3} mms^{-1}$. This rate was significantly higher than with CuZr5 (w-%). At the end of the experiment the contact angle started to increase again, which was verified by the decrease of the diameter of the droplet. This is most likely occurring due to the evaporation of silver, which has a high evaporation tendency at 980°C. From the weighed sample mass loss of 19% can be calculated. Contact angle and drop radius vs. time-curves are shown in Figure 6.22. and according to the curves 50 s from the end of the experiment should be neglected. It is obvious from the contact angle vs. time curve that the final contact angle value will remain the same even though the final result is taken at 350 s.

a)

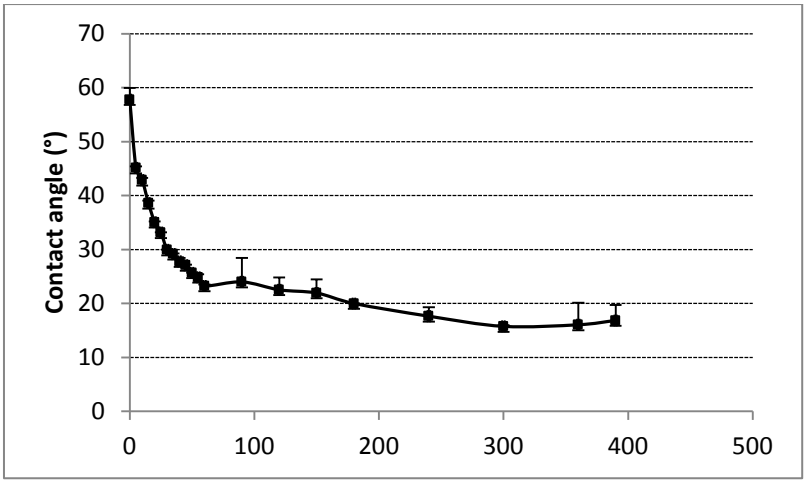

b)

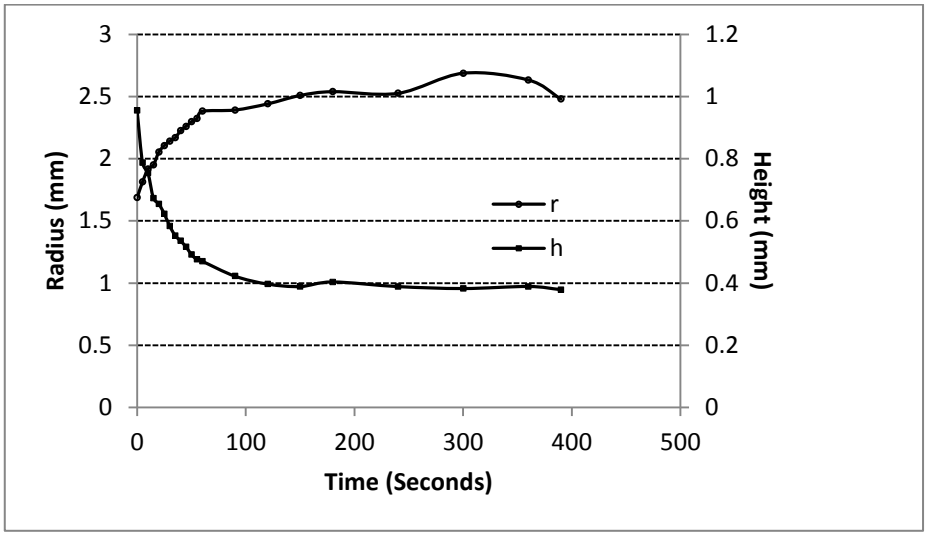

Figure 6.22. The wetting in AlN – AgZr3 (w-%) system: a) contact angle vs. time, b) drop radius and height of drop as a function of time.

Characterisation of AlN – AgZr interface after wetting experiment

The duration of the AlN-AgZr3 wetting experiment and therefore the time for interfacial reactions was about 7 minutes. Figure 6.23 shows a SEM image of the top of the solidified AgZr3 (w-%) drop after the wetting experiment. There are four different areas in the image.

Area at the centre is the topographically highest point of the drop and the solidification structure is visible. EDS analysis shows that this area consists of the original

AgZr3 (w-%) alloy with the oxygen content as high as 18 at-%. Most probably the oxygen is in the form of an oxide, but it is not possible to detect it with the used analysing method. Next to the metallic area is an area where the droplet is covered with needle-like structure (area 2 in the image). Needles are too small to be analysed separately. The spot-analysis gives zirconium as the main metallic element (40 at-%) and smaller amounts of Ag (11 at-%) and Al (11 at-%). The rest consists of oxygen and nitrogen.

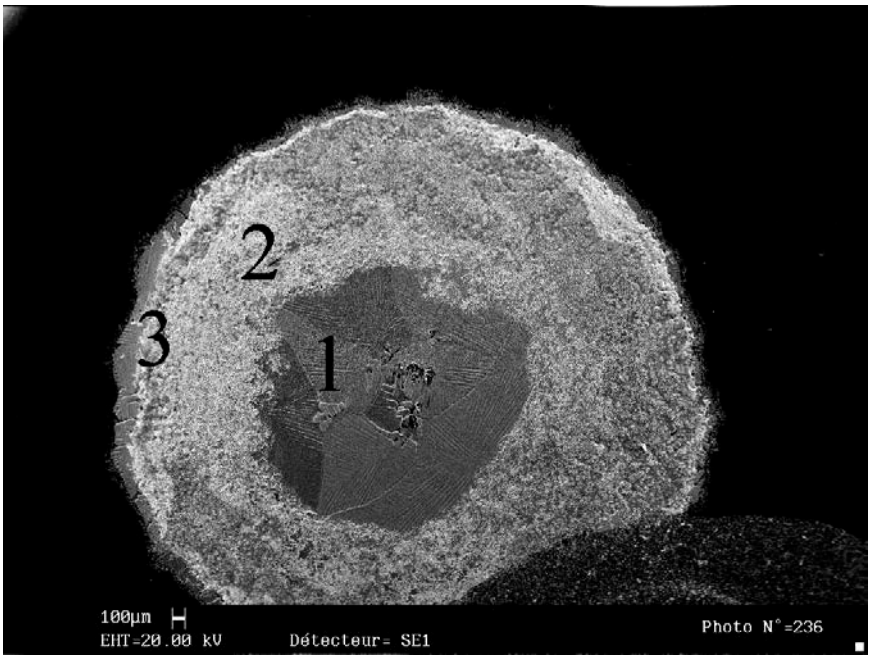

Figure 6.23. Top view SEM image of the solidified AgZr3 (w-%) drop on the AlN surface. Phases: 1) AgZr3 (w-%) alloy, 2) needle-like ceramic, mainly ZrN and ZrO_2 and 3) see Fig 6.24. Surrounding dark area is the original AlN substrate.

The amounts of oxygen and nitrogen in area 2 are 14 at-% and 24 at-%, respectively. All the nitrogen cannot be in the substrate AlN due to the ratio of Al to N; therefore at least some part of AlN must have reacted to ZrN and Al is either dissolved in Ag or it has reacted with Zr to form aluminides. Of all these elements, zirconium has the highest affinity to oxygen and most probably all the detected oxygen is in the ZrO_2 phase.

Edge area no. 3 is magnified in Figure 6.24. Several different phases are visible. Phase no 1 is the needle-rich phase analysed in the previous chapter. One needle (no

4) is visible at the de-wetted zone (no 3). The analysis from this detached needle area suggests that the needle is ZrO_2 located in the reacted area.

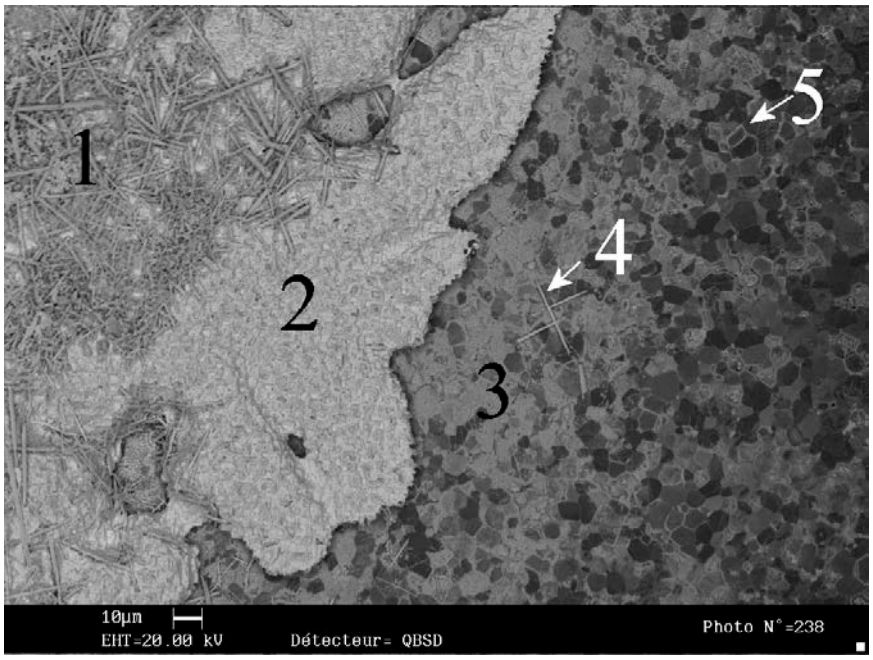

Figure 6.24. A magnified SEM -image from the edge area in Fig. 6.23. Phases: 1)ZrO_2, 2) AgZr3 (w-%) with oxygen, 3) reacted substrate area with ZrN-AlN mixed structure after the withdrawal of the triple line due to the evaporation of silver 4) single ZrO_2 needles on the surface of reacted ceramic and 5) high reactivity shown with larger Zr contents found in the grain boundaries of AlN.

The lightest uniform phase (no 2 in Fig. 6.24.) has the composition of the original AgZr3 (w-%) with oxygen content similar to centre area (16 at-%). Due to the evaporation of silver during the wetting experiment the area no 3 is disclosed and the reaction layer is left on the top of the original AlN substrate. At some points there is strong reactivity visible at grain boundaries. In the AlN substrate there is also a YAG binder phase which reacts with Zr, as was discussed earlier in the case of CuZr – AlN system. Since the reaction layer is thin at the edge area, it is not possible to distinguish clearly the differences between the non-reacted substrate and the reaction layer. The oxygen content of the reaction layer is smaller than that of ZrO_2 needle and therefore the Zr probably exists as nitride, oxynitride or aluminide on the top of AlN substrate. The detected silver content is negligible.

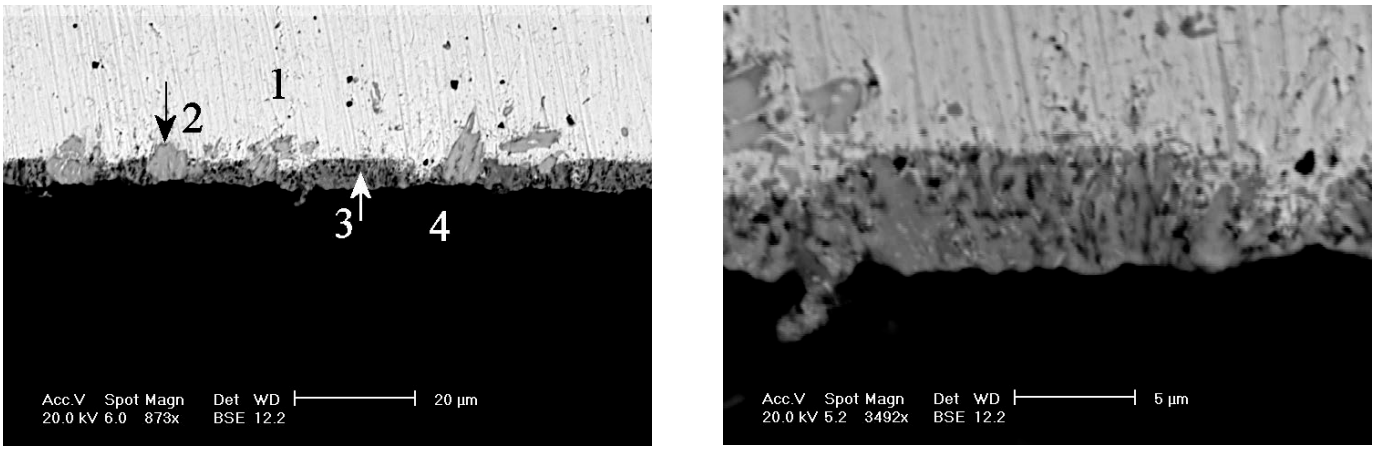

a) b)

Figure 6.25 SEM-images from the interface between AlN and AgZr3 (w-%) after the wetting experiment: a) phase 1 is the AgZr3 (w-%) alloy, phase 2 and 3 are different phases at the interface and 4 is the AlN substrate, b) larger magnification of the phase 3.

Analysis of the cross-section after 7 minutes experiment shown in Figure 6.25 indicates the existence of two different phases at the interface. The total thickness of reaction layer is 5µm. Since the theoretical equilibrium thickness is 32µm it is assumed that the reaction time is not sufficient to reach equilibrium. Phase number 2 in the image is close to the intermetallic composition of Zr_2Ag which must have been formed during the solidification stage before the solidus temperature. The fact that it is embedded into reaction layer suggests that it was formed either simultaneously or even before the reaction layer. These precipitates can be found mostly at the interface but also in the matrix alloy. More heterogeneous phase number 3 is ZrN phase with residual AlN and Ag metal. At the points touching the substrate binder phase, there are significant amounts of oxygen in the composition. This phase is most likely YAG binder reacted with Zr to form ZrO_2 as was found in the CuZr - AlN system.

The influence of matrix metal on the reactive wetting was significant. AgZr reacted much faster than the Zr alloy with copper matrix. Koltsov et al /66/ suggested this to depend on the thermodynamic activity of Zr in the alloy which caused a difference in the non-stoichiometry of the formed ZrN_{1-y} alloy. The determined activities in the article varied as follows: $a_{(Zr)Ag} : a_{(Zr)Ag,Cu} : a_{(Zr)Cu} = 1 : 0,3 : 0,05$. The difference in the surface tension of silver (903 dyn/cm) to copper (1360 dyn/cm) is significant but

possibly the interfacial phenomena have the largest influence on the wetting behaviour. Interesting difference is also the behavior of oxygen in the copper and silver matrices. With the copper matrix the drop is oxidized and spreading pinned by the blocking oxides, while with the silver matrix drop is not at least visibly oxidized and pinning doesn't occur. Even though the ZrO_2 formation is the most probable process there seems to be differences to it. This question is interesting and should be further studied in future.

6.3. Experiments on silicon nitride

Same studies were carried out with another common nitride ceramic, the silicon nitride Si_3N_4.

6.3.1. Wetting and reactivity between Si_3N_4 and copper

With silicon nitride the first experiment was carried out with pure oxygen free copper in horizontal metallic furnace. The initial contact angle was 122° ± 2°. This value is slightly lower than the value observed on SiO_2 (130°) /101/. The molten Cu-drop seemed to migrate on Si_3N_4 surface as was also reported by Tomsia and Pask /69/. During the experiment the contact angle value oscillated between 112° - 122°. This kind of oscillation can be caused by possible reaction and gas bubble formation at the interface as observed with Ni-Al_2O_3 by Labrousse /102/. In this case the reaction would be the decomposition of Si_3N_4 and dissolution of silicon into copper and the release of nitrogen gas into atmosphere since it doesn't dissolve in copper:

$$Si_3N_4 + Cu \Rightarrow Si_{[Cu]} + 2N_2 \uparrow \qquad (24)$$

After 30 minutes experiment the drop was lightly adhered to the substrate, and evidence of any reactivity was searched for from the substrate and from the solidified drop. Slight change of colour and traces from a migrating drop were visible on substrate surface, and the amount of Si in the bottom surface copper drop was analysed to be between 0,3 – 0,6 at-%. It is likely that if the experiment had lasted long enough

wetting might have occurred due to the increasing amount of silicon in copper, since the contact angle of Si on Si_3N_4 is 48° /71/. Despite of its significance this kind of a study was not carried out since it was considered to be outside the scope of this work.

6.3.2. Si_3N_4 – CuZr system

The influence of zirconium on wetting was studied with Cu-Zr alloys of 1 w-% and 5 w-% Zr.

Wetting between Si_3N_4 - CuZr1 (w-%)

Wetting experiment for CuZr1 w-% on Si_3N_4 was carried out in the horizontal metallic furnace with *in-situ* alloying. All possible precautions were taken to prevent oxygen from disturbing the experiment. The initial contact angle was 163° ± 2°, and after 70 minutes the final angle was 146° ± 2°. These angles are even larger than the contact angle of pure copper on Si_3N_4. Throughout the experiment there was a continuous oxide layer on the surface of the drop which caused a propagation barrier at the triple line front. The experimental conditions were not able to distort the layer and that way promote the spreading. Therefore these contact angles are apparent and not real. The wetting curve is shown in Figure 6.26. Spreading kinetics is evaluated in the next subchapter together with CuZr alloy with 5 w-% Zr.

a)

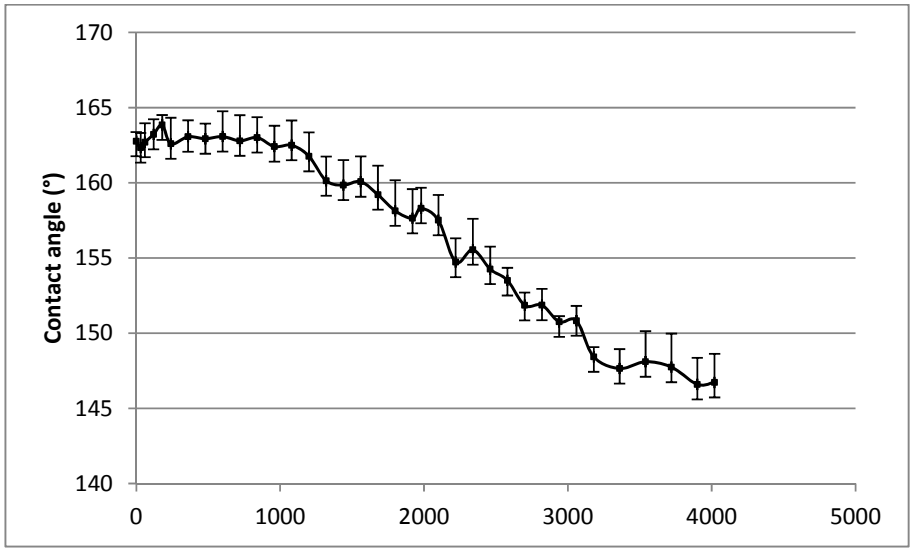

b)

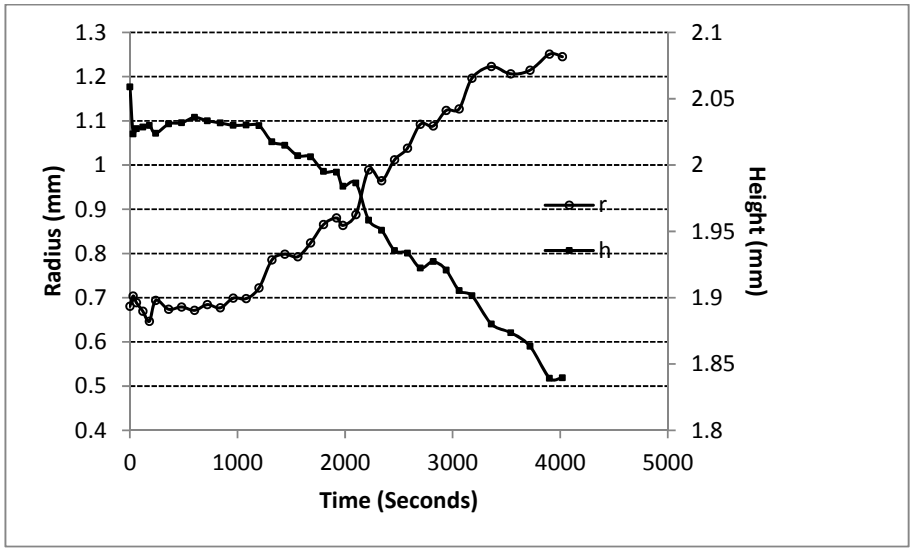

Figure 6.26. Results of the wetting experiment on Si_3N_4 – CuZr1 (w-%) system a) Si_3N_4 – CuZr1 (w-%) contact angle vs. time wetting curve and b) the drop diameter and height development during the experiment.

Reactive wetting between Si_3N_4 - CuZr5 (w-%)

The amount of zirconium in the CuZr alloy was increased to 5 w%, and wetting test was carried out as previously. Now the initial contact angle was 152° ± 2° and there was again an oxide layer at drop surface. It was, however, not continuous and

therefore spreading was able to occur. Other factor enhancing the reactivity is the larger amount of Zr, i.e., higher activity of liquid $Zr_{[Cu]}$. Final contact angle was 107° ± 2° after 50 minutes experiment. Kinetic values from this experiment are presented in Figure 6.27 and Table 6.5. Discontinuities in the spreading are assumed to be due to the local disruption of the ZrO_2 layer at the triple line. Spreading rate varies: it is 2,7 x 10^{-3} mm/s directly after the formation of the initial contact angle, then it stops almost completely in the second stage. In the third stage there is a drop of nearly 20° in the contact angle value with 1,4 x 10^{-3} mm/s and then the spreading continues to final contact angle value with the rate of 1,1 x 10^{-4} mm/s. It is not possible to make conclusions from the spreading of oxidized drops since the oxide deviates the spreading from the ideal behaviour.

Table 6.5. The spreading behavior of CuZr1 (w-%) and CuZr5 (w-%) on Si_3N_4 in the wetting experiments.

	1st stage dR/dt	duration	2nd stage dR/dt	duration	3rd stage dR/dt	duration	4th stage dR/dt	duration
w-%	mm/s	s	mm/s	s	mm/s	s	mm/s	s
CuZr1	0	1080	$1,9*10^{-4}$	3000				
CuZr5	$2,7*10^{-3}$	150	0	450	$1,4*10^{-3}$	480	$1,1*10^{-4}$	1800

Major differences in wetting behaviour exist between the two CuZr alloy concentrations. For CuZr1 (w-%) there is a linear regime where the triple line propagates slowly indicating the existence of some kind of reaction. The difference to the experiment on AlN is large. Now the final contact angle is not indicating the presence of metallic reaction products as was the case with AlN where the contact angle was close to that of 5-w% alloy. With Si_3N_4 the adsorption of Zr to the substrate and the driving force for new layer formation are obviously not as strong or the oxide layer on drop surface is thicker in the experiment with Si_3N_4.

On the other hand the behaviour of CuZr5 (w-%) in reactive wetting is very similar on both nitride ceramics. There are linear regimes in the triple line propagation as a function of time. The spreading with decreasing rate is not found in the curves and

therefore the assumption is similar as with AlN: the the reactive spreading is controlled by the rate of the occurring reactions and not as much by the diffusion of the reactive elements to the triple line. This will be discussed further after the characterisation of the interfacial layers.

a)

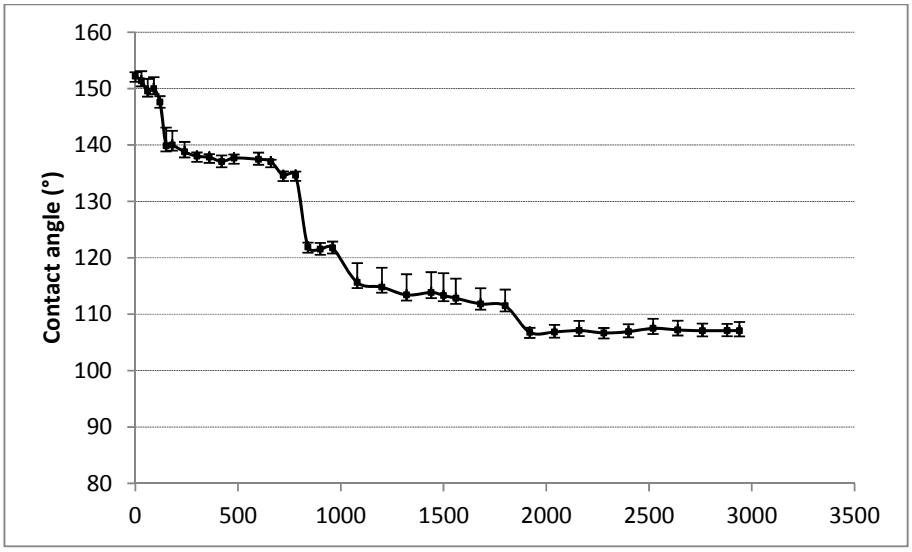

b)

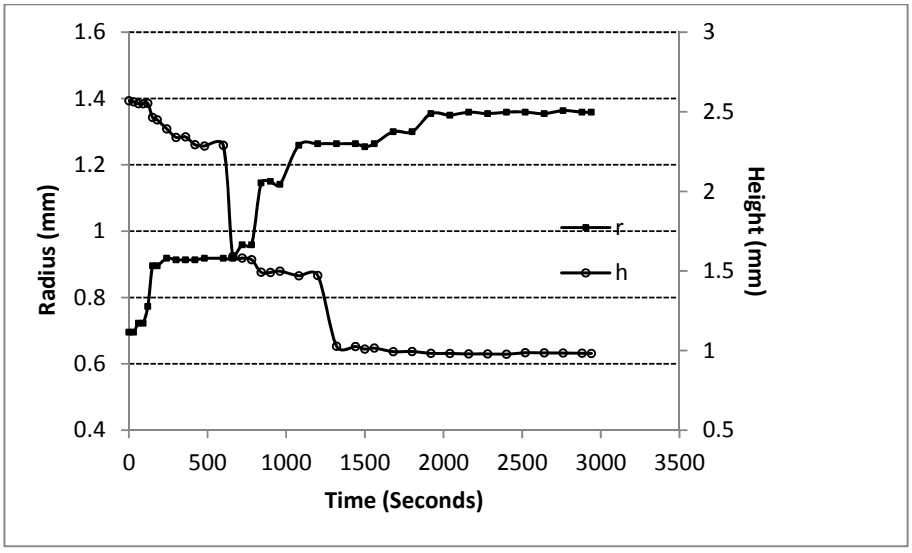

Figure 6.27. Wetting experiment with the Si_3N_4 – CuZr5 (w-%) system: a) contact angle as a function of time, b) the diameter and height of the drop as function of time in the experiment.

Characterisation of Si_3N_4 – CuZr5 (w-%) interfaces

Adherence of the drop to the substrate was strong indicating reactivity between the substrate and the alloy. A SEM image of the interface is in the Figure 6.29. A white layer can be seen at interface (phase no.3), but to confirm that it is not the Cu_5Zr eutectic alloy, elementary mapping was carried out. From the Zr distribution in the mapping shown in Figure 6.29 it is possible to state that the intensity of Zr in the eutectic is lower than in the reaction layer. This indicates that Zr is adsorbing to the interface in large extent. The reaction of the interface starts directly after the melting of the alloy by the formation of a new compound. From the literature it is predicted to be ZrN formation even though it is thermodynamically not the most stable of all possible compounds as is shown in Appendix. The formula for this reaction is:

$$4Zr_{[Cu]} + Si_3N_4 \Rightarrow 4ZrN + 3Si_{[Cu]} \qquad (25)$$

EDS analysis taken from the interface showed the existence of nearly continuous ZrN layer, but also oxygen was found with varying concentrations. It is known from the literature that the adsorption of the reactive Zr to the interface can actually occur as oxygen-rich clusters Zr-O. Therefore, since a lot of oxygen was found, the layer phase consists either of Zr-oxynitride or of the mixture of ZrO_2 and ZrN. Zirconium oxynitride formation is identified in the literature as was mentioned in the case of AlN /91, 92/. On the other hand the elementary mapping does not indicate heavy oxygen concentration at the interface and therefore the layer can be concluded to consist mostly of ZrN.

The thickness of the reaction layer was between 0,2 –0,4 μm after 50 minutes experiment and therefore a more accurate identification of layer composition with SEM/EDS is not possible. The reaction layer thickness was exactly the same as was theoretically calculated for ZrN formation. In the study carried out by Nakao et al /64/ the CuZr10 (w-%) reaction layer formation with Si_3N_4 was studied at 1373 – 1473 K. In this study the formation of both ZrN and Zr_5Si_3 compound was identified.

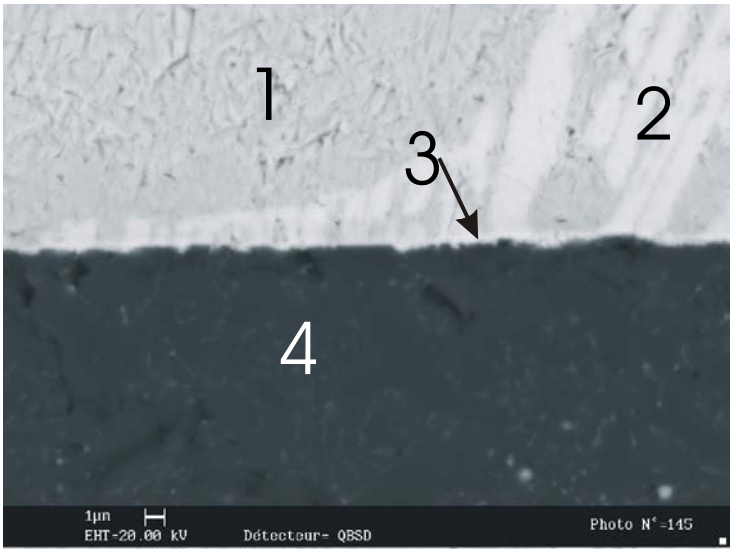

Figure 6.28. A SEM image of the interface in the system Si_3N_4 – CuZr5 (w-%) containing the following phases: 1) Cu with dissolved Zr, 2) Cu_5Zr/Cu eutectic alloy, 3) reaction layer and 4) substrate Si_3N_4 with Al_2O_3/Y_2O_3-binder phase.

Due to the spreading rates and the shape of the wetting curve as a function of time it was predicted previously that the actual reaction at the interface controls the wetting. After verifying that the interfacial reaction layer is ZrN, which can be estimated to grow very slowly, it is possible to confirm that the wetting - controlling mechanism is the ZrN formation by the reaction shown in equation 25.

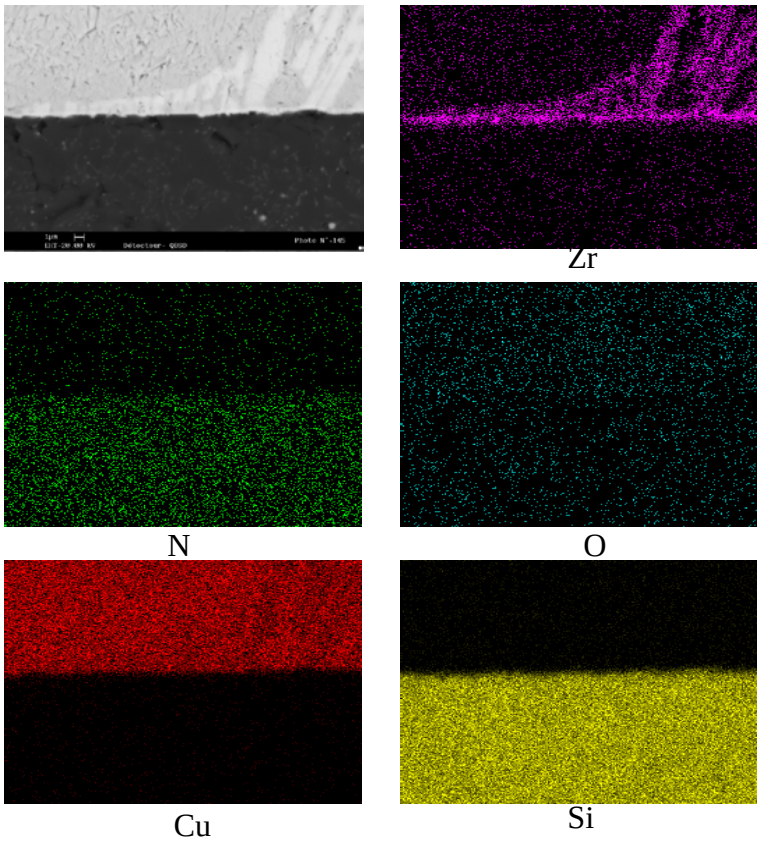

Figure 6.29. Elemental distribution maps of the interface in the system Si_3N_4 – CuZr5 (w-%) after the wetting experiment. The place for mapping and the magnification are the same as in Figure 6.28.

6.3.3. Si_3N_4 – CuCr system

Characterization of Si_3N_4 – CuCr1,5 (w-%) interface

After the experiment the drop was strongly adhered to the substrate. A rather thick interfacial reaction layer was found at the interface in the characterisation. With support of the chemical analysis carried out with SEM it is assumed to be formed according to the reaction shown in equation (26):

$$8Cr_{[Cu]} + Si_3N_4 \Rightarrow 4Cr_2N + 3Si_{[Cu]} \qquad (26)$$

The formed interfacial layer is shown in Figures 6.30 and 6.31, where two different zones in the layer can be distinguished. Both parts of the layer are Cr_2N with variable amount of oxygen. Si_3N_4 inclusions in the lower part of layer, their absence from the upper part and the irregular shape of substrate surface suggest that the reaction layer has grown to both directions, and it can be assumed that the original substrate surface follows the interface between lower and upper layers. White inclusions in the reaction layer are copper captured inside the forming ceramic reaction layer. The results do not enable the conclusion whether the oxygen is dissolved in the Cr_2N phase or whether it forms an oxynitride phase. The existence of several chromium oxynitrides has been identified in literature /103, 104/. The thickness of the formed layer after 50 minutes was 10 μm at the center of the drop and 3 μm near the triple line The difference to calculated theoretical thickness ($1x10^{-7}$ μm) is significant implying to non-equilibrium condition in reaction.

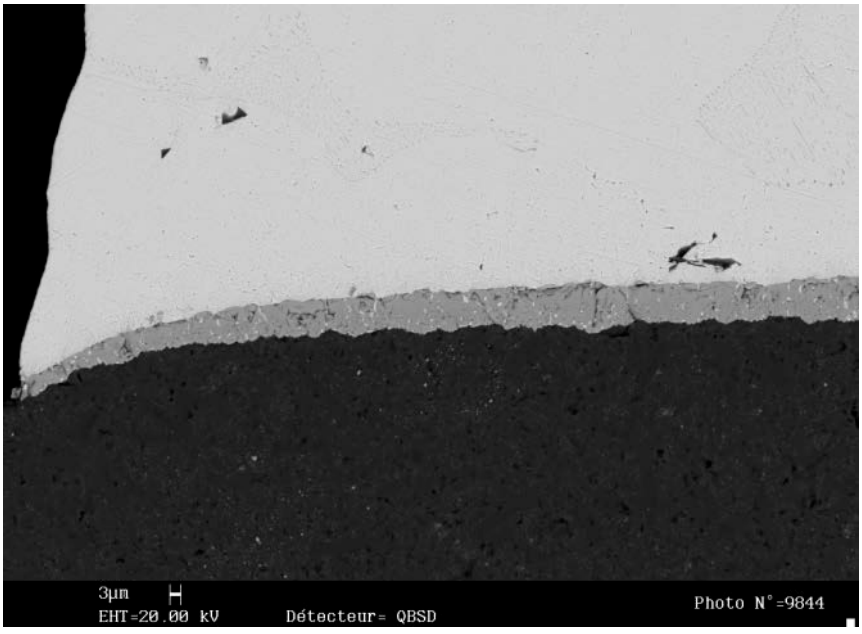

Figure 6.31. A SEM-image of the interface and the triple line in the system Si_3N_4 – CuCr1,5 (w-%) after the wetting experiment.

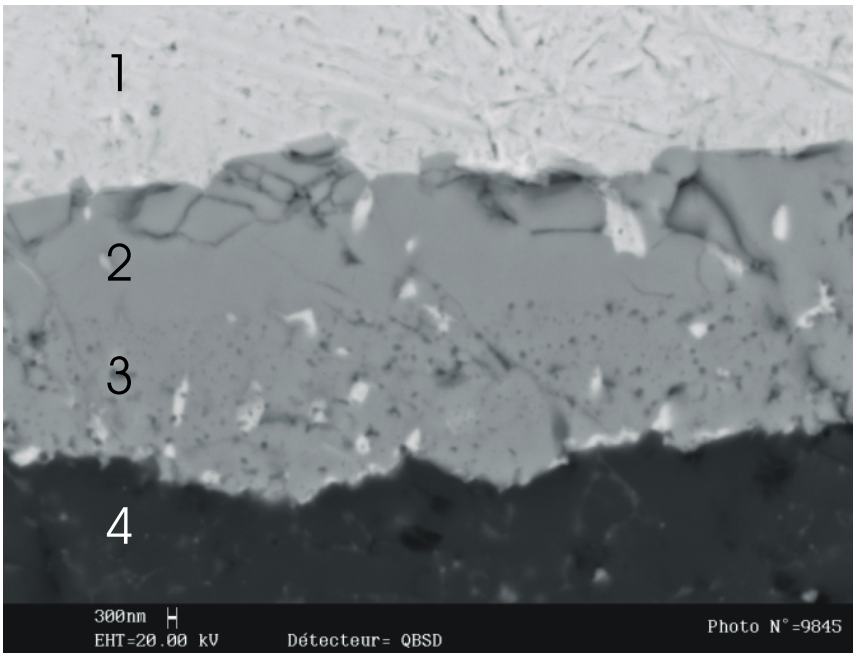

Figure 6.32. A SEM image of the interfacial layer in fig. 6.32 with the following phases: 1) CuCr alloy, 2) upper part of reaction layer, 3) lower part of reaction layer with Si_3N_4 inclusions and 4) substrate.

The beneficial influence of Cr on the wetting of Cu may be attributed to the formation of the metal-like Cr_2N at the interface. Nakao et al studied the reaction layer growth in brazing trials between Si_3N_4 and CuCr5 w-% alloy at 1573 K in /64/ and concluded that solid state reactions between Si_3N_4 and Cr cause the growth of reaction layer toward the substrate and the reactions between N and Cr are taking place when the reaction layer grows towards the Cu-rich drop. In their 60 min experiment the reaction products were Cr_2N, CrN and $CrSi_2$.

The difference between experiments with Zr and Cr as alloying elements in Cu is visible from the thickness of the reaction layer. The thickness of the Cr_2N layer is 10 μm, while the ZrN layer thickness was only 1 μm after experiments with the same duration. One explanation to this is that the diffusion of Cr and N through Cr_2N layer is easier than the diffusion of Zr and N through the ZrN layer. Oxygen was found with EDS analysis in some parts of the reaction layer. The composition of such points was found to be in the range corresponding to the compounds $Cr_3(ON)_2$ – $Cr_5(ON)_4$. Since the accurate phase structures cannot be analysed in the reaction layer it can be stated

that the layer consists mostly of Cr_2N with varying amount of chromium oxide dissolved or mixed to this layer.

The spreading mechanism can be stated to be controlled by the nitride forming reaction and not the diffusion of Cr to the triple line. Chromium diffusion is fast under the conditions of the experiment and also the spreading curve shape indicates it. The reaction layer thickness which decreases from the centre of the drop/substrate interface towards the triple line acts as an evidence for the reaction rate controlled spreading.

Reactive wetting between Si_3N_4 and CuCr1,5 (w-%)

The influence of chromium on the wetting between Cu and Si_3N_4 was studied with a CuCr1,5 w-% alloy. The sessile drop experiment was carried out for this system in horizontal metallic furnace at 1100 °C. The initial contact angle after melting of the drop was 123° ± 2°, which is very close to the contact angle of Cu on Si_3N_4. Some oxide particles were observed at the surface of the drop throughout the entire experiment but still the drop was able to spread until the final contact angle value of 75° ± 2° was reached. Time of spreading was about 60 minutes. The propagation of spreading is presented in Figure 6.33. For the first stage 0-720 s the spreading rate is $1,7*10^{-4}$ mm/s and for the rest of the experiment the average rate is approximately $5,4*10^{-4}$ mm/s. The reproducibility of the experiment was rather poor since in another experiment the initial and final contact angles were 115°± 2° and 90°± 2°, respectively, and the spreading time was 30 minutes. Despite this scatter in the results it can be concluded that small additions of Cr cause a significant decrease, by several tens of decrees, in the contact angle of Cu with Si_3N_4 leading to a transition from non-wetting to moderate wetting in this system. There are some differences as compared with the CuCr1,5 (w-&) wetting on AlN. The alloy CuCr1,5 (w-%) can be stated to wet Si_3N_4 with contact angle 75°± 2° while the angle was 113°± 2° on AlN.

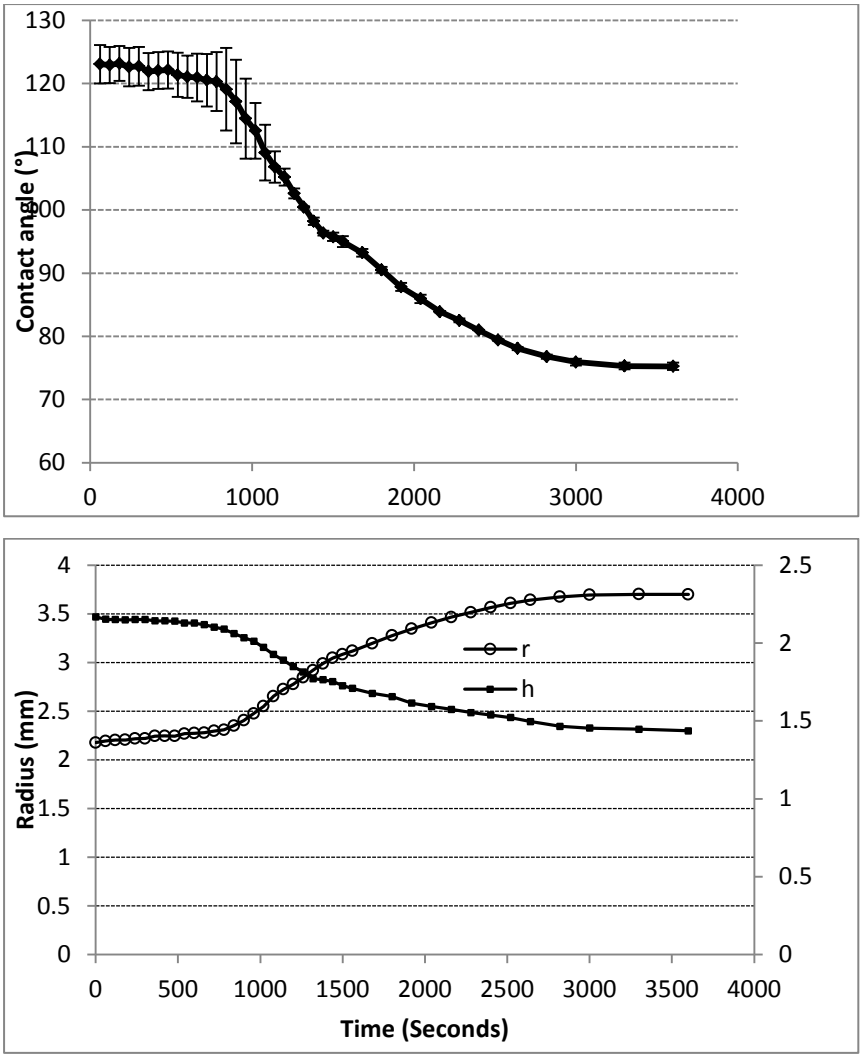

Figure 6.33. Wetting angle as function of time in the Si_3N_4 – CuCr1,5 (w-%) system at 1100°C (upper part). The lower part shows the radius and the height of the drop as a function of time during the wetting experiment.

6.3.4. Si_3N_4 – AgZr3 (w-%) system

Reactive wetting between Si_3N_4 and AgZr3 (w-%)

For the next experiments the base metal was changed to silver which itself is non-wetting, with contact angle on Si_3N_4 132° as reported in /105/. Addition of 3w-% zirconium was made *in-situ* and wetting test performed as before with AlN in alumina tube furnace at 980°C. The propagation of wetting with time is presented in Figure

6.34. After complete melting of the alloy the initial contact angle was 60° which indicated from the beginning different behavior as compared with copper matrix. Spreading was rapid for the first 20 s the rate being as high as 3,6 x 10^{-2} mm/s and the final contact angle corresponds almost perfect wetting. The spreading rate after initial 20 s was 4,4 x 10^{-3} mm/s. The duration of the experiment was six minutes. Deviations from continuous spreading occurred also in this experiment. In comparison with the same experiment on AlN it was noticed that with Si_3N_4 the final wetting angle was nearly 0° while with AlN it was 15°.

Characterisation of Si_3N_4 – AgZr3 (w-%)

The cross-section of the solidified AgZr drop at the interface is shown in Figure 6.35. Figure 6.36 is taken at the withdrawn triple line. The withdrawal is either due to the shrinkage during the solidification or due to the significant evaporation of the alloy in the experiment.

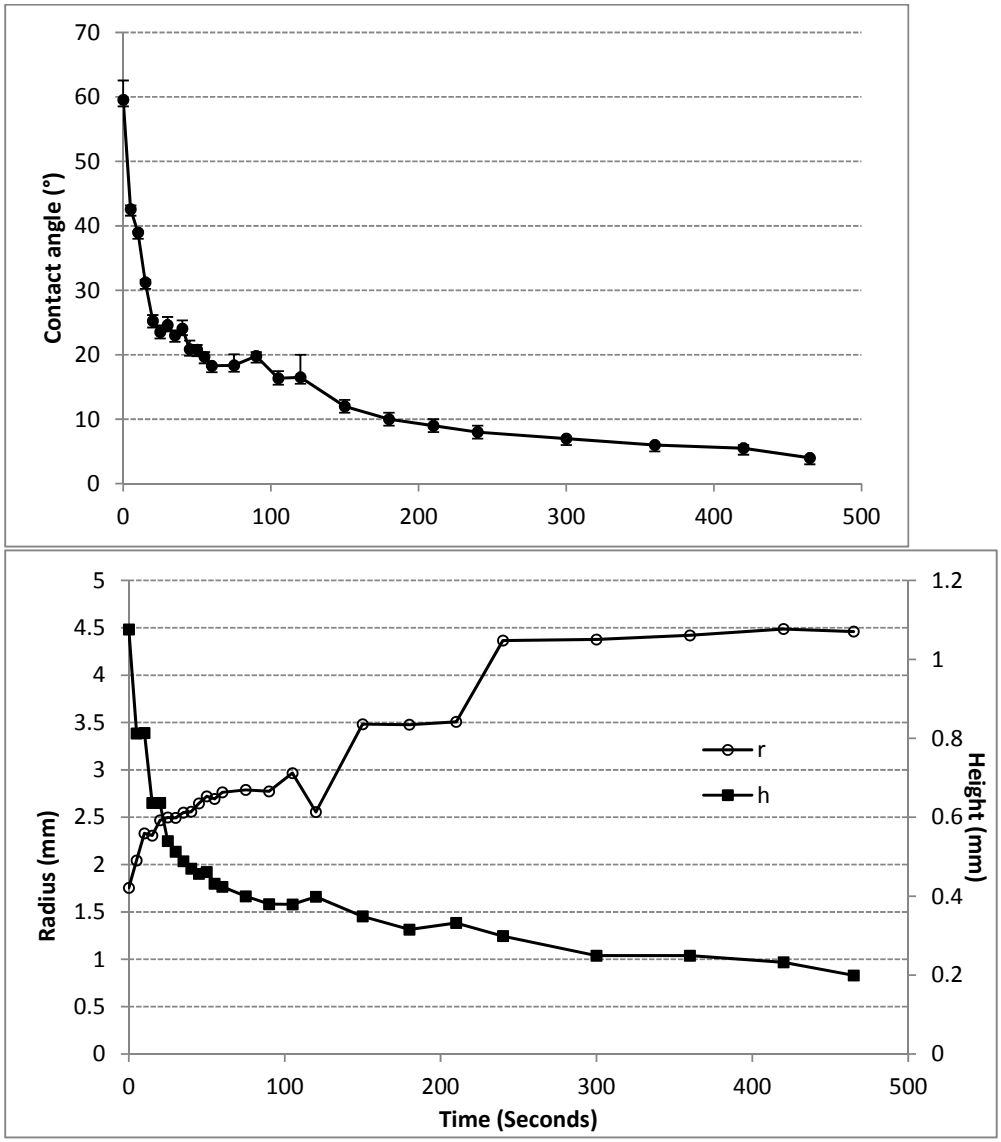

Figure 6.34. The propagation of wetting with time in the Si_3N_4 – AgZr3 (w-%) system. The upper part of the figure represents the contact angle as a function of time and the lower part shows the time dependence of the drop radius and height respectively.

This behaviour is called de-wetting. There is an obvious reaction layer at the interface with thickness varying between 1,5 μm and 2 μm. The actual reaction layer thickness is significantly larger than was the calculated theoretical equilibrium thickness of ZrN (15nm) in Appendix. This can be either an indication of the existence of other layer or non-equilibrium condition. EDS analysis of the layer taken after de-wetting shows that the reaction zone consists of two different areas in the interface. The first one

which seems to be ZrN, is located mostly on the surface of the silicon nitride sub-substrate. The other phase seems to be rich in Zr and Si closest to Zr_5Si composition. It is located on the side of the alloy. It can also be noted that the oxygen concentration in the two layers is also significantly high (23 at-%) in ZrN rich layer and smaller in the silicide, (3-4 at-%). It was not possible to make conclusions on any other actual phases at the interface than the ZrN due to the large spot size of EDS analysis which resulted in large variations in the elemental compositions.

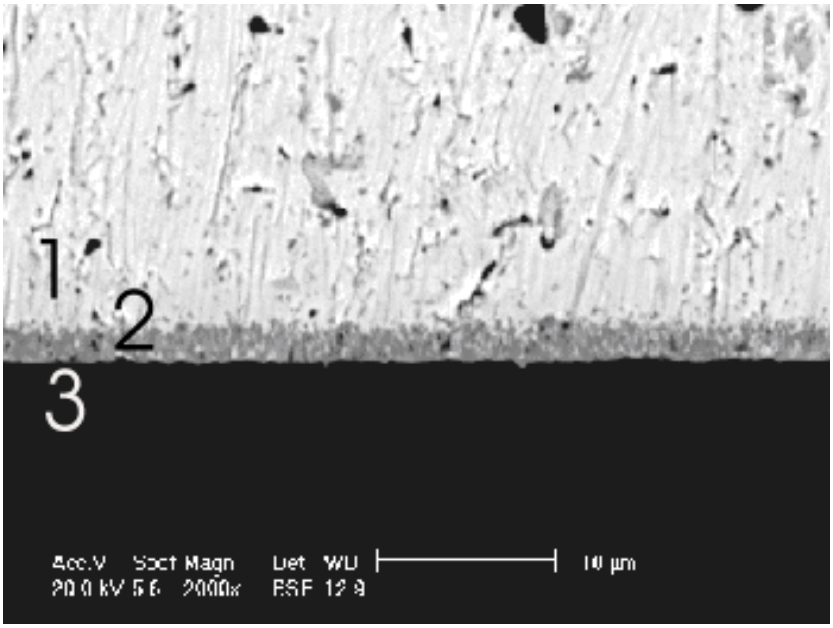

Figure 6.35. The interface after wetting experiment between Si_3N_4 and AgZr alloy. The show phases are 1) AgZr3 (w-%) alloy, 2) reaction layer at the interface and 3) Si_3N_4 substrate. SEM image, magnification 2000X.

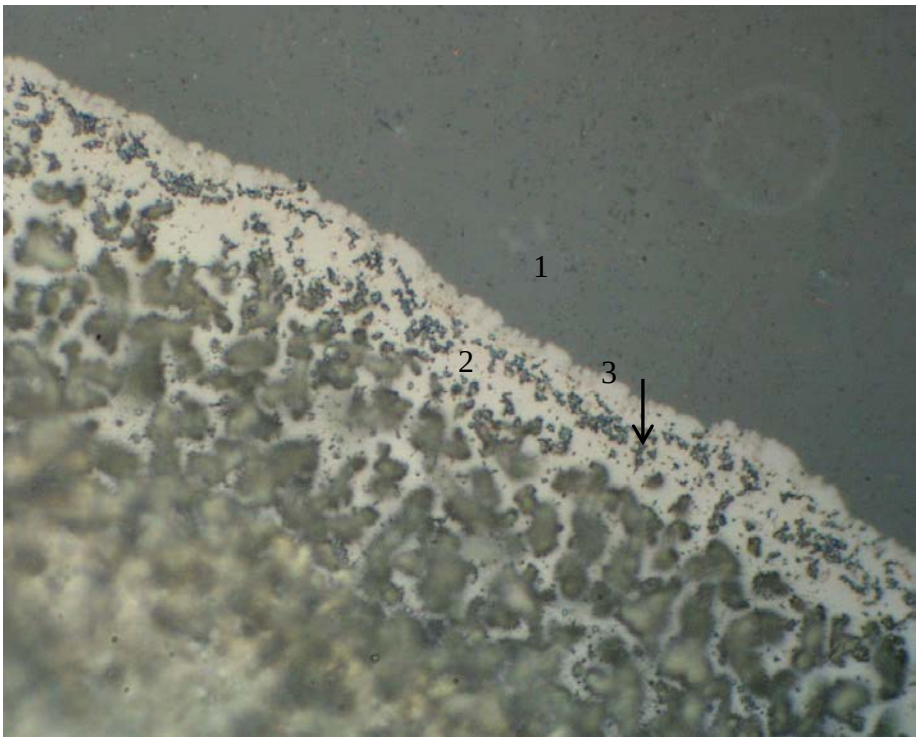

Figure 6.36. Top view of the triple line and the de-wetted area in the Si_3N_4 –AgZr alloy wetting experiment:.1) Si_3N_4 substrate, 2) ZrN phase (white), 3) Zr_3Si metal alloy. Optical micrograph, magnification 100X.

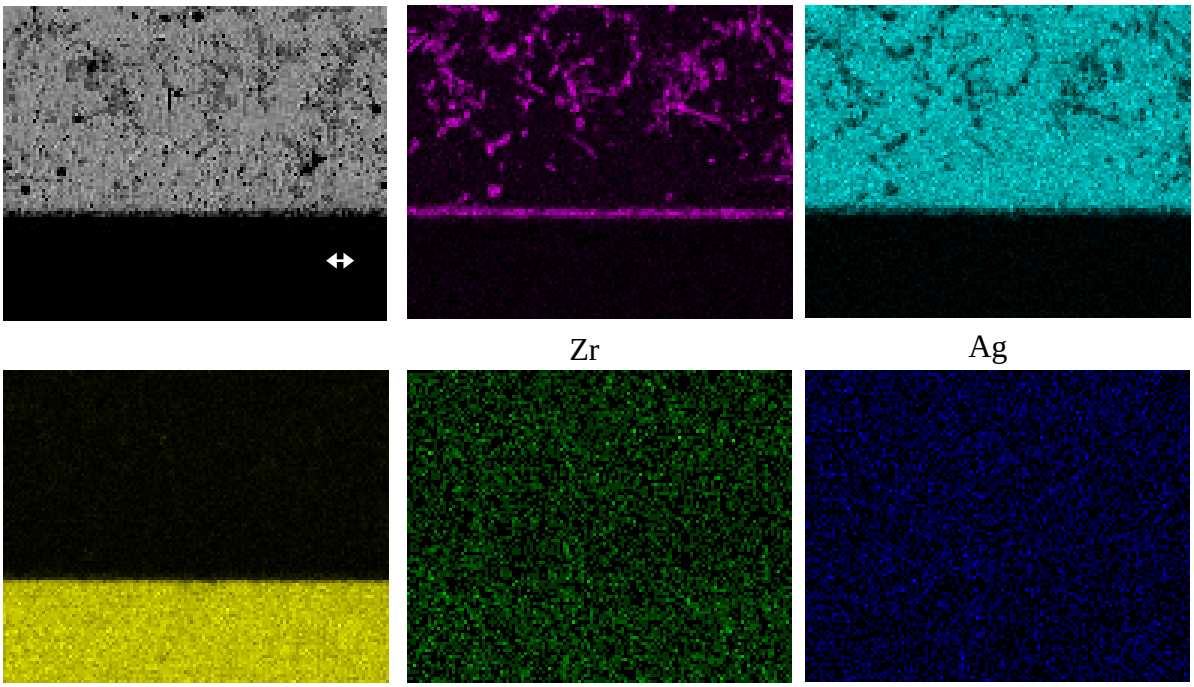

Figure 6.37. Elemental distribution mapping of the interface after the wetting experiment with AgZr3 (w-%) on Si_3N_4

The influence of zirconium on wetting was stronger in the silver alloy than in the copper alloy. This can be caused by different zirconium activity in silver as compared with that in copper as was the case with AlN. Better wetting of AgZr would indicate that the activity of Zr in Ag is markedly higher than in Cu. Activities are known to be different: $a_{(Zr)Ag} : a_{(Zr)Cu} = 1 : 0{,}05$, which supports the assumption. It is reported by Niessen et al./106/ that the partial enthalpy of solution at infinite dilution of Zr in Cu is more negative than in Ag (-110 kJ/mol against –87 kJ/mol). The thickness of the reaction zone for the CuZr5 (w-%) alloy is by one order of magnitude smaller than the thickness of this zone for the AgZr3 (w-%) alloy although both the experimental temperature and time in the AgZr3 (w-%) case are significantly lower than in the CuZr5 (w-%) case (960°C against 1100°C and 10 minutes against 50 minutes). The compound Zr_3Si seems also to form with the Ag matrix but not with Cu matrix.

The comparison of the reaction layers between AlN and Si_3N_4 shows that there is a difference. The needle-like oxide layer which was seen with AlN substrate was not present with Si_3N_4 even though the oxygen amounts in the analyses are almost the same. The formation of ZrO_2 seems to be different with different ceramics. More detailed analysis of this behaviour was not carried out. The wetting angle on AlN was 15° and on Si_3N_4 near 0°, which may be due to the differences in ZrSi and ZrAl formation. This could also influence the ZrO_2 phase formation. Further verification of these phenomena would form a good subject for future studies.

Chapter 7. CONCLUSIONS

Wetting experiments with CuZr, CuCr and AgZr alloys were carried out on AlN and Si_3N_4 ceramics. The desirable properties of these metals and ceramics make them good candidates for demanding applications, where better performance of materials is constantly looked for. Joining of different materials is needed and reactive additions to otherwise inert metals are often an easy solution in cases where strong bonding is needed. Reactivity will guarantee the bonding even though wetting may not occur. Other interesting case is in materials manufacturing where the wetting and reactivity determine the possibilities to use different high temperature materials with highly reactive metals.

Copper and silver do not wet aluminum nitride or silicon nitride ceramic under the studied conditions. Addition of zirconium to copper or silver, and chromium to copper improves wetting due to the formation of metallic nitrides, ZrN or Cr_2N at the ceramic – metallic interface. On AlN material

the wetting angle below 90° was reached only with AgZr3 (w-%) alloy. None of the studied reactive alloying element additions to copper were able to wet AlN. On Si_3N_4 good wetting was obtained with chromium addition to copper and zirconium addition to silver. All the wetting results are given in Table 7.1.

Table 7.1. Measured final contact angle values and revealed compounds in wetting experiments.

Metal alloy	Substrate	Contact angle θ_f	Reaction Products
Cu	AlN	127°±2°	-
Cu	Si_3N_4	122°±2°	$Si_{[Cu]}$
CuZr1	AlN	116°±2°	ZrN
CuZr1	Si_3N_4	146°±2°	Not analysed
CuZr5	AlN	107°±2°	ZrN
CuZr5	Si_3N_4	107°±2°	ZrN
CuCr1,5	AlN	113°±2°	Cr_2N
CuCr1,5	Si_3N_4	75°±2°	Cr_2N
AgZr3	AlN	15°±2°	ZrN
AgZr3	Si_3N_4	4°±2°	ZrN

The high affinity of Zr and Cr to oxygen and consequent oxide formation can cause apparent contact angles as high as 150° due to the formation of oxide layers on the surface of the molten alloy which inhibits wetting. As a consequence the wetting in these kinds of systems depends strongly on furnace atmosphere and on the content of oxygen in the initial alloy and in the ceramic. Oxygen generally helps the adsorption of reactive elements to the interfaces. It also decreases the surface tension of metal-oxygen solutions. With AlN and Si_3N_4 the surfaces are in practice always contaminated by oxygen in air. Depending on the oxygen partial pressure in the wetting experiment atmosphere these experiments will be markedly influenced by the behavior of oxygen on the substrate surface. With both AlN and Si_3N_4 the contaminated layers were to some extent de-oxidized and final contact angles were different from those of Al_2O_3 and SiO_2. Still in some cases in this study the reaction layers contained large amount of dissolved oxygen which most likely has some influence on the results.

Differences in behavior between the matrix metals copper and silver was concluded to arise from the different activities of Zr in Cu and Ag varying with the ratio 0,05 : 1. This variation causes non-stoichiometry in the formed $ZrN_{(1-y)}$ reaction product and therefore also variation to wetting. The differences between alloying elements Zr and Cr on the other hand were found to arise from different stabilities of their oxides, different activities in copper and different diffusion coefficients of their atoms in their nitrides. Zirconium has more stable oxide, higher activity in copper but a much lower diffusion rate in its nitride than chromium. The faster kinetics of chromium reactivity resulted finally in better wetting properties and thicker reaction layers at metal-substrate interface.

Ceramics AlN and Si_3N_4 had in some cases similar wetting and reactivity properties. This occurred when the same interfacial reaction products were found in the reaction layers and no other phases were formed at the interface. Silicon nitride as well as many Zr – silicides are thermodynamically more stable than AlN and aluminium silicides. An example from this was seen when in the case of Ag-based metal alloy the Zr –silicide formation promoted the wetting. It can be concluded that Si_3N_4 is more easily wetted and more reactive than AlN with the studied metal alloys.

From the studied alloys only AgZr alloy could really cause wetting on both AlN and Si_3N_4. The alloy AgZr is therefore best suitable for brazing AlN and Si_3N_4 to other materials. With other combinations the wetting and reactivity could be enhanced by increasing the active metal concentration or the temperature. When considering the liquid metal handling with the studied alloys Si_3N_4 can be used only if the reactivity is not a crucial factor, or if it appears that the formed reaction product layer is dense enough to protect the interface, as could be the case with ZrN. The nitride AlN is not as reactive and not as well wetted and therefore it is a better candidate for liquid metal handling applications including CuZr and CuCr alloys. The influence of oxygen in all these phenomena can make a difference in real applications where atmosphere is not as well controlled. For applications in various atmospheres the final wetting and reactivity behavior needs to be tested separately, as the results of this study cannot be directly applied.

References

1. Young, T. An essay on the cohesion of liquids. Philosophical Transactions of the Royal Society of London, (94) 1805, p 65-87.

2. Dupré, A. Théorie mecanique de la chaleur, Chapter IX, Actions moléculaires, Gauthier-Villars, Paris. 1869.

3. Wenzel, R.N., Resistance of solid surfaces to wetting by water. Industrial and Engineering Chemistry, 28 (8), 1936, p. 988-994.

4. Shuttleworth, R. and Bailey, G.L.J., Discussions of the Faraday Society (3), 1948, p. 16.

5. Dettree, R.H. and Johnson, R.E., Contact angle, wettability and adhesion; Advances in Chemistry Series, American Chemical Society, Washington D.C., 1964, pp.136-144.

6. Eick, J.D., Good, R.J. and Neuman, A.W., Thermodynamics of contact angles II, Rough solid surfaces. Journal of Colloid and Interface Science, 53 (2), 1975, pp. 235-248.

7. Cassie, A.B.D., Contact angles. Discussions of the Faraday Society (3), 1948, p.11-22.

8. Tanner, L.H. Applied Physics, (12), 1979, p.1473.

9. de Gennes, P.G. Wetting: statics and dynamics. Reviews of Modern Physics, 57 (3), 1985, pp. 827-863.

10. Protsenko, P., Kozlova, O., Voytovych, R. and Eustathopoulos, N. Dissolutive wetting of Si by molten Cu. Journal of Materials Science 43 (16) 2008, p. 5669.

11. Saiz, E. and Tomsia, A.P. Atomic dynamics and Marangoni films during liquid-metal spreading. Nature Materials, 3 (12) 2004, p 903.

12. Kozlova, O., Voytovych, R., Protsenko, P. and Eustathopoulos, N. Non-reactive versus dissolutive wetting of Ag-Cu alloys on Cu substrates. Journal of Materials Science 45, 2010, p. 2099.

13. Smith, C.S. Grains, Phases and interfaces: An interpretation of microstructure. Transactions of the American Institute of Mining, Metallurgical, and Petroleum Engineers, 175, 1948, p.15.

14. Carre, A. and Shanahan, M.E.R., Influence of the “wetting ridge” in dry patch formation. Langmuir, (11), 1995, pp. 3572-75.

15. Saiz, E., Cannon, M. and Tomsia, A.P. Reactive spreading: adsorption, ridging and compound formation. Acta Materialia 48, 2000, pp. 4449-4462.

16. Eustathopoulos, N. Progress in understanding and modeling reactive wetting of metals on ceramics. Current opinion in Solid State and Materials Science 9, 2005, pp. 152-160.

17. Passerone, A., Muolo, M.L., Valenza, F., Monteverde, F. and Sobczak, N. Wetting and interfacial phenomena in Ni-HfB_2 systems. Acta Materialia 57, 2009, pp. 356-364.

18. Warren, J.A., Boettinger, W.J. and Roosen, A.R., Modeling reactive wetting. Acta Materialia. 46 (9), 1998, pp.3247-64.

19. Ogino, K., Nogi, K. and Yamase, O. Effect of Selenium and Tellurium on the Surface Tension of Moltern Iron and the Wettability if Alumina by Molten Iron. Transactions of ISIJ, 23, 1983, p. 234.

20. Voytovych, R., Koltsov, A., Hodaj, F. and Eustathopoulos, N. Reactive vs non-reactive wetting of ZrB_2 by azeotropic Au-Ni. Acta Materialia, 55(18), 2007, pp. 6316-6321.

21. Yin, L., Meschter, J. and Singler, J. Wetting in the Au-Sn system. Acta Materialia, 54, 2004, pp. 2873-2888.

22. Yin, L., Murray, B.T. and Singler T.J. Dissolutive wetting in the Bi-Sn system. Acta Materialia, 54, 2006, pp. 3561-3574.

23. Bougiori, V., Voytovych, R, Dezellus, O. and Eustathopoulos, N. Wetting and reactivity in Ni-Si/C system: experiments versus model predictions. Journal of Materials Science, 42, 2007, pp. 2016-2023.

24. Espié, L., Drevet, B. and Eustathopoulos, N., Experimental study of the influence of interfacial energies and reactivity on wetting in metal/oxide systems. Metallurgical and Materials Transactions A, 25A, 1994, pp. 599-605.

25. Kritsalis, P., Coudurier, L., Parayre, C. and Eustathopoulos, N., Influence of adsorption and interfacial reactions induced by chromium and titanium on the wettability of vitreous carbon by NiPd alloys. Journal of Less-Common Metals, (175), 1991, pp.13-27.

26. Landry, K., Kalegeropoulou, S. and Eustathopoulos, N., Wettability of carbon by aluminium and aluminium alloys. Materials Science and Engineering A254, 1998, pp.99-111.

27. Landry, K. and Eustathopoulos, N. Dynamics of wetting in reactive metal/ceramic systems: linear spreading. Acta Materialia 44, 1996, p. 3923.

28. Dezellus, O., Contribution à l'étude des mécanismes de mouillage réactif. Doctoral thesis, Institut national polytechnique de Grenoble, 2000.

29. Mortensen, A., Drevet, B. and Eustathopoulos, N., Kinetics of diffusion-limited spreading of sessile drops in reactive wetting. Scripta Materialia, 26 (6), 1997, pp. 645-651.

30. Hodaj, F., Dezellus, O., Barbier J.N., Mortensen, A. and Eustathopoulos, N., Diffusion-limited reactive wetting: effect of interfacial reaction behind the triple line. J. Mater. Sci. 42, 2007, pp 8071-8082.

31. Dezellus, O., Hodaj, F. and Eustathopoulos, N., Progress in modeling of chemical-reaction limited wetting. Journal of the European Ceramic Society 23, 2003, pp 2797-2803.

32. Eustathopoulos, N., Nicholas, M.G. and Drevet, B., Wettability at high temperatures. Pergamon Materials Series 3, 1999, p 97.

33. Muolo, M., Ferrera, E., Morbelli, L. and Passerone, A. Wetting, spreading and joining in the alumina-zirconia-Inconel 738 system. Scripta Materialia, 50, 2004, pp. 325-330.

34. Calderon, N.R., Voytovych, R., Narciso, J. and Eustathopoulos, N. Wetting dynamics versus interfacial reactivity of AlSi alloys on carbon. Journal of Materials Science, 45, 2010, pp. 2150-2156.

35. Yang, L., Shen, P., Lin, Q., Qiu, F. and Jiang, Q. Effect of Cr on the wetting in Cu/graphite system. Applied Surface Science, 257, 2011,pp. 6276-6281.

36. Drevet, B., Voytovych, R., Israel, R. and Eustathopoulos, N. Wetting and adhesion of Si on Si_3N_4 and BN substrates. Journal of the European Ceramic Society, 29, 2009, pp. 2363-2367.

37. Koltsov, A. Dumont, M., Hodaj, F. and Eustathopoulos, N. Infuence of Ti on wetting of AlN by Ni-base alloys. Materials Science and Engineering A, 415, 2006, pp. 171-176.

38. Li, J.G., Coudurier, L. and Eustathopoulos, N. Work of adhesion and contact-angle isotherm of binary alloys on ionocovalent oxides. Journal of Materials Science, 24, 1989, p. 1109.

39. Jacob, K.T. and Alcock, C.B. Quasichemical equations for O and S in liquid binary alloys. Acta Metallurgica 20, 1972, p 221.

40. Dezellus, O. and Eustathopoulos, N. Fundamental issues of reactive wetting by liquid metals. Journal of Materials Science, 45, 2010, pp. 4256-4264.

41. Eustathopoulos, N., Nicholas, M.G. and Drevet, B., Wettability at high temperatures. Pergamon Materials Series 3, 1999, p 251.

42. Eustathopoulos, N., Nicholas, M.G. and Drevet, B., Wettability at high temperatures. Pergamon Materials Series 3, 1999, p 219.

43. Nexhip, C., Davidson, R. and Sun, S. Surface tension of Cu-O alloys at 1400 K, VII International Conference on Molten Slags, Fluxes and Salts, The South African Institute of Mining and Metallurgy, 2004, p.271.

44. Chakadler, A.C.D., Gill, W.W. and Mehrotra, S.P. Predictive model for interfacial phenomena between molten metals and sapphire in varying oxygen partial pressures. Materials Science Research 14, 1981, pp 421-432.

45. Naidich, Y.V., Progress in Surface and Membrane Science, (edited by Cadenhead, D.A.) Academic Press, 1981.

46. Kritsalis, P., Li, J.G., Coudurier, N. and Eustathopoulos, N. Role of clusters on the wettability and work of adhesion of the Cu-Cr/Al_2O_3 system. Journal of Materials Science Letters, 9, 1990, pp.1332-35.

47. Rivollet, I., Chatain, D. and Eustathopoulos, N. Mouillabilité de l'alumine monoocristalline par l'or et l'etain entre leur point de fusion et 1673 K. Acta Metallurgica, 35, 1987, p.835.

48. Jarrige, J., Joyeux, T., Lecompte, J.P. and Labbe, J.C. Influence of oxygen on the joining between copper and aluminium nitride. Journal of the European Ceramic Society, 27, 2007, pp. 337-341.

49. Tanaka, S.-I., Direct bonding of Cu to oxidized silicon nitride by wetting of molten Cu and Cu(O). Journal of Materials Science, 45, 2010, pp. 2181-2187.

50. Kubaschewski, O. and Alcock, G.B., Metallurgical Thermochemistry, 5th ed., Pergamon, 1979.

51. Eustathopoulos, N., Nicholas, M.G. and Drevet, B., Wettability at high temperatures. Pergamon Materials Series 3, 1999, p.285.

52. Nicholas, M.G., Mortimer, D.A., Jones, L.M. and Crispin, R.M., Some observations on the wetting and bonding of nitride ceramics. Journal of Materials Science, 25, 1990, pp. 2679-89.

53. Rosazza Prin, G., Baffie, T., Jeymond, M. and Eustathopoulos, N. Contact angles and spreading kinetics of Al and Al-Cu alloys on sintered AlN. Materials Science and Engineering A 298, 2001, pp. 34-43.

54. Taranets, N. Yu. and Naidich, Yu.V., Wettability of aluminium nitride by molten metals. Powder Metallurgy and Metal Ceramics, 35 (5-6), 1996, pp. 74 – 78.

55. Beer, S.Z. (editor), Liquid metals. Chemistry and physics. 1972. p.175.

56. Rhee, S.K., Wetting of AlN and TiC by liquid Ag and liquid Cu. Journal of the American Ceramic Society, 53 (12), 1970, pp. 639-641.

57. Tomsia, A.P. and Loehman, R.E., Reactions and microstructure at selected ceramic/metal interfaces. Materials and Manufacturing Processes, 9 (3), 1994, pp. 547-561.

58. Kida, M., Bahraini, M., Molina, J.M., Weber, L. and Mortensen, A. High-temperature wettability of aluminum nitride during liquid metal infiltration. Materials Science and Engineering A, 495, 2008, pp. 197-202.

59. Labbe, J.C. et Brandy, G., Mouillabilité d'une céramique à base de nitrure d'aluminium par le cuivre liquide. Rev. Int. Hautes Tempér. Réfract., (26), 1990, pp.121-130.

60. Rhee, S.K., Wetting of AlN and TiC by liquid Pb. Journal of the American Ceramic Society, 53 (12), 1970, pp. 426.

61. Dezellus, O., Andrieux, J., Bosselet, F., Sacerdote-Peronnet, M., Baffie, T., Hodaj, F., Eustathopoulos, N. and Viala, J.C. Transient liquid phase bonding of titanium to aluminium nitride. Materials Science and Engineering A, 495, 2008, pp. 254-258.

62. Olesińska, W., Pawłowska, M. Kaliński, D. and Chmielewski, M. Reactive metallic layers produced on AlN, Si_3N_4 and SiC ceramics. Journal of Materials Science: Materials in Electronics, 15, 2004, pp. 813-817.

63. HSC Chemistry for Windows 4.1. Outokumpu Research Oy, 1999.

64. Nakao, Y., Nishimoto, K. and Saida, K., Reaction layer formation in nitride ceramics (Si_3N_4 and AlN) to metal joints bonded with active filler metals. ISIJ International, 30 (12), 1991, pp.1142-50.

65. He, X., Size, Y., Du, Y., Tao, K. and Fan, Y., Reaction layer formation at the interface between Ti and Zr and AlN. Phys. Stat. Sol. (a), 157, 1996, pp. 99-106.

66. Koltsov, A., Hodaj, F., Eustathopoulos, N., Dezellus, A. and Plaindoux, P. Wetting and interfacial reactivity in Ag-Zr/sintered AlN system. Scripta Materialia 48, 2003, pp. 351-357

67. Ljungberg, L. and Warren, R. Wetting of Silicon Nitride with Selected Metals and Alloys. Ceramic engineering and science proceedings, American Ceramic Society. Pittsburgh, April 1987, paper 14-F11-87.

68. Naka, M., Kubo,M. and Okamoto, I. Wettability of silicon nitride by aluminium, copper and silver. Journal of Materials Science Letters, 6, 1987, pp. 965-966.

69. Tomsia, A.P. and Pask, J.A. Joining nitride ceramics. Ceram. Eng. Sci. Proc. 11-12, 1989, pp. 1631-1654.

70. Naka, M. and Okamoto, I. Wetting of silicon nitride by copper-titanium or copper-zirconium alloys. Transactions of JWRI, 14 (1), 1985, pp. 29-34.

71. Li, J.G. and Hausner, H. Influence of oxygen partial pressure on the wetting behaviour of silicon nitride by molten silicon. Journal of the European Ceramic Society, 9, 1992, pp. 101-105.

72. Luz, A.P. and Ribeiro, S. Wetting behavior of silicon nitride ceramics by Ti-Cu alloys. Ceramics International 34, 2008, pp. 305-309.

73. Xiao, P. and Derby, B. The wetting of silicon nitride by chromium-containing alloys. Journal of Materials Science, 30, 1995, pp. 5915 - 5922.

74. He, Y.M., Zhang, J., Wang, X. and Sun, Y. Effect of brazing temperature on microstructure and mechanical properties of Si_3N_4/Si_3N_4 joints brazed with Ag-Cu-Ti + Mo composite filler. Journal of Materials Science, 46, 2011, pp. 2796-2804.

75. Zhang, J., He, Y.M., Sun, Y. and Liu, C.F. Microstructure evolution of Si_3N_4/Si_3N_4 joint brazed with Ag-Cu-Ti + SiCp composite filler. Ceramics International, 36, 2010, pp. 1397-1404.

76. Hess, N., Maupin, L., Chick, L., Sundberg, D., McCreedy, T. and Armstrong, T. Synthesis, analysis and processing of novel materials in the yttrium oxide – aluminium oxide system. Journal of Materials Science, 29, 1994, pp. 1873 – 1878.

77. Eustathopoulos, N., Nicholas, M.G. and Drevet, B., Wettability at high temperatures. Pergamon Materials Series 3, 1999, p 108.

78. Baffie, T. Contribution a l'amélioration des propriétés thermiques d'assemblages cuivre/nitrure d'aluminium poly cristallin destines a l'électronique de puissance. Doctoral thesis, Institut national polytechnique de Grenoble, 2000.

79. Maguire, H.G. and Augustus, P.D. The detection of silicon-oxynitride layers on the surfaces of silicon nitride films by Auger electron emission. Journal of the Electrochemical Society: Solid-State Science and Technology, 119 (6), 1972, pp. 791-793.

80. Rocabois, P., Chatillon, C. and Bernard, C. Thermodynamics of the Si-O-N system: II, Stability of Si_2N_2O(s) by high-temperature mass spectrometric vaporization. Journal of the American Ceramic Society, 79 (5), 1996, pp. 1361-65.

81. McCauley, R.A., Corrosion of ceramics, Marcel Dekker, Inc. USA, 1995.

82. Laurent, V., Mouillabilité et réactivité dans les systèmes composites métal/céramique: Etude du couple Al/SiC. Doctoral thesis, Institut national polytechnique de Grenoble, 1988.

83. Du, H., Tressler, R.E. and Spear, K.E., Thermodynamics of the Si-N-O system and kinetic modeling of oxidation of Si_3N_4. Journal of Electrochemical Society, 136 (11), 1989, pp.3210-3215.

84. Vaughn, W.L. and Maahs, H.G., Active-to-passive transition in the oxidation of silicon carbide and silicon nitride in air. Journal of the American Ceramic Society, 73 (6), 1990, pp. 1540-43.

85. Labrousse, L. Mouillage et reactivité des alliages refractaires Ni-Al-Ti sur l'alumine p.65.

86. Ohuchi, F.S. and Kohyama, M., Electronic structure and chemical reactions at metal-alumina and metal-aluminium nitride interfaces. Journal of the American Ceramic Society, 74 (6), 1991, pp.1163-87.

87. Massalski, T.B., Binary phase diagrams. Ohio, USA, 1986, American Society for metals.

88. MTDATA Phase diagram software, National Physical Laboratory, Hampton Road, Teddington, Middlesex.

89. Gribaudo, L., Arias, D. and Abriata, J. Reactions between U-Zr alloys and nitrogen. Journal of Phase Equilibria, 15 (4), 1994, pp. 441-449.

90. Nicholas, M.G. Active metal brazing. Journal of British Ceramic Transactions, 85, 1986, p.144.

91. Gilles, J.C., Formation of oxynitrides from refractory oxides. Rev. Hautes Temp. Refract., (2), 1965, pp. 237-62.

92. Collongues, R., Gilles, J.C., Lejus, A.M., Perez, M., Jorba, Y. and Michel, D., Investigations on the metallic oxynitrides. Materials Research Bulletin, (2), 1967, pp.837-48.

93. Ondik, H.M. and McMurdie, H.F. Phase diagrams for Zirconium and Zirconia systems. The American Ceramic Society, 1998

94. Matzke, H.J. Advances in Ceramics 1987;23 p.617.

95. Beer, S.Z. (editor), Liquid metals. Chemistry and physics. 1972. p.169.

96. Chakrabarti, D.J. and Laughlin, D.E. The Cr-Cu system. Bulletin of alloy phase diagrams. Vol 5, Nr 1. 1984 p 59.

97 Eom, J.Y. Rao, V.S. Experiments and modeling study on growth behavior of Cr-nitrides formed on electroplated hard Cr during ion-nitriding. J.Mater.Res .18, 4, 2003, pp 861- 867.

98. Eustathopoulos, N., Nicholas, M.G. and Drevet, B., Wettability at high temperatures. Pergamon Materials Series 3, 1999, p.300.

99. Karakaya, I. and Thompson, W.T. Ag-O system. Journal of phase equilibria, vol. 13, no 2, 1992, pp 137-142.

100. Bricard, A., Eustathopoulos, N., Joud, J-C. and Desré, P. Surface tension of liquid Ag-Cu alloys by the sessile-drop method. Compt. Rend. Vol 276C, no22. Acad Sci Paris 1973, p. 1613.

101. Sangiorgi, R., Muolo, M.L., Chatain, D. and Eustathopoulos, N. Wettability and work of adhesion of nonreactive liquid metals on silica. Journal of American Ceramic Society, 71, 1988, p. 742.

102. Labrousse, L. Mouillage et réactivité des alliages réfractaires Ni-Al-Ti sur l'alumine. Doctoral thesis, Institut national polytechnique de Grenoble, 2001.

103. Baborowski, J., Charbonnier, M. and Romand, M., X-ray emission characterization of chromium oxide and oxynitride films deposited by reactive magnetron sputtering. J. Phys. IV, 6(C4, Rayons X et Matiere), 1996, pp. C4/429-C4/439.

104. Gouin, X., Le Gendre, L., Marchand, R. and Laurent, Y., A new family of high specific surface area chromium oxynitrides: preparation and characterization. Ann. Chim. (Paris), 20 (5), 1995, pp. 293-299.

105. Naka, M., Kubo,M. and Okamoto, I. Wettability of silicon nitride by aluminium, copper and silver. Journal of materials science letters, 6, 1987, pp. 965-966.

106) Niessen, A.K., De Boer, F.R., Boom, R., Dechatel, P.F. Mattens W.C.M. and Miedema, A.R. Calphad, (1983) 51.

Thermodynamic data and calculations on studied materials

The most probable reactions are selected on the basis of the formation energies of various possible compounds, found from phase diagrams and other literature. The compound with the most negative formation energy should represent the most stable alternative compound. However, also other factors have an influence on the reactivity, for example the reaction kinetics and atmosphere and therefore the selection of thermodynamically studied reactions is based on the results of previous studies. Additionally it is possible to calculate the possible thicknesses of reaction layers by equaling the reaction equation to zero, representing the case where there is no more driving force for reaction.

Reaction at AlN – CuZr interfaces

Table 1. The Gibbs energies of reaction of binary compounds which are possible in the studied AlN – CuZr system.

Compound	$G_f°(T)$ (1100°C) J/mol	Ref.*
AlN	-386988	1
ZrN	-466763	1
Al_2Zr	-102501	1
Al_2Zr_3	-146826	2
Al_3Zr	-122793	2
Al_3Zr_2	-174151	2
Al_3Zr_5	-150595	2
Al_4Zr_5	-283119	2
AlZr	-65606	2
$AlZr_2$	-76025	2
$AlZr_3$	-77272	2

Reaction energy is calculated for the ZrN formation reaction at 1150°C:

$(Zr)_{Cu} + AlN = ZrN + (Al)_{Cu}$

Calculated reaction energy represents the driving force of the reaction.

*) The Appendix has its own reference list at the end

Thermodynamic data and calculations on studied materials (cont.)

$$\Delta G_M = \left\{\Delta G_M^0 + RT\ln\gamma_{Al}^{\infty} - RT\ln\gamma_{Zr}^{\infty}\right\} + RT\ln x_{Al} - RT\ln\left[x_{Zr}^0 - x_{Al}\right]$$

$$x_{Zr} \to 0, T = 1150°C = 1423K$$

$$RT\ln\gamma_{Zr}^{\infty} = \overline{\Delta G}_{Zr(Cu)}^{xs} = -48180\,J/mol^* /2/$$

$$RT\ln\gamma_{Al}^{\infty} = \overline{\Delta G}_{Al(Cu)}^{xs} = -70890\,J/mol^* /4/$$

$$\Delta G_M^0 = \Delta G_f^0(ZrN) - \Delta G_f^{\circ}(AlN)$$

$$\langle Zr\rangle + \frac{1}{2}N_2 \to \langle ZrN\rangle; \Delta G_f^{\circ} = -233299\,J/mol$$

$$(Zr) \to \langle Zr\rangle; \Delta_{fus}G_{Zr} = 4038\left(1 - \frac{1423K}{2125K}\right) * 4{,}1868\,J/mol = 5585\,J/mol$$

– – – – – – – – – – – – –

$$(Zr) + \frac{1}{2}N_2 \to \langle ZrN\rangle$$

$$\Delta G_f^0\left(ZrN/(Zr)\right) = \Delta G_f\left(ZrN/\langle Zr\rangle\right) - \Delta H_m\left(1 - \frac{T}{T_m}\right)$$

$$= -233299\,J/mol - 5585\,J/mol = -238884\,J/mol$$

$$(Al) + 1/2N_2 \to AlN; \Delta G_f^{\circ} = -162027\,J/mol$$

$$\Delta G_M = (-238884 + 162027 - 70890 + 48180) + RT\ln x_{Al} - RT\ln\left[x_{Zr}^0 - x_{Al}\right]$$

$$x_{Zr}, x_{Al} \to 0$$

$$\Rightarrow \Delta G_M = -99567\,J/mol$$

By setting the $\Delta G_M = 0$, and inserting the actual amount of Zr it is possible to calculate the thicknesses (e) for the possible ZrN reaction layers with varying Zr contents. The calculation is presented here:

If $\Delta G_M = 0$ and $x_{Zr} = 10^{-2} \rightarrow x_{Al} = 9{,}998 * 10^{-3}$

Assuming mass balance:

$\theta \approx 90°$
m = 100 mg
M_{Cu} = 63,54 g/mol

$$n = \frac{0{,}1g}{63{,}54g/mol} = 1{,}574 * 10^{-3} mol$$

$\rightarrow n_{Zr}(ZrN) = x_{Al}^{*} * 1{,}574 * 10^{-3}$ mol

$V_{ZrN} = (\pi R^2) * e = \frac{n_{Zr} * M_{ZrN}}{\rho_{ZrN}}$

$$R \rightarrow V = \frac{m}{\rho_{Cu}} = \frac{0{,}1g}{8{,}95g/cm^3} \approx 0{,}0111732cm^3 = \frac{1}{2} * \frac{4}{3}R^3\pi$$

Thermodynamic data and calculations on studied materials (cont.)

→ R = 0,8mm

M_{ZrN} = 105,2267 g/mol

ρ_{ZrN} = 7,35 g/cm^3

$V = \pi R^3 * e = \frac{n_{Zr} * M_{ZrN}}{\rho_{ZrN}}$

$\rightarrow e = \frac{1{,}574 * 10^{-3} mol * x^*_{Al} * 105{,}2267 g/mol}{\frac{7{,}35 g}{cm^3} * \pi * (0{,}174743 cm)^2}$

Inserting $x_{Al}^* = 9{,}998 * 10^{-3}$

e = 0,002344 cm ≈ 23,4 µm

The results for different Zr contents are listed in Table 2.

Table 2. Theoretical reaction layer thicknesses for different CuZr alloys on AlN

CuZr0,1 (w-%)	2,34 µm
CuZr1 (w-%)	23,4 µm
CuZr5 (w-%)	117 µm
CuZr10 (w-%)	234 µm

Reaction at AlN – CuCr interfaces

In the related articles the reaction product has been identified to be Cr_2N, and in the following calculation its formation is studied. Table 3 lists all possible compounds and their Gibbs energies of reaction

Table 3. The Gibbs energies of reaction for binary compounds, which are possible in the studied AlN – CuCr system.

Compound	$G_f°(T)$ (1100°C) J/mol	Ref.
AlN	-386988	1
CrN	-220610	1
Cr_2N	-294068	1
$AlCr_2$	-44769	2
Al_4Cr	-115181	2
Al_8Cr_5-L	-229515	2
Al_8Cr_5-H	-228053	2
Al_9Cr_4-L	-208653	2
Al_9Cr_4-H	-211541	2
$Al_{11}Cr_2$	-140070	2
$Al_{13}Cr_2$	-143924	2

$2(Cr)_{Cu} + AlN = Cr_2N + (Al)_{Cu}$

T = 1373K

$$\Delta G_m = (\Delta G_m^0 + RT\ln\gamma_{Al}^{\infty} - RT\ln\gamma_{Cr}^{\infty}) + RT\ln x_{Al} - RT\ln\left[x_{Cr}^0 - x_{Al}\right]$$

$$\mathrm{RT}\ln\gamma_{Cr}^{\infty} = \overline{\Delta G}_{Cr(Cu)}^{xs} = (1-x_{Cr})^2\cdot(81200 + 6070x_{Cr} - 27{,}9\cdot T)$$

$$x_{Cr} \to 0$$

$$\overline{\Delta G}_{Cr(Cu)}^{xs} = 1\cdot(81200 + 6070\cdot 0 - 27{,}9\cdot 1373) = 42893 J/mol/4/$$

$$\mathrm{RT}\gamma_{Al}^{\infty} = \overline{\Delta G}_{Al(Cu)}^{xs} = \left[-8625 - T\cdot 5{,}838\right]\cdot 4{,}1868 = -69671 J/mol/4/$$

$$\Delta G_M = \Delta G_M^{\circ} + RT\ln\gamma_{Al}^{\infty} - RT\ln\gamma_{Cr}^{\infty} + RT\ln x_{Al} - RT\ln(x_{Cr}^{\circ} - x_{Al})$$

$$\Delta G_M^{\circ} = \Delta G_f^{\circ}(Cr_2N) - \Delta G_f^{\circ}(AlN)$$

$$2\langle Cr\rangle + 1/2N_2 \to Cr_2N \qquad \Delta G^{\circ} = -95997 J/mol$$

Thermodynamic data and calculations on studied materials (cont.)

$$2(Cr) \rightarrow 2\langle Cr \rangle ; \Delta_{fus} G_{Cr} = 20500 \cdot \left(1 - \frac{T}{2130}\right) = 7286 J / mol$$

$$2(Cr) + 1/2 N_2 \rightarrow Cr_2N$$

$$\Delta G_f^{\circ}\left(Cr_2N / \langle Cr \rangle\right) - \Delta G_{fus} = -95997 J / mol - 2 \cdot 7286 J / mol = -110569 J / mol$$

$$(Al) + 1/2 N_2 \rightarrow AlN \qquad \Delta G_f^{\circ} = -167900 J / mol$$

$$\Delta G_M = (-110569 + 167900 - 69671 - 42893) + RT \ln x_{Al} - RT \ln(x_{Cr}^{\circ} - x_{Al})$$
$$x_{Cr,Al} \rightarrow 0$$
$$\Delta G_M = -53568 J / mol$$

The thickness of the reaction layer is calculated with the help of the mass balance in the same way as in the case of CuZr alloys on AlN.

The theoretical reaction layer thickness for CuCr1,5 (w-%) is 3,7µm.

Reaction at AlN – AgZr interfaces

On AgZr - AlN only ZrN has been found in the interfacial layer and therefore the calculation here studies the formation of ZrN. Possible compounds were listed in Table 1.

$(Zr)_{Ag} + AlN = ZrN + (Al)_{Ag}$

$$\Delta G_M = \left\{\Delta G_M^0 + RT\ln\gamma_{Al}^{\infty} - RT\ln\gamma_{Zr}^{\infty}\right\} + RT\ln x_{Al} - RT\ln\left[x_{Zr}^0 - x_{Al}\right]$$

$$x_{Zr} \to 0, T = 980°C$$

$$RT\ln\gamma_{Zr}^{\infty} = \overline{\Delta G}_{Zr(Ag)}^{xs} \approx -13000 J/mol^* /5/$$

$$RT\ln\gamma_{Al}^{\infty} = \overline{\Delta G}_{Al(Ag)}^{xs} \approx -33950 J/mol^* /6/$$

$$\Delta G_M^0 = \Delta G_f^0(ZrN) - \Delta G_f^0(AlN)$$

$$\langle Zr\rangle + \frac{1}{2}N_2 \to \langle ZrN\rangle; \Delta G^\circ = -248791 J/mol$$

$$(Zr) \to \langle Zr\rangle; \Delta_{fus}G_{Zr} = 4038\left(1 - \frac{1253K}{2125K}\right) * 4{,}1868 J/mol = 6938 J/mol$$

– – – – – – – – – – – – –

$$(Zr) + \frac{1}{2}N_2 \to \langle ZrN\rangle$$

$$\Delta G_f^0\left(ZrN/(Zr)\right) = \Delta G_f\left(ZrN/\langle Zr\rangle\right) - \Delta H_m\left(1 - \frac{T}{T_m}\right)$$

$$= -248791 J/mol - 6938 J/mol = -255729 J/mol$$

$$(Al) + 1/2 N_2 \to AlN; \Delta G_f^\circ = -181999 J/mol$$

$$\Delta G_M = (-255729 + 181999 - 33950 + 13000) + RT\ln x_{Al} - RT\ln\left[x_{Zr}^\circ - x_{Al}\right]$$

$$x_{Zr}, x_{Al} \to 0$$

$$\Rightarrow \Delta G_M = -94680 J/mol$$

The mass balance calculation for reaction layer thickness e is carried out the same way than with CuZr/AlN system and the result for the ZrN layer in the system AgZr3 (w-%) on AlN is 32 μm.

Reaction at Si_3N_4 – CuZr interfaces

In the related articles the formation of ZrN was found in most cases. Some studies also reported silicide formation. All the possible compounds are listed in Table 4. Here the reaction calculation is made for ZrN formation.

Table 4. The Gibbs energies of reaction for binary compounds which are possible in the studied Si_3N_4 – CuZr system.

Compound	$G_f°(T)$ (1100°C) J/mol	Ref.
Si_3N_4	-1027192	1
ZrN	-466763	1
Zr_2Si	-423704	1
ZrSi	-284527	1
$ZrSi_2$	-329783	1
Zr_5Si	-1141043	1

$4(Zr)_{Cu} + Si_3N_4 = 4ZrN + 3(Si)_{Cu}$

Thermodynamic data and calculations on studied materials (cont.)

$$\Delta G_M = \left\{\Delta G_M^0 + RT\ln\gamma_{Si}^{\infty} - RT\ln\gamma_{Zr}^{\infty}\right\} + RT\ln x_{Si} - RT\ln\left[x_{Zr}^0 - x_{Si}\right]$$

$$x_{Zr} \to 0, T = 1150°C$$

$$RT\ln\gamma_{Zr}^{\infty} = \overline{\Delta G}_{Zr(Cu)}^{xs} = -48180 J/mol/2/$$

$$RT\ln\gamma_{Si}^{\infty} = \overline{\Delta G}_{Si(Cu)}^{xs} = -19900 J/mol/3/$$

$$\Delta G_M^0 = \Delta G_f^0(ZrN) - \Delta G_f^0(Si_3N_4)$$

$$\langle Zr\rangle + \frac{1}{2}N_2 \to \langle ZrN\rangle; \Delta G_f^{\circ} = -233299 J/mol$$

$$(Zr) \to \langle Zr\rangle; \Delta_{fus}G_{Zr} = \left[4038\left(1 - \frac{1423K}{2125K}\right)\right]\cdot 4{,}1868 J/mol = -5585 J/mol$$

– – – – – – – – – – – – –

$$(Zr) + \frac{1}{2}N_2 \to \langle ZrN\rangle$$

$$\Delta G_f^0\left(ZrN/(Zr)\right) = \Delta G_f\left(ZrN/\langle Zr\rangle\right) - \Delta H_m\left(1 - \frac{T}{T_m}\right)$$

$$= (-233299 + 5585) J/mol = -238884 J/mol$$

$$3Si + 2N_2 \to Si_3N_4; \Delta G_f^{\circ} = -273844 J/mol$$

$$\Delta G_M = (-238884 + 273844 - 19900 + 48180) + RT\ln x_{Si} - RT\ln\left[x_{Zr}^{\circ} - x_{Si}\right]$$

$$x_{Zr}, x_{Si} \to 0$$

$$\Rightarrow \Delta G_M = 63240 J/mol$$

The theoretical reaction layer thicknesses are calculated with mass balance calculation to be 65 nm for the CuZr1 (w-%) alloy and 0,3 μm for the CuZr5 (w-%) alloy.

Reaction at Si_3N_4 – CuCr interfaces

In the related articles the reaction product has been identified to be Cr_2N, and the calculation here studies its formation. Gibbs energies of reaction for other possible compounds are listed in Table 5.

Table 5. The Gibbs energies of reaction for binary compounds which are possible in the studied Si_3N_4 – CuCr system

Compound	$G_f°(T)$ (1100°C) J/mol	Ref.
Si_3N_4	-1027192	1
CrN	-220610	1
Cr_2N	-294068	1
CrSi	-186868	1
$CrSi_2$	-250103	1
Cr_3Si	-363488	1
Cr_5Si_3	-796264	1

$8(Cr)_{Cu} + Si_3N_4 = 4Cr_2N + 3(Si)_{Cu}$

T = 1373K (1100°C)

$$\Delta G_m = (\Delta G_m^0 + RT\ln\gamma_{Si}^{\infty} - RT\ln\gamma_{Cr}^{\infty}) + RT\ln x_{Si} - RT\ln\left[x_{Cr}^0 - x_{Si}\right]$$

$$RT\ln\gamma_{Cr}^{\infty} = \overline{\Delta G}_{Cr(Cu)}^{xs} = -42893{,}3J/mol/4/$$

$$RT\gamma_{Si}^{\infty} = \overline{\Delta G}_{Si(Cu)}^{xs} = -19900J/mol/3/$$

$$\Delta G_M = \Delta G_M^{\circ} + RT\ln\gamma_{Si}^{\infty} - RT\ln\gamma_{Cr}^{\infty} + RT\ln x_{Si} - RT\ln(x_{Cr}^{\circ} - x_{Si})$$

$$\Delta G_M^{\circ} = \Delta G_f^{\circ}(Cr_2N) - \Delta G_f^{\circ}(Si_3N_4)$$

$$2\langle Cr\rangle + 1/2N_2 \rightarrow Cr_2N \qquad \Delta G^{\circ} = -95997J/mol$$

$$2(Cr) \rightarrow 2\langle Cr\rangle \qquad \Delta_{fus}G_{Cr} = 20500\cdot\left(1 - \frac{T}{2130}\right) = 7286J/mol$$

$$2(Cr) + 1/2N_2 \rightarrow Cr_2N$$

$$\Delta G_f^{\circ}\left(Cr_2N/\langle Cr\rangle\right) - \Delta G_{fus} = -95997J/mol - 2\cdot 7286J/mol = -110569J/mol$$

$$3Si + 2N_2 \rightarrow Si_3N_4; \Delta G_f^{\circ} = -290164J/mol$$

$$\Delta G_M = (-110569 + 290164 + 19900 + 42893) + RT \ln x_{Al} - RT \ln(x_{Cr}^{\circ} - x_{Al})$$
$$x_{Cr,Al} \to 0$$
$$\Delta G_M = 242388 J / mol$$

The theoretical Cr_2N reaction layer thickness calculated in the same way as in previous examples for CuCr1,5 (w-%) is $1*10^{-10}$ mm.

Reaction at Si_3N_4 – AgZr interfaces

In AgZr-Si_3N_4 system no previous results were found. From earlier experiments in this study, the formation of ZrN is predicted even though there are more stable compounds as can be seen in Table 4.

$(Zr)_{Ag} + Si_3N_4 = ZrN + (Si)_{Ag}$

$$\Delta G_M = \left\{\Delta G_M^0 + RT \ln \gamma_{Si}^{\infty} - RT \ln \gamma_{Zr}^{\infty}\right\} + RT \ln x_{Si} - RT \ln\left[x_{Zr}^0 - x_{Si}\right]$$
$$x_{Zr} \to 0, T = 980°C$$
$$RT \ln \gamma_{Zr}^{\infty} = \overline{\Delta G}_{Zr(Ag)}^{xs} = -13000 J / mol / 5 /$$
$$RT \ln \gamma_{Si}^{\infty} = \overline{\Delta G}_{Si(Ag)}^{xs} = 4990 J / mol / 4 /$$
$$\Delta G_M^0 = \Delta G_f^0(ZrN) - \Delta G_f^0(Si_3N_4)$$
$$\langle Zr \rangle + \frac{1}{2} N_2 \to \langle ZrN \rangle; \Delta G^{\circ} = -248791 J / mol$$
$$(Zr) \to \langle Zr \rangle; \Delta_{fus} G_{Zr} = 4038\left(1 - \frac{1253K}{2125K}\right) * 4{,}1868 J / mol = 6938 J / mol$$
$$- - - - - - - - - - - - - -$$
$$(Zr) + \frac{1}{2} N_2 \to \langle ZrN \rangle$$
$$\Delta G_f^0\left(ZrN / (Zr)\right) = \Delta G_f\left(ZrN / \langle Zr \rangle\right) - \Delta H_m\left(1 - \frac{T}{T_m}\right)$$
$$= -248791 J / mol - 6938 J / mol = -255729 J / mol$$

$$3Si + 2N_2 \to Si_3N_4; \Delta G_f^{\circ} = -329494 J / mol$$
$$\Delta G_M = (-255729 + 329494 + 4990 + 13000) + RT \ln x_{Al} - RT \ln\left[x_{Zr}^{\circ} - x_{Al}\right]$$
$$x_{Zr}, x_i \to 0$$
$$\Rightarrow \Delta G_M = 79965 J / mol$$

The theoretical ZrN reaction layer thickness calculated in the same way as in previous examples for AgZr3 (w-%) is 15 nm

Thermodynamic data and calculations on studied materials (cont.)

REFERENCES IN THE APPENDIX

1. HSC Chemistry for Windows 4,1, Outokumpu Research Oy, 1999.
2. Ansara, I., Dinsdale, M. and Rand, M. H., Thermochemical database for light metal alloys, volume 2. COST 507, July 1998.
3. Lüdecke, D. A thermodynamic assessment of the Cu-Si system. CALPHAD 11, 2, 1987, p.135.
4. Kubaschewski, O. and Alcock, C.B., Metallurgical Thermochemistry, 5th ed., Pergamon, 1979.
5. Kubaschewski O, Alcock, C.B. and Spencer, P.J. Materials Thermochemistry, 6th ed. Pergamon, 1993, p.324.
6. Fitzner, K., Kleppa, O.J. Thermochemistry of binary alloys of transition metals: The Me-Ti, Me-Zr, and Me-Hf (Me= Ag, Au) systems. Metallurgical Transactions 23 A, 1992, p. 997.

Tampereen teknillinen yliopisto
PL 527
33101 Tampere

Tampere University of Technology
P.O.B. 527
FI-33101 Tampere, Finland

ISBN 978-952-15-2813-2
ISSN 1459-2045